FABRICATION AND CHARACTERIZATION OF GERMANIUM PHOTODETECTORS

WANG JIAN

NATIONAL UNIVERSITY OF SINGAPORE
2011

FABRICATION AND CHARACTERIZATION OF GERMANIUM PHOTODETECTORS

WANG JIAN
B. Sci. (Peking University, P. R. China) 2006

A THESIS SUBMITTED
FOR THE DEGREE OF DOCTOR OF PHILOSOPHY

DEPARTMENT OF
ELECTRICAL AND COMPUTER ENGINEERING

NATIONAL UNIVERSITY OF SINGAPORE
2011

Acknowledgements

First, I would like to express my sincere gratitude to my advisors, Dr. Lee Sungjoo and Prof. Kwong Dim-Lee for their invaluable guidance, encouragement throughout my Ph.D. study at NUS. Dr. Lee Sungjoo has been a great supervisor for his kindness and patience, giving me continuous encouragement, allowing me to make some mistakes along the way. And no one can ask for a better guider. I am also truly grateful to Prof. Kwong's wise guidance and foresight to choose Si photonics, one of the hottest topic in Si microelectronics as my Ph.D research target.

I would also like to express my deepest appreciation for Dr. Loh Wei Yip, Dr. Yu Mingbin and Dr. Lo Guoqiang Patrick, from the Institute of Microelectronics, Singapore, for their valuable advice and technical discussions for my research work. I benefited greatly through interactions with them. They gave me inspiration throughout all my projects during my graduate study. I would like to thank all the technical staff in NanoEP department for their kindness, help and suggestions for my research work. I would not have been able to do my doctoral research smoothly.

Special thanks to my seniors in at NUS, especially Dr. Zang Hui, Dr. Jiang Yu, Dr. Fu Jia, Shen Chen, Gao Fei, Song Yan, Zhao Hui and Chen Yu for their assistance on many of my technical problems encountered during my graduate study. Many thanks to my research buddies, Peng Jianwei, Xie Ruilong, Chin Yoke King, and all the SNDL students for their indispensable help for my research work and for the great academic atmosphere created.

My deepest love goes out to my parents who have given me their support and encouragement during my doctorial studies. Last but not least, I would like to express my gratitude towards my wife, Wei Yuan for her unconditional support and love over the years.

Table of Contents

Summary

Si photonics has become one of the most intensive research domains in the world since it holds great promise for maintaining the performance roadmap known as Moore's Law.

First, the recent progresses in the development and integration of Ge-photodetectors on Si-based photonics is comprehensively reviewed, along with remaining technological issues to overcome and future research trend. Second, the impact of selective-epitaxial-germanium is discussed, specifically its local strain effects, on high-performance PIN photodetector for near-infrared applications. Then Si-waveguide-integrated lateral Ge-PIN photodetectors using novel Si/SiGe buffer and two-step Ge-process are demonstrated. Comparative analysis between lateral Ge PIN and vertical p-Si/i-Ge/n-Ge PIN are made. Furthermore, device performance of scaled thin-film-Ge lateral PIN photodetectors integrated on Si-waveguide is presented. The photodetectors are with closely spaced p+/n+ regions (0.8 μm) on Ge region with short length (5-20 μm) and narrow width (2.4 μm). Though with thin Ge-layer (~220 nm including bottom SiGe buffer), light is evanescent-coupled from Si waveguide effectively to the overlying Ge detector. The device exhibits f_{3dB} bandwidth of 18 GHz with external responsivity of 0.13 A/W for 1550 nm at -1V. Considering the coupling loss and waveguide loss, the internal responsivity is as high as 0.65 A/W. It is shown that with increasing detector length, device's internal quantum efficiency can be improved to ~90% and by suppressing parasitic effects, speed can be boosted further towards several tens of GHz.

To address the photodiodes' scalability issue, this work demonstrates a scalable (with gate length of 1 μm) Ge-photodetector based on junction field-effect-transistor (JFET) structure with high sensitivity and improved response time. To overcome the low detection efficiency issue of typical JFET photodetectors, a high quality Ge epi-layer as

the gate of JFET was achieved using a novel epi-growth technique. By laser surface-illumination of 3 mW on the Ge gate, an I_{on}/I_{off} ratio up to 185 was achieved at wavelength of 1550 nm for the first time. Moreover, SOI wafers are utilized to improve the Ge JFET detector's 3dB bandwidth. The results on high-speed silicon-waveguided Ge JFET-based photodetector are reported. While the Ge layer's footprint on wafer is as small as 2 μm×2 μm, low stand-by current (0.5 μA@1 V), high responsivity (642 mA/W) and high speed (8 GHz) are achieved. The reported Ge JFET is a promising candidate for the further scale-downed photodetector in the next-generation Si photonics.

List of Tables

List of Figures

List of Symbols

$\hbar$	Planck's constant
C_{ox}	Gate dielectric capacitance
E_g	Bandgap
ε	Permittivity
κ	Dielectric constant
μ_e	Mobility of electron
μ_h	Mobility of hole
μ_{eff}	Effective mobility
Φ_{be}	Electron Schottky barrier height
Φ_{eh}	Hole Schottky barrier height
I_p	Photocurrent
η	Quantum efficiency
GHz	Gigahertz
n	Reflection index
g_m	Transconductance
V_{th}	Threshold voltage
I_{dark}	Dark current
R	Responsivity
V_D	Drain voltage
J_g	Gate leakage current density

List of Abbreviations

AFM	Atomic force microscopy
BARC	Bottom anti-reflective coatings
CMOSFET	Complementary metal oxide semiconductor field effect transistors
CMP	Chemical mechanical polishing
CV, C-V	Capacitance versus Voltage
DI	De-ionized
DWDM	Dense wavelength division multiplexing
EOT	Equivalent oxide thickness
$E_{buid\text{-}in}$	Build-in electric field
FWHM	Full width at half maximum
GIDL	Gate induce drain leakage
HP	High-performance
HF	Hydrofluoric acid
HR-TEM	High resolution transmission electron microscopy
IC	Integrated circuit
ITRS	International technology roadmap of semiconductor
I-V	Current versus voltage
MBE	Molecular beam epitaxy
MSM	Metal-semiconductor-metal
MGM	Metal-germanium-metal
MBE	Molecular beam epitaxy
OEIC	Optoelectronic integrated circuit

PDA	Post-deposition annealing
PECVD	Plasma enhanced chemical vapor deposition
PR	Photo resist
RMS	Root mean square
RTA	Rapid thermal annealing
RTP	Rapid thermal processor
RIE	Reactive ion etching
RC delay	Resistance-capacitance delay
SEM	Scanning electron microscopy
SB	Schottky barrier
SBH	Schottky barrier height
SOI	Si on isolator
SIMS	Secondary ion mass spectrometry
TEM	Transmission electron microscopy
TCE	Thermal coefficient of expansion
ULSI	Ultra-large scale integrated circuits.
UHV-CVD	Ultra-high vacuum chemical vapor deposition
$V_{buid\text{-}in}$	Build-in voltage

CHAPTER 1

1. Introduction

1.1 Overview of Opto-Electronics Integrated Circuits and Photodetectors

In the past decade, Si photonics has become one of the most active research domains in the world since it holds great promise for maintaining the performance roadmap known as Moore's Law, which predicts that the number of transistors per unit area in the integrated circuits would double approximately every 18 months.

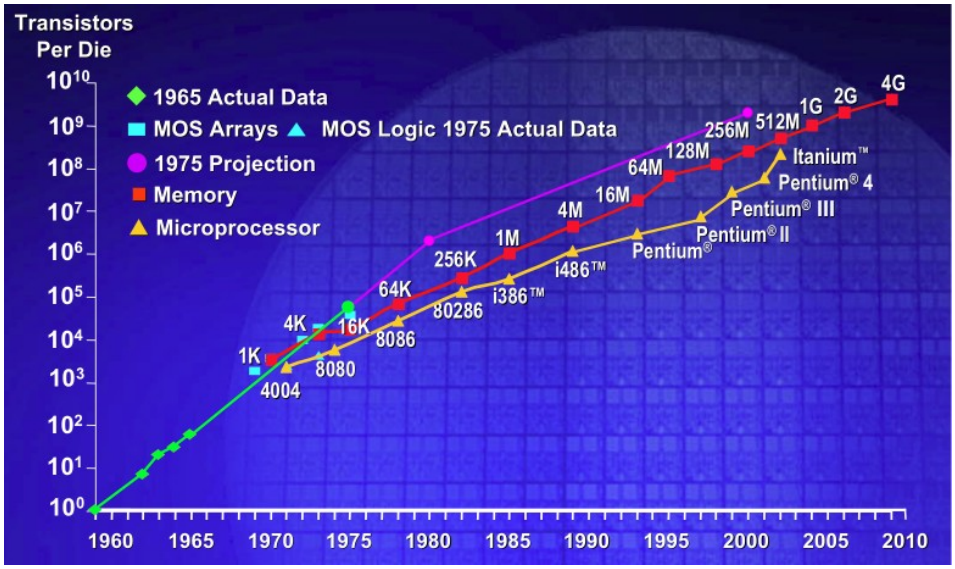

Fig. 1.1: Moore's law for memory chips and microprocessors. [1.1]

As the short-distance data exchange rate approaches 10 Gb/s, metal interconnection is facing a number of inevitable issues such as slow resistance-capacitance limit speed and large heat dissipation. Under these circumstances, it is well known that for data communication beyond 10 Gb/s, optical signal delivery is more advantageous compared to today's copper interconnections. As a result, combining sophisticated process technique, low cost and mass production, Si based Opto-Elelctronics Integrated Circuits (OEIC) emerges as one of the most promising solutions for next generation interconnection technique (Fig. 1.2).

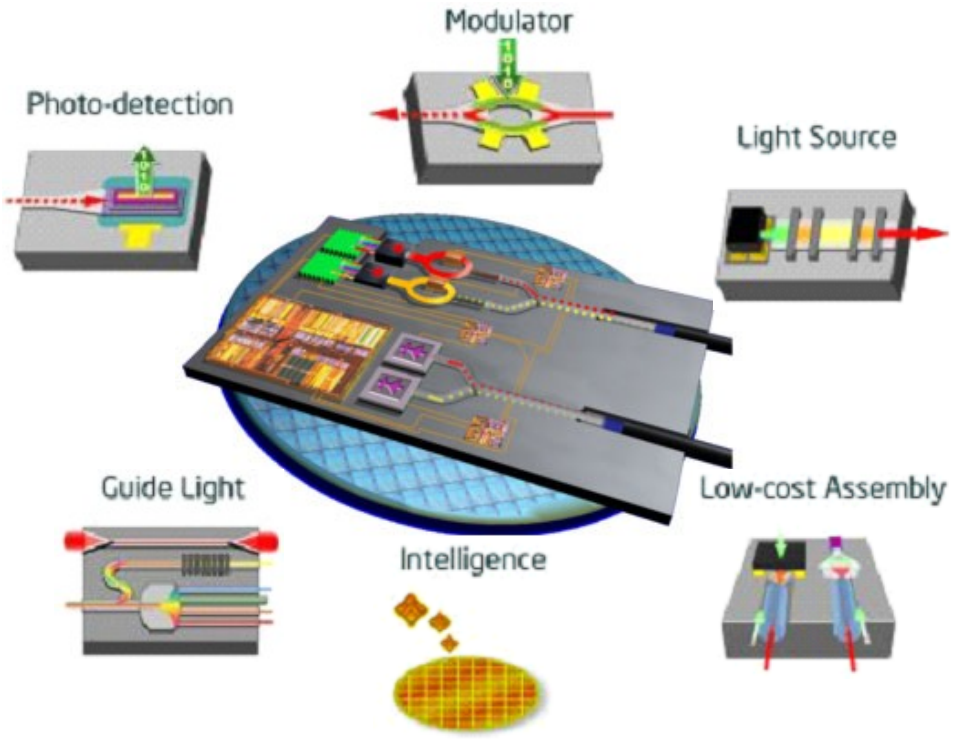

Fig. 1.2: OEIC building blocks: light source, modulator, photodetector and passive components like waveguide [1.1].

As a signal-delivery system, OEIC comprises several different types of photonics devices:

1) Light sources: to generate optical signal;

2) Modulators: to convert electrical 0 s and 1 s into optical 0 s and 1 s;

3) Optical waveguides: to deliver optical signals across the chip;

4) Photodetectors: to convert optical signal back to electrical signal.

To date, enormous efforts have been invested into Si photonics techniques and critical breakthroughs and millstones have been achieved. Various passive components [1.2], active devises like lasers[1.3], and high speed modulators [1.4] have been reported. Being the device that ends the optical path, photodetectors, which convert light back into electrical signals, are vital component for Si photonic integrated circuits. In fact, the trigger of the past decade's Si photonics upsurge was the first successful demonstration of the high-efficiency Germanium photodetector [1.5].

In principle, photodetector is an Opto-Electronic device which absorbs optical energy and converts it into electrical power. In its most common form, semiconductor-based photodetectors are widely used in optical communication systems. In semiconductor-based photodetectors, incoming photons with energy higher than semiconductor bandgap are aborbed and electron-hole pairs (EHP) are

generated. These EHPs are then separated by the electric field and contribute to external current or voltage.

The the performance of the photodetectors can be quantified by several indices, including, dark current, sensitivity/responsivity at certain wavelength, and response speed/bandwidth. To meet the photodetector performance criteria, material selection also needs serious consideration.

1.2 Material Choices for Photodetectors in Si OEIC

The long-haul communications have been based on fiber optics technique for the last 30 years. The wavelength used for the majority of long-distance data transition is in the 1.3-1.55 μm range corresponding to the minimum loss window of silica optical fiber. If the same wavelength can be utilized in the future short-distance data transfer including intra-chip, chip-to-chip and Fiber-To-The-Home (FTTH) communications, all end users will be able to connect directly to the external servers without the need for wavelength conversion, making global communication much easier and cheaper. As a result, Si OEIC working in 1.3-1.55 μm wavelength has become aggressively pursued by researchers worldwide.

Although photodetectors based on silicon have been widely used in optical receiver in the wavelength range around 850 nm, its relatively large bandgap of 1.12 eV corresponding to an absorption cutoff wavelength of ~1.1 μm hinders Si

photodetectors' application in the longer wavelength range of 1.3 and 1.55 μm. For a more seamless integration with current long-haul communication technology, a material with strong absorption coefficient in the 1.30-1.55 μm is very desirable.

Among the available choices, III-V compound semiconductors possess the advantage of high absorption efficiency, high carrier drift velocity and mature design and fabrication technology for optical devices. Therefore, integration of high performance III-V photodetectors onto the Si platform by flip-chip bonding or direct heteroepitaxy has been widely reported. However, the introduction of III-V material into Si process is at the expense of high cost, increased complexities and potential introduction of doping contaminants into the Si CMOS devices since III-V materials also act as dopants for group IV materials.

Germanium, a group IV material the same as Si, avoids the cross contamination issue. Though Ge is also an indirect bandgap (Eg = 0.66 eV) material like Si, its direct bandgap of 0.8 eV is only 140 meV above the dominant indirect bandgap. As a result, Ge offers much higher optical absorption in 1.3-1.55 μm wavelength range, thus making Ge-based photodetectors promising candidate for Si photonics integration. Although the 4% lattice mismatch between Ge and Si places challenging obstacle towards monolithic integration of high-quality low dislocation density Ge devices through Ge on Si heteroepitaxy; nevertheless, to date, device-

grade single-crystalline Ge films have been demonstrated by many groups with practically high performance Ge photodetectors.

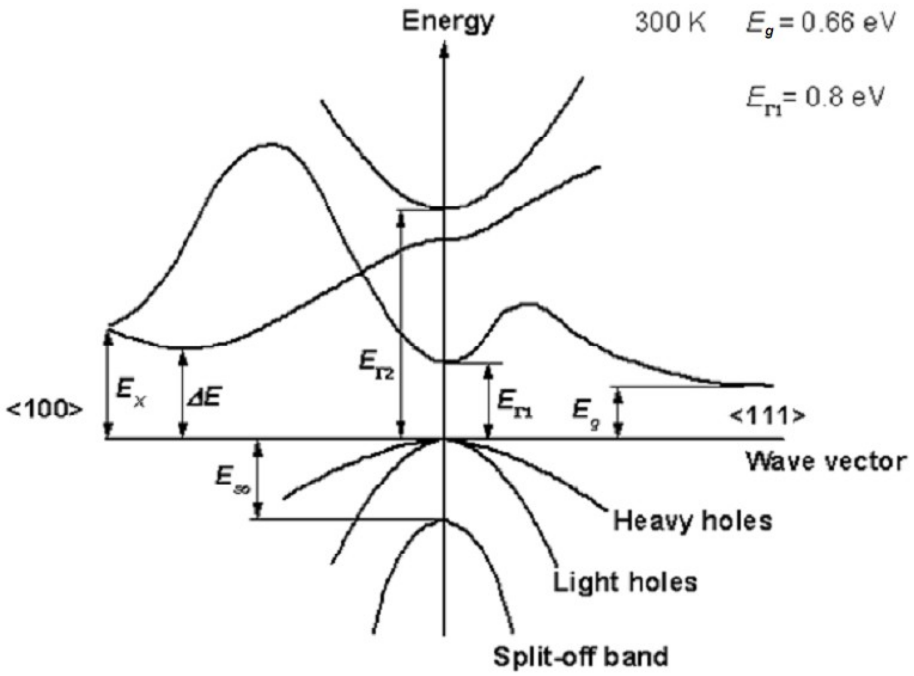

Fig. 1.3: Band diagram of Germanium at 300 K. [1.6]

1.3 Photodetector Electrical Structures

Several types of semiconductor-based photodetectors exist, i.e., PIN photodetector, Metal-Semiconductor-Metal (MSM) photodetector and avalanche photodetectors.

1.3.1 PIN Detectors

PN junctions are one of the most commonly used configurations for semiconductor photodetectors. The PIN diode with “I” stands for intrinsic, includes an intrinsic region in between P and N regions. Due to the built-in potential or

external reverse bias, the intrinsic region is depleted and has high resistivity so that voltage drop takes place mainly in this region, giving rise to high electric field for effective collection of photo-generated electron-hole pairs (EHP).

In this configuration, the thickness of the intrinsic region is always many times larger than the highly-doped regions so that most of the EHP's are generated within the intrinsic region where strong electric field helps to sweep the EHP to the adjacent p+/n+ region faster than diffusion. Another advantage of the PIN structure is that the depletion-region thickness (the intrinsic layer) can be tailored to optimize both the quantum efficiency and response bandwidth.

In Ge PIN photodetectors, while the photoabsorption intrinsic layer is usually Ge for effective absorption around 1.55 μm , the p+ and n+ region can be formed either by implantation [1.7] or in-situ dope to form p+ and n+ regions for PIN structure [1.8]. Another way is to use p+/n+ single crystalline Si substrate or deposited polycrystalline Si heterojunction [1.9].

1.3.2 Metal-Semiconductor-Metal (MSM) detectors

PIN photodiodes produce a voltage drop across the diode terminals in response to an external optical input. Such device is categorized as photovoltaic devices. On the other hand, MSM photodetectors are photoconductive devices whose conductivity alters when an optical illumination is imposed. Therefore, MSM photodetectors are only functional under non-zero external bias. MSM photodetectors possess the advantage of low capacitance and relative ease of fabrication. The

intrinsically low capacitance resulting from its configuration has always been utilized to fabricate high-speed large area detectors.

One issue in early Ge MSM photodetectors is its high dark current density which gives rise to high stand-by power consumption thus making Ge MSM photodetectors unfavorable and not practical. Due to the narrow bandgap and strong Fermi-level pinning of the metal/Ge interface at valence band, hole injection over Schottky Barrier Height (SBH) is the major component of dark current in Ge MSM detectors. Regarding this issue, application of dopant segregation (DS) to Ge MSM photodetectors for dark current suppression is experimentally demonstrated by H. Zang et al [1.10]. Metal-Ge Schottky barrier height modification by an intermediate layer of large bandgap material such as amorphous Ge and SiC is also proposed [1.11]. While the demonstrated Ge MSM detectors are able to achieve dark current suppression of two to four orders of magnitude, it is still an open question whether these MSM Ge photodetectors are competitive to PIN devices.

1.3.3 Avalanche PD

The simplest avalanche photodiode (APD) has a similar device structure to a PIN photodiode. However, a voltage close to its breakdown is usually applied to APD for detection of low power signal with high sensitivity. Under sufficiently higher external bias, electrical field in the photodiode's depletion region becomes high enough to initiate impact ionization which is responsible for carrier multiplication. Therefore, one absorbed incoming photon does not only generate one electron/hole

pair but rather a large number of EPHs leading to a quantum efficiency potentially large than unity.

The most important performance indice for APD is excess noise factor quantified by effective ratio of electron and hole ionization rate (k_{eff}), gain-efficiency product and sensitivity.

1.4 Criteria for photodetectors' dark current

An important issue in the integrated photodetectors is dark current, which increases the power consumption of the receiver. Most importantly, shot noise associated with this leakage current undesirably degrades the Signal-to-Noise Ratio (SNR) leading to increased bit error rate (BER).

Generally, dark currents less than 1 μA are referred to as acceptable value for a high-speed receiver design, below which the transimpedance amplifier (TIA) noise is the main noise source [1.12-1.14].In practice, a precise value of the required dark current depends upon the speed of operation and the amplifier design. In the recent successful demonstration of Ge-on-Si photodetector-based receiver, photodetectors with dark current of both ~10 nA [1.13] and ~2 μA [1.15] are reported.

Depending on the receiver design, higher dark current level is tolerable with certain sacrifice in the receiver parameters. For example, L. Vivien et al [1.16] showed that with an increase of the input power of about 20% in comparison with

photodetector without dark current, a photodetector with 300 μA dark current is still able to ensure a BER of 10^{-18} at frequency close to 50 GHz. The conclusion was drawn based on SPICE simulation taking into account of feedback resistance noise, the shot noise from detector dark current and photocurrent sources, and the transistor channel noise [1.17].

1.5 Objectives and Scope

The main aim of this thesis was to demonstrate fabrication and characterization of high performance Ge infrared photodetectors integrated on Si platform. The specific objectives of this research were to:

(1) grow device-quality thick Ge layer on Si substrate. The criterion for high-quality Ge includes: low intrinsic doping level, low threading dislocation, and highly-ordered crystal structure.

(2) integrate tensile-strained Ge PIN photodetector into CMOS platform. With the tensile strain applied to Ge, the material's light absorption range can be extended to ~1600 nm, which makes Ge a promising next-generation photodetector candidate covering the whole range of modern communication wavelength.

(3) integrate evanescent-coupled Ge-PIN photodetectors with Si-waveguide and study the influence of different dimensional parameters on the final

performance index of the photodetector (dark current, responsivity and response speed). On the basis of simulation and experimental data, optimization of the device structure can be achieved.

(4) explore new structures of Ge photodetectors capable of infra-red laser signal detection. Although photodiode is the majority device structure for high speed photodetectors, it suffers from intrinsically low detection sensitivity. New types of photodetectors possessing both attributes of high speed and high sensitivity are needed for future performance requirement.

The result of the present study may have impact on theoretical and experimental studies of the domain of Si OEIC. The fabricated photodetectors, being an important building block of Si OEIC, can be readily integrated into Si OEIC to serve a more complete function as optical signal processor, which is the foundation of next-generation central-processing-unit (CPU).

1.6 Thesis Organization

The organization of the thesis is divided in the following chapters.

In **Chapter 2**, the recent progresses in the development and integration of Ge-photodetectors on Si-based photonics is reviewed, along with remaining technological issues to be overcome and research trend.

Chapter 3 discussess the impact of selective-epitaxial-germanium, specifically its local strain effects, on high-performance PIN photodetector for near-infrared

applications. Combining a thin compliant Si epitaxial layer (~6 nm) with SiGe buffer (10-15 nm), a high quality Ge-film (~150 nm) prepared by two-step growth is demonstrated. Without using high-temperature cyclic anneal, Ge films with smooth surface (rms ~0.67 nm) and low dislocation density (4×10^6 cm^{-2}), have been achieved. Lateral PIN Ge photodetector has been demonstrated with enhanced photoresponse of ~190 mA/W at 1520 nm and 3dB bandwidth of 5.2 GHz at 1 V.

Chapter 4 Si-waveguide-integrated lateral Ge-PIN photodetectors using Si/SiGe buffer and two-step Ge-process are demonstrated. Comparative analysis between lateral Ge PIN and vertical p-Si/i-Ge/n-Ge PIN are made. Light is evanescently coupled from Si waveguide to overlaying Ge-detector, achieving high responsivity of 1.16 A/W at 1550 nm with f_{3dB} bandwidth of 3.4 GHz for lateral Ge PIN detector at 5V reverse bias. In contrast, vertical p-Si/i-Ge/n-Ge PIN has lower responsivity of 0.29 A/W but higher bandwidth of 5.5 GHz at -5 V bias.

Chapter 5 presents the device performance of scaled thin-film-Ge lateral PIN photodetectors integrated on Si-waveguide. The photodetectors are with closely spaced p+/n+ regions (0.8 μm) on Ge region with short length (5-20 μm) and narrow width (2.4 μm). Though with thin Ge-layer (~220 nm including bottom SiGe buffer), light is evanescent-coupled from Si waveguide effectively to the overlying Ge detector. The device exhibits f_{3dB} bandwidth of 18 GHz with external responsivity of 0.13 A/W for 1550 nm at -1 V. Considering the coupling loss and waveguide loss, the

internal responsivity is as high as 0.65 A/W. It is shown that with increasing detector length, devices' internal quantum efficiency can be improved to ~90% and by suppressing parasitic effects, speed can be boosted further towards several tens of GHz.

Chapter 6 demonstrates a scalable (with gate length of 1 μm) Ge-photodetector based on junction field-effect-transistor (JFET) structure with high sensitivity and improved response time. To overcome the low detection efficiency issue of typical JFET photodetectors, a high quality Ge epi-layer as the gate of JFET was achieved using a novel epi-growth technique. An I_{on}/I_{off} ratio up to 185 was achieved at wavelength of 1550 nm for the first time. In addition, the device shows a temporal response time of 110 ps with rise time of 10 ps, indicating that the scalable Ge JFET photodetector is promising candidate to replace large size photodiode in future opto-electronics integrated circuit and as image sensor integrated with CMOS circuit for its comparable size in respect to the modern MOSFETs.

Chapter 7 reports results on high-speed silicon-waveguided germanium junction-field-effect-transistor (JFET) -based photodetector. While the Ge layer's footprint on wafer is as small as 2 μm×2 μm, low stand-by current (0.5 μA@1V), high responsivity (642 mA/W) and high speed (8 GHz) are achieved. The reported Ge JFET is a promising candidate for the further scale-downed photodetector in the next-generation Si photonics.

Chapter 8 summarizes the major results and findings. It also offers some suggestions on future research based on the results of this thesis.

REFERENCES

[1.1] Intel Corporation, http://www.intel.com

[1.2] J. Michel, J. Liu, D. Ahn, D. Sparacin, R. Sun, C. Hong, W. Giziewicz, M. Beals, L. Kimerling and A. Kopa, "Advances in fully CMOS integrated photonic devices", in SPIE, pp. 64770P, 2007.

[1.3] J. Liu, X. Sun, R. Camacho-Aguilera, L. Kimerling and J. Michel, "Ge-on-Si laser operating at room temperature", Optics Letters, vol.35, no.5, pp. 679-681, 2010.

[1.4] J. Liu, M. Beals, A. Pomerene, S. Bernardis, R. Sun, J. Cheng, L. Kimerling and J. Michel, "Waveguide-integrated, ultralow-energy GeSi electro-absorption modulators", Nature Photonics, vol. 2, pp.433-437, 2008.

[1.5] L. Colace, G. Masini, G. Assanto, H. Luan, K. Wada and L. Kimerling, "Efficient high-speed near-infrared Ge photodetectors integrated on Si substrates", Applied Physics Letters, vol.76, pp. 1231, 2000.

[1.6] O. Madelung, M. Schulz and H. Weiss, *Intrinsic properties of group IV Elements and III-V, II-V, and I-VII Compounds*, Berlin: Springer, 1982.

[1.7] J. Wang, W. Y. Loh, H. Zang, M. B. Yu, K. T. Chua, T. H. Loh, J. D. Ye, R. Yang, X. L. Wang, S. J. Lee, B. J. Cho, G. Q. Lo and D. L. Kwong, "Integration of tensile-strained Ge p-i-n photodetector on advanced CMOS platform", in Group IV Photonics, 2007 4th IEEE International Conference on, pp. 1-3, 2007.

[1.8] M. Jutzi, M. Berroth, G. Wohl, M. Oehme and E. Kasper, "Ge-on-Si vertical incidence photodiodes with 39-GHz bandwidth", IEEE Photonics Technology Letters, vol.17, no.7, pp. 1510-1512 2005.

[1.9] J. Liu, J. Michel, W. Giziewicz, D. Pan, K. Wada, D. Cannon, S. Jongthammanurak, D. Danielson, L. Kimerling and J. Chen, "High-performance, tensile-strained Ge PIN photodetectors on a Si platform", Applied Physics Letters, vol.87, pp. 103501, 2005.

[1.10] H. Zang, S. Lee, W. Loh, J. Wang, M. Yu, G. Lo, D. Kwong and B. Cho, "Application of dopant segregation to metal-germanium-metal photodetectors and its dark current suppression mechanism", Applied Physics Letters, vol.92, pp. 051110, 2008.

[1.11] K. Ang, S. Zhu, J. Wang, K. Chua, M. Yu, G. Lo and D. Kwong, "Novel silicon–carbon (Si: C) schottky barrier enhancement layer for dark-current suppression in Ge-on-SOI msm photodetectors", IEEE Electron Device Lett, vol.29, no.7, pp. 704–707, 2008.

[1.12] D. Ahn, C. Hong, J. Liu, W. Giziewicz, M. Beals, L. Kimerling, J. Michel, J. Chen and F. Kartner, "High performance, waveguide integrated Ge photodetectors", Opt. Express, vol.15, pp. 3916-3921, 2007.

[1.13] S. Koester, C. Schow, L. Schares, G. Dehlinger, J. Schaub, F. Doany and R.

John, "Ge-on-SOI-detector/Si-CMOS-amplifier receivers for high-performance optical-communication applications", J. Lightwave Technol, vol.25, pp. 46-57, 2007.

[1.14] S. Koester, J. Schaub, G. Dehlinger and J. Chu, "Germanium-on-SOI infrared detectors for integrated photonic applications", Selected Topics in Quantum Electronics, IEEE Journal of, vol.12, no.6, pp. 1489-1502, 2007.

[1.15] G. Masini, G. Capellini, J. Witzens and C. Gunn, "A 1550 nm, 10 Gbps monolithic optical receiver in 130nm CMOS with integrated Ge waveguide photodetector", in Group IV Photonics, 4th IEEE International Conference on, pp. 1-3, 2007.

[1.16] L. Vivien, M. Rouvière, J. Fédéli, D. Marris-Morini, J. Damlencourt, J. Mangeney, P. Crozat, L. El Melhaoui, E. Cassan and X. Le Roux, "High speed and high responsivity germanium photodetector integrated in a silicon-on-insulator microwaveguide", Optics Express, vol.15, no.15, pp. 9843-9848, 2007.

[1.17] E. Cassan, D. Marris, M. Rouviere, S. Laval, L. Vivien and A. Koster, "Comparison between electrical and optical clock distribution for CMOS integrated circuits", in SPIE, pp. 89-100, 2004.

CHAPTER 2

2. Literature and Technology Review

As discussed in Chapter 1, Ge-on-Si photodetectors evolves rapidly in the last decade. New methodologies and schemes have been proposed to solve various technical issues and contribute to the development of Ge photodetectors.

In this chapter, various Ge growth techniques are first introduced in section 2.1. Different photodetector light coupling schemes are described in sections 2.2. In section 2.3, the historical research trends along with performances of Ge photodetectors reported by research groups are summarized. Finally, the remaining technical issues and future research directions will be discussed in section 2.4.

2.1 Ge Growth Techniques

Tracing back in history, the first Ge on Si detector was reported in 1984 by S. Luryi et al [2.1] . The demonstrated detector showed 41% quantum efficiency at wavelength of 1.45 μm, where an MBE-grown 1800 Å n+ Ge_xSi_{1-x} alloy (graded in ten steps from x=0 to x=1) act as buffer layer for the heteroepitaxy of Ge on Si.

Since then, various techniques have been pursued for the growth of Ge film on Si surface with their own pros and cons. The main quality criterion of the Ge layer can be categorized as: procedure complexity, material cost, growth temperature, and the resulting Ge layer's dislocation density and strain.

2.1.1 Poly Ge films

For ease of integration of near-infrared detectors with standard Silicon process line for signal acquisition, amplification and processing, low temperature growth of Ge layers is much desired. In 2000, Ge deposition approach based on the thermal evaporation with process temperature as low as ~300 °C was first proposed in the pioneer work conducted by G. Masini et al [2.2] . It was found that polycrystalline Ge deposition could be possible at substrate temperature as low as 300 °C, confirmed by the Raman spectra results. This method allows simple and low cost integration with Si process. Monolithic integration of an array of 8 polycrystalline Ge pixels with CMOS readout electronics was demonstrated based on this method [2.3] shortly after which, L. Colace et al [2.4] reported the realization of a digital camera further confirming the process compatibility of the low-temperature approach.

Moreover, although the low temperature deposition introduces relatively high density of defects and dislocations into the poly-Ge layer and worsens the electrical properties compared to crystalline Ge films, it was shown recently that by a careful design, acceptable performance of the polycrystalline Ge photodetector for Si

photonics integration can be obtained, with responsivities between 0.1 A/W and 0.3 A/W [2.5] .

2.1.2 Crystalline Ge growth with graded SiGe buffer layers

In the early stage of crystalline Ge film epitaxy on Si wafers, a compositionally graded SiGe region was commonly adopted as buffer layer. This approach was first adopted in the SiGe/Si system by S. Luryi et al [2.1] and later improved by E. A. Fitzgerald et al. in 1990 [2.6] . Multiple buffer layers with increasing Ge content was adopted to relax high strain between Ge and Si, which minimizes dislocation nucleation and reduces the threading dislocations. The final strain-relaxed $Si_{1-x}Ge_x$ layers grown on these graded layers showed low density of threading-dislocations, 4×10^5 cm^{-2} for x = 0.23 and 3×10^6 cm^{-2} for x = 0.50.

However, the graded SiGe buffer method usually requires a thick 10 μm buffer for pure Ge epitaxy on Si, while in modern Si photonics technology, Ge photodetectors are favorably fabricated in close adjacency with Si optical waveguide facilitating evanescent or butt-coupling of the optical power. As a result, new technique with thin buffer layers is still needed.

2.1.3 Two step LT/HT Ge growth

The origin of the two-step LT/HT (low temperature/high temperature) growth technique can be traced back to 1986 for GaAs growth on Si by Fan et al. [2.7] . Its application in the epitaxially grown Ge on Si was first proposed and utilized by

Colace et al. [2.8] in a ultra high vacuum chemical vapor deposition (UHVCVD) growth reactor in 1998, since when it has attracted wide interest for Ge epitaxial growth.

In the procedure of the two-step Ge growth, first, after thorough cleaning, the substrate is maintained at low- temperature (~300-400 °C), a thin layer of Ge buffer layer (~ 50-100 nm) is grown to prevent strain release through undesirable island growth. Second, the substrate temperature is elevated to ~550-700 °C and a thick Ge layer with reduced threading dislocation density is grown on top of the low-temperature thin Ge buffer. It should be noted that the two-step Ge method can be adopted not only in UHVCVD systems, but also in growth tools such as reduced-pressure CVD (RPCVD) [2.9] and molecule beam epitaxy (MBE) [2.10] .

The Ge layers growth by two-step Ge epitaxy typically suffers from a high threading dislocation density (TDD) in the order of 10^8-10^9 cm^{-2}. Therefore, high temperature anneal is employed to reduce the TDD to an acceptable level by many groups. For example, the research of Luan et al [2.11, 2.12] indicate that the TDD in two-step Ge layer can be significantly reduced by cyclic thermal annealing. The optimized annealing condition (900 °C/10 min, 780 °C/10 min, cycle number: 10) can reduce the threading dislocation density to ~2×10^7 cm^{-2}. Ge photodetectors based on this process were successfully demonstrated with improved performance [2.11, 2.13] . However, the annealing process increases the thermal budget undesirable for

photodetectors' integration with Si MOSFET. Therefore, a number of experiments have been reported to demonstrate high Ge detector performance. These experiments are based on low-temperature anneal or even no additional thermal anneal [2.14, 2.15] . In table 2.1, some of the currently active groups' Ge growth methods are summarized.

Table 2.1: Summary of recent Ge epitaxy method from selected groups.

	Group	Year	Ref.	Tool	Low Temp. buffer	High Temp. Ge	Anneal	Aneal condition	RMS (nm)	TDD (cm^{-2})
two-step LT/HT growth	IEF	2004	[2.9]	RPCVD	400 °C 25 nm Ge	<750 °C 730 nm	yes	750/875 °C, 10 cycles	2.2	$<2 \times 10^8$
	IEF	2009	[2.16]	RPCVD	400 °C 40 nm Ge	730 °C 300 nm	yes	not specified	-	-
	Intel	2006	[2.17]	RPCVD	400 °C 100 nm Ge	670 °C 1.2 µm	yes	900 °C, 15 min	-	$\sim 1 \times 10^7$
	IBM	2004	[2.18]	UHVCVD	350 °C 50 nm Ge	600 °C 400 nm	yes	780/900 °C, 10 cycles	-	$\sim 1 \times 10^8$
	Univ. stuttgart	2005	[2.10]	MBE	thin LT buffer	550° C 1 µm	no	-	-	-
	MIT	1999	[2.12]	UHVCVD	350 °C 30 nm Ge	600 °C 1 µm	yes	780/900 °C, 10 cycles	-	$\sim 2 \times 10^7$
	MIT	2007	[2.19]	UHVCVD	360 °C 60 nm Ge	730 °C 1.1 µm	yes	650/850 °C, cyclic	-	-
	Luxtera	2007	[2.20]	RPCVD	no buffer	350 °C 200 nm	no	-	-	-
	Kotura	2010	[2.15]	CVD	400 °C 100 nm Ge	670 °C 1.1 µm	yes	not specified	-	-
	ETRI	2009	[2.21]	RPCVD	400 °C 100 nm Ge	650 °C 1.2/1.7 µm	no	-	1.3	-
	Univ. Roma Tre	2006	[2.14]	UHVCVD	350 °C thin Ge	600 °C 1 µm	no	-	-	-
SiGe buffer	Unvi. Texas	2004	[2.22]	UHVCVD	1 µm SiGe	400 °C 2.5 µm	yes	750 °C, 15 min	-	-
	Canon ANELVA	2006	[2.23]	UHVCVD	450–520 °C 13 nm SiGe 370 °C 30 nm Ge	550–600 °C 1 µm	yes	800 °C, 15 min	0.44	-
	IME	2007	[2.24]	UHVCVD	350–400 °C 30 nm SiGe 350–400 °C 30 nm Ge	550–600 °C 100 nm	no	-	1.4	$\sim 1 \times 10^7$
H_2 anneal	Stanford	2008	[2.25]	RPCVD	350 °C 200 nm Ge	600 °C 400 nm	yes	800 °C, 30 min, in H_2	~1	$0.8–1 \times 10^7$
LEPECVD	Como	2009	[2.26]	LEPECVD	no buffer	500–600 °C 1 µm	yes	600/780 °C, 3 cycles	-	2×10^7

2.1.4 Other Ge Growth Methods

Many attempts have been reported to modify the two-step Ge growth procedure. An UHV-CVD growth of high quality Ge on Si substrate using modified two-step Ge growth method combining with intermediate thin SiGe buffer layers was proposed first by Z. Huang et al in 2004 [2.22] .The buffer region consisted of 0.6-μm-thick $Si_{0.45}Ge_{0.55}$ and 0.4-μm-thick $Si_{0.35}Ge_{0.65}$ layers. In-situ anneal for 15 min at 750 °C was carried out to further reduce the dislocation density.The thickness of the SiGe buffer is further reduced by Nakatsuru et al [2.23] by employing 13-nm-thick $Si_{0.5}Ge_{0.5}$ buffer layer grown at 450-520 °C. After post-deposition anneal of 800 °C/15 min, the Ge layer shows a low roughness of 0.44 nm. T. Loh et al [2.24] also reported epi-Ge layer based on the SiGe buffer method, where the SiGe buffer is grown at low temperature of 350-400 °C with the thickness of around 30 nm (Fig. 2.1 a & b).

Another way to improve Ge film quality is H_2 annealing which is reported by Choi et al [2.25] . They demonstrated 800 °C/30 min anneal in H_2 ambient which is able to effectively improve the Ge film quality in terms of surface roughness and TDD. It is proposed that the increased atom mobility caused by Hydrogen/Ge bond is the main mechanism for the improved film surface planarity and defect density.

Another new Ge epitaxy procedure is demonstrated based on low-energy plasma-enhanced chemical vapor deposition (LEPECVD) [2.26] . Thanks to the high deposition rates and high concentration of atomic H present in the chamber, Ge film with smooth surface and TDD $\sim 2\times10^7$ are achieved under low thermal budget.

Moreover, the fabricated diode shows much lower dark current compared to the devices from UHVCVD method with comparable dislocation density. This is attributed to the improved passivation arising from the dense plasma in LEPECVD which is known to be efficient in generating atomic hydrogen radicals.

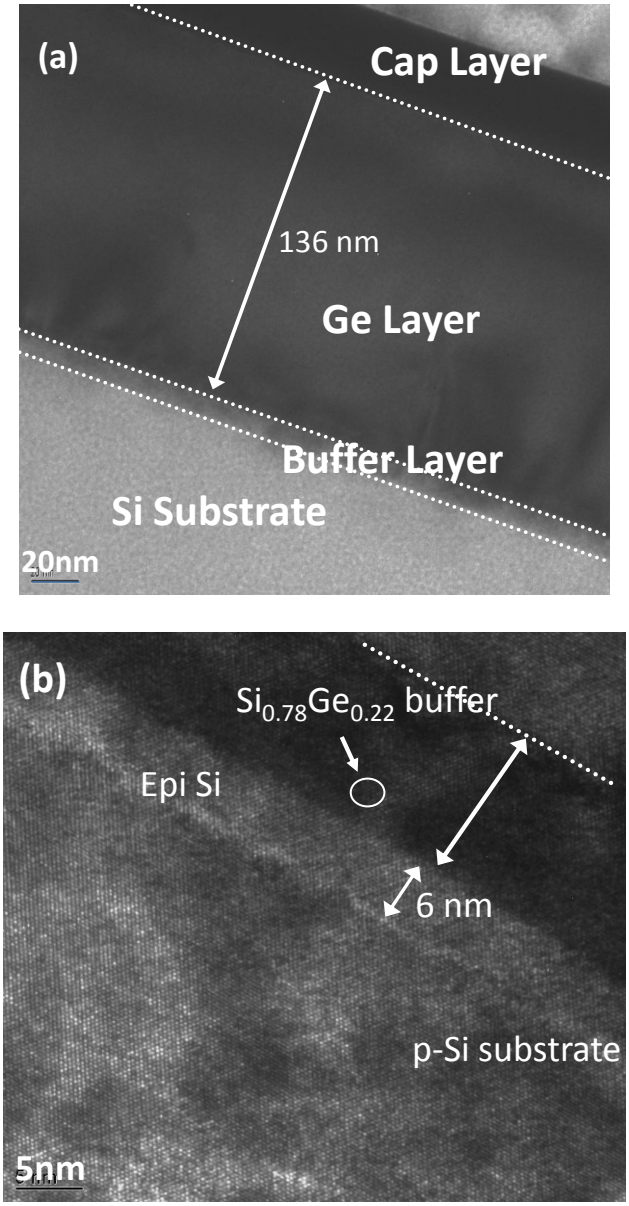

Fig. 2.1: (a) HR-TEM image of epitaxial Ge layer using two-step Ge growth method combining with an intermediate SiGe buffer layer. (b) Zoom-in image of the heterostructure epitaxial layers of Si/$Si_{0.75}Ge_{0.25}$/Ge.

2.2 Ge Photodetector light coupling schemes

2.2.1 Normal incidence photodetectors and the bandwidth-efficiency tradeoff

Normal incidence (NI) photodetectors are also known as vertical photodetectors or surface illuminated photodetectors. Normal incidence is the simplest light coupling scheme with incoming light illuminated on the top or bottom surface of the detector (Fig. 2.2). Almost all the electrical structures, i.e., PIN, MSM and avalanche, can be fabricated in the fashion of NI photodetectors. Due to its low process complexity, NI photodetectors are widely used in communication technologies. However, NI photodetectors suffer from an inherent drawback due to the bandwidth-efficiency tradeoff. This tradeoff results from the opposite requirement of the thickness of the photoabsorption layer for high bandwidth and high efficiency [2.29] .

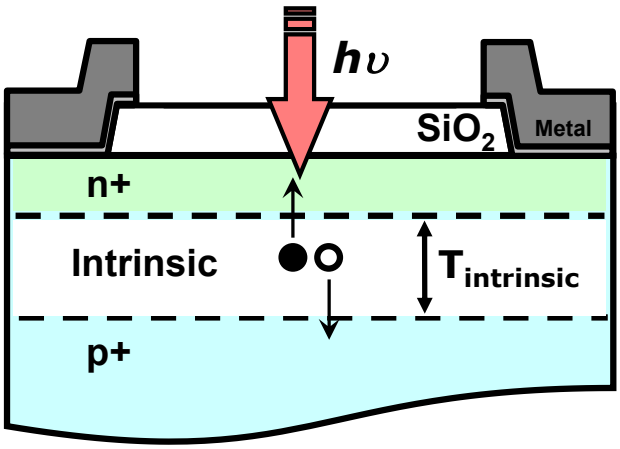

Fig. 2.2: Schematic of a normal incidence photodetector.

The carrier-transit-time-limiting bandwidth can be expressed as [2.30] :

$$f_t \cong 0.45 \times \frac{\upsilon}{d} \qquad \text{(Eq 2.1)}$$

While the ideal efficiency η assuming zero reflection and full carrier collection is:

$$\eta \cong 1 - e^{-\alpha \times d} \qquad \text{(Eq 2.2)}$$

Where υ is carrier transit velocity, d is intrinsic region's thickness and α is material's absorption coefficient. Using $\upsilon = 6\times10^6$ cm/s for Ge and $\alpha = 4000$ cm^{-1}, the carrier-transit-time-limiting bandwidth and efficiencies versus intrinsic region thickness can be plotted as Fig. 2.3. As can be seen, for Ge device with 3dB bandwidth of 100 GHz, an intrinsic layer thinner than 0.27 μm is required with resulting efficiency of ~10%.

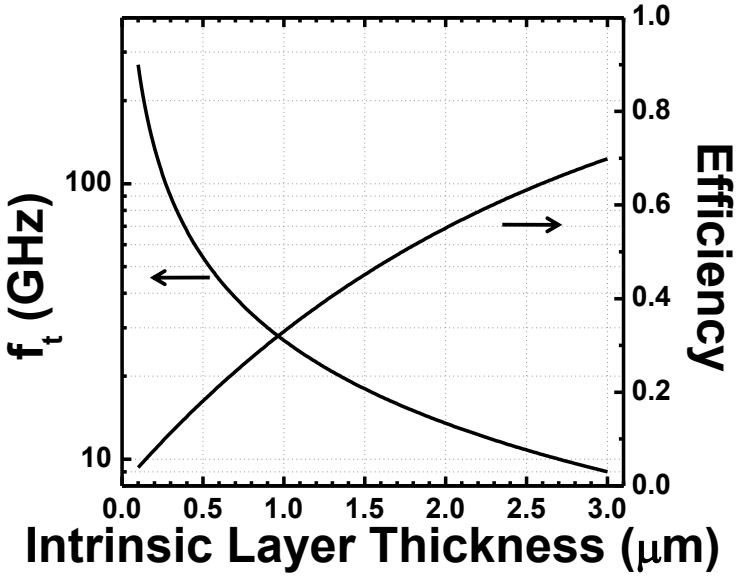

Fig. 2.3: A Calculated carrier-transit-time-limiting bandwidth and efficiencies of normal incidence PIN Ge photodetector.

2.2.2 Resonant Cavity Enhanced (RCE) detectors

To overcome the tradeoff between bandwidth and efficiency in NI detectors, one method is to sandwich a thin layer of photo absorbing material between two light reflectors therefore cavity resonance is enhanced [2.31, 2.32] . Ideally in this structure, light is trapped between the two reflectors and travels through the center light absorber multiple times until fully absorbed. At the same time, the photoabsorption layer can be thin enough to achieve high bandwidth. Another advantage of RCE detectors is the wavelength selectivity. When the light reflector is fabricated in the form of Bragg reflector, only light in small range of certain wavelength is reflected effectively so as to produce high efficiency. RCE device's light selectivity makes it especially useful for wavelength division multiplexing (WDM) systems.

Ge RCE Schottky photodetectors were demonstrated by Dosunmu et al. [2.31] in 2005. The resonant cavity was formed between the Au reflecting top metal contact and the SOI substrate. The backside of the SOI wafer was polished to facilitate light coupling. Schottky contact was formed between the top contact Au and the Ge layer whereas the bottom contact of Au and p+ Si was ohmic contact. The resonant wavelength was found at around 1538 nm leading to increased quantum efficiency of 59%.

Although RCE photodetectors solves the bandwidth-efficiency tradeoff to some extent, the fabrication of high reflectivity mirror increases the design and process complexity significantly. The multiple layers needed for effective reflection

also make RCE detectors difficult to be integrated with other functional devices. Therefore, other methods are still required with more process and integration friendliness.

2.2.3 Waveguide photodetectors

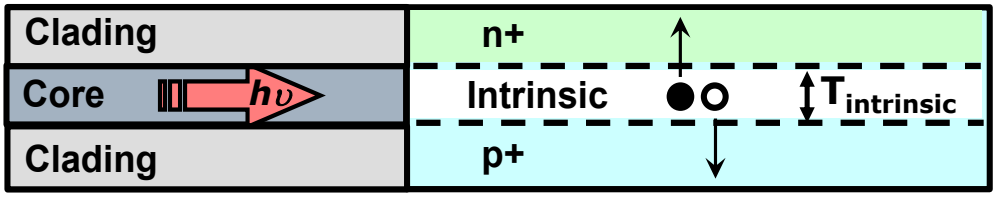

Fig. 2.4: Schematic of a waveguide-fed photodetector.

The waveguide integrated photodetectors (Fig. 2.4) have been considered to be one of the most promising candidates for overcoming the bandwidth-efficiency tradeoff in normal incidence detectors. In this configuration, a light signal is delivered to the device by in-plane optical waveguide rather than top down, permitting the bandwidth and efficiency to be determined almost independently because the efficiency is no longer specified by the photoabsorption layer thickness, but rather by the waveguide length.

Furthermore, large scale integration of Si optical and electrical devices requires all devices to be fabricated on the same planar wafer which makes optical waveguides indispensable. Thus integration of waveguides with photodetectors seems to be a natural choice.

Table 2.2: Summary of performances from selected Ge photodetectors.

Year	Ref	Structure	I_{dark}(μA) @-1V	Responsivity @λ=1.55μm @-1V (A/W)	Highest Electrical Bandwidth (GHz)	APD Gain-Bandwidth Product (GHz)
2000	[2.33]	NI PIN	12	0.25	~0.4@-4V	
2002	[2.13]	NI PIN	1.2	0.75	2.5@-1V	-
2005	[2.10]	NI PIN	0.08	0.035@0V	39@-2V	-
2005	[2.34]	NI PIN	~0.8	0.56	8.5@-1V	-
2005	[2.31]	NI PIN RCE	0.38@-5V	0.73	12.1@-3V	-
2006	[2.14]	NI PIN	~10	0.2	10@-1V	-
2007	[2.35]	WG MSM	130	1	25@-6V	-
2007	[2.19]	WG PIN	0.9	0.87	7.5@-3V	-
2007	[2.36]	WG PIN	0.267@-2V	1.16@-2V	29.4@-2V	-
2009	[2.38]	WG MSM	4@-5V	~1	40@-5V	-
2009	[2.39]	NI PIN	~0.10	0.05@-2V	49@-2V	-
2009	[2.21] ,	NI PIN	0.042	0.47	36@-3V	-
2009	[2.16]	WG PIN	~1	1	42@-4V	-
2009	[2.40] ,	WG PIN	0.072	0.8	47@-3V	-
2010	[2.15]	WG PIN	1.3	1.1	36.8@-3V	-
2010	[2.41]	WG MSM	90	0.14	40@-2V	-
2008	[2.42]	NI SACM APD	~10@25V	~15.6@~25V@ 1.3μm	~12@~25V	340
2010	[2.43]	WG SACM APD	~100@23V	16.8@~23V	5@~23V	105
2010	[2.44]	WG MSM APD	~100	-	~35@1.5V	350

The development of Ge-on-Si photodetectors has been going on for more than ten years. In Table 2.2 and Fig. 2.5, performances reported for some typical Ge photodetectors are summarized.

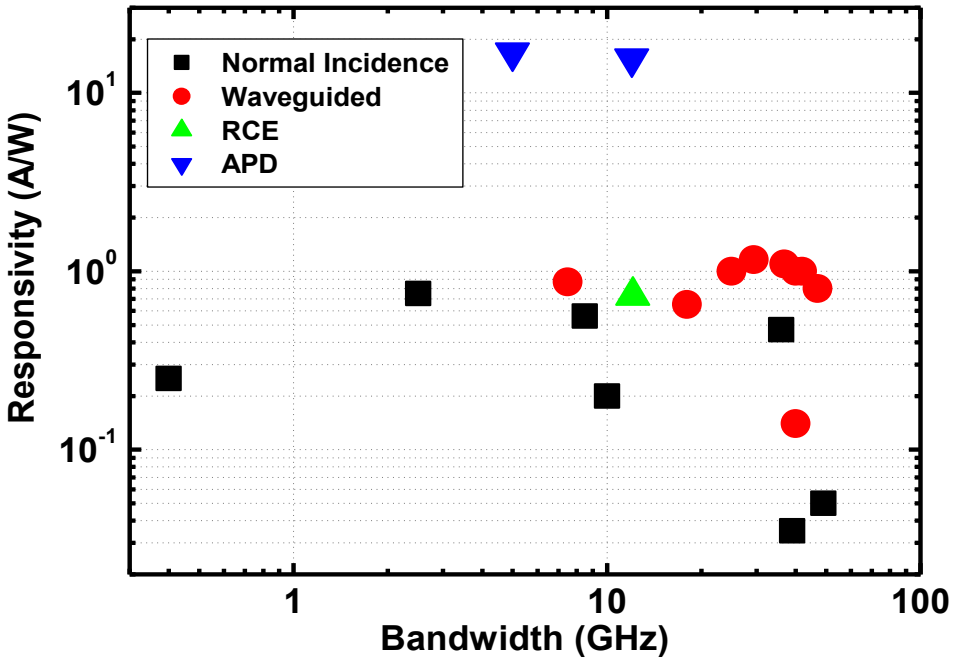

Fig. 2.5: Bandwidth and responsivity of selected Ge photodetectors.

2.3 Research trends in Ge photodetectors

In this section, research trends are identified and described.

2.3.1 zero-bias PIN photodiode

High dark current leads to high stand-by power consumption in addition to the degraded SNR. Moreover, it is desirable for the detector and the receiver circuit to operate on a single power supply which often restricts the bias voltage for

photodetector to be less than 1.5 V [2.45] . As a result, there has been an increasing research interest in the development of low-bias or even zero bias PIN photodiode.

In terms of responsivity, J. Liu et al [2.34] measured their Ge PIN detector's responsivity over the wide spectrum of 650 nm – 1650 nm. The reported responsivity at 0 V bias is more than 98% of the saturated value at 2 V reverse bias, which attributed to high carrier collection efficiency resulted from the high built-in electric field in the diode's depletion region.

High speed operation at zero-bias is demonstrated by M. Jutzi et al [2.10] . From PIN Ge detectors with diameter of 10 μm, a record high zero-bias 3dB bandwidth of 25.1 GHz is obtained.

2.3.2 Avalanche photodetectors

For Ge photodetector's application in Si photonics IC, next level pre-amplifier is necessary to further transform the current signal into voltage signal for later CMOS IC process. Avalanche photodetectors offer much lower signal-to-noise ratio compared to PIN or MSM structures. Therefore, more and more interest is being casted onto Ge-based avalanche photodetectors. To date, Intel [2.42] , IBM [2.44] and IME [2.43] have reported successful fabrication of such devices.

The first Ge-based APD was demonstrated by Y. Kang et al [2.42] . For the reported device, a separate-absorption-charge-multiplication (SACM) configuration is used to take advantage of both Si's low noise property and Ge's strong absorption near 1.55 μm wavelength. The device exhibits low excess noise with low k_{eff} of ~0.09.

The reported sensitivity of -28 dBm at 10 Gb/s is equivalent to commercial III-V APD. And the bandwidth-efficiency product of 340 GHz is even higher than its III-V counterpart, thanks to much lower k value of Si compare to InP material.

Another configuration for Ge APD is conventional MSM structure with nano-engineered metal-to-metal spacing as small as 200 nm reported by S. Assefa et al [2.44] . With low bias voltage of ~1.5 V, the electric field in the immediate vicinity of the metal contact is already high enough to initiate avalanche amplification. Although the whole APD structure is built on Ge, whose properties is not optimized for APD, the device exhibits excess noise factor with k_{eff} ~ 0.2, high speed of ~40 GHz, and bandwidth-efficiency product of 350 GHz at the wavelength of 1.3 μm. Although the high dark current due to the small metal spacing requires more optimization, the Ge MSM APD shows great potential for Ge's application in avalanche photodetection.

The APD devices reported above are working at 1.3 μm due to the incorporation of Si into Ge which gives rise to undesired reduction of the absorption efficiency at 1550 nm. Using two-step Ge growth with SiGe buffer layer method, the first waveguide-base Ge APD working at 1.55 μm is reported by K. Ang et al [2.43] . The device is fabricated based on SACM structure. Waveguide was used to increase device efficiency and facilitate future Si photonics integration. The reported high responsivity at unity gain was as high as ~0.8 A/W and bandwidth-efficiency product 105 GHz was achieved.

2.3.3 Normal incidence to waveguide integration

At the starting stage of Ge-on-Si photodetector development for Si photonics applications, normal incidence Ge photodetectors were first fabricated and comprehensively studied [2.10, 2.13, 2.14, 2.18, 2.33, 2.34, 2.39, 2.42, 2.46-2.54] due to its ease of process.

Due to the bandwidth-efficiency tradeoff, typical NI incidence Ge photodetectors offer moderate quantum efficiencies and bandwidths. Among the reported NI photodetectors, S. Klinger et al. [2.39] reported the highest bandwidth of 49 GHz for Ge-based photodetectors. The Ge PIN photodiode was fabricated in Ge grown by MBE two-step Ge growth. Given the nominal Ge intrinsic layer thickness of 300 nm, detector diameter of 10 μm and the series resistance of 25 Ω, the theoretical bandwidth of 54.3 GHz corresponds well with the experiment. It should be noted that the reported improved 3dB frequency of 49 GHz from previous result (39 GHz) [2.10] is mainly due to the reduced series resistance (Rs) of 15 Ω from 32 Ω. The reported responsivity at 1550 nm is ~0.05 A/W limited by small device footprint and relatively large density of defects in the Ge layer.

In terms of high responsivity, thick Ge absorption layer is need. The highest reported value at 1550 nm wavelength for NI photodetector is 0.75 A/W from a PIN diode with ~4 μm thick Ge layer fabricated and reported by S. Fama and coworkers [2.13] . The Ge layer was epitaxial grown on Si substrate by two-step UHVCVD

combined with high temperature cyclic anneal for the reduction of dislocation density. A time response of less than 200 ps and operation >2.5 Gb/s was also demonstrated.

The study of the Ge normal incidence photodetectors gives valuable insight into the Ge/Si system and its properties. As the Ge growth technique becomes mature and the particulars of Ge/Si device have been studied in details, researches are gradually redirected to the integration of Ge photodetectors on Si waveguides to decouple the tradeoff between bandwidth and efficiency mentioned before. Also since Si photonics require devices to be monolithically integrated on the same Si substrate using on-wafer optical waveguide, Ge photodetector's integration with waveguide seems mandatory.

To date, a number of groups demonstrate their results on waveguided Ge photodetectors, including MIT[2.19, 2.55-2.58] , IEF[2.16, 2.35] , IME[2.37, 2.43, 2.59-2.61] , INTEL [2.36, 2.62] , IBM [2.41, 2.44, 2.63] , Kotura [2.15, 2.64] . Both PIN and MSM structures are reported in these waveguide photodetector with comparable performance and high speed around 40 Gbit/s.

2.3.4 Improvement of speed performance of waveguide Ge photodetectors

Another trend of the Ge photodetectors continuous evolvement is the increasing of the detector bandwidth. At the starting point of Ge detector's integration with Si waveguide, Ge growth on SOI wafers, optical coupling between Ge detector and Si optical waveguide is first explored. The reported detectors are ~100 μm long to

make sure full absorption of light around 1.55 μm wavelength, inevitably leading to large device capacitance so that the bandwidth are <10 GHz limited by RC delay.

Nowadays, special care in design is given to detector's bandwidth performance. With the adoption of shorter device, sophisticated radio-frequency coplanar waveguide (CPW) metal interconnections and frequency measurement technologies, 40 Gbit/s operation was reported by several groups [2.36, 2.38, 2.41, 2.65] , with waveguide detector's bandwidth as high as 47 GHz [2.65] .

2.4 Summary

This chapter summarizes the Ge growth techniques as well as the development of Ge-on-Si photodetectors. Various electrical structures (PIN, MSM, and avalanche) and optical coupling schemes (normal incidence, resonant cavity enhancement and waveguide integration) have been adopted in the Ge photodetectors.

The Ge photodetectors have been widely reported with improving performance. Nevertheless, there are still areas to be explored, especially on the local strain effects of selective-epitaxial-germanium on high-performance PIN photodetectors for near-infrared applications. There are typically two types of device configurations adopted for waverguide Ge-on-Si photodetectors, namely, lateral and vertical PIN. To conduct a comparative study of these two configurations is also of great interest.

Moreover, the reported Ge photodetectors are mostly p-n/PIN diode based detectors. Due to its inherent limitations, current PN/PIN diode based Ge photodetectors suffer from serious scalability issues where further scaling-down of photodiodes inevitably leads to insufficient light absorption and decreases quantum efficiency. Thus, novel structures of photodetectors have to be proposed. In the following chapters, the above mentioned issues are addressed by employing new solutions.

REFERENCES

[2.1] S. Luryi, A. Kastalsky and J. Bean, "New infrared detector on a silicon chip", Electron Devices, IEEE Transactions on, vol.31, no.9, pp. 1135-1139 1984.

[2.2] G. Masini, L. Colace, F. Galluzzi and G. Assanto, "Advances in the field of poly-ge on si near infrared photodetectors", Materials Science and Engineering B, vol.69, pp. 257-260 2000.

[2.3] G. Masini, V. Cencelli, L. Colace, F. De Notaristefani and G. Assanto, "Monolithic integration of near-infrared ge photodetectors with si complementary metal–oxide–semiconductor readout electronics", Applied Physics Letters, vol.80, pp. 3268 2002.

[2.4] L. Colace, G. Masini, V. Cencelli, F. DeNotaristefani and G. Assanto, "A near-infrared digital camera in polycrystalline germanium integrated on silicon", IEEE Journal of Quantum Electronics, vol.43, no.4, pp. 311-315 2007.

[2.5] V. Sorianello, M. Balbi, L. Colace, G. Assanto, L. Socci, L. Bolla, G. Mutinati and M. Romagnoli, "Guided-wave photodetectors in germanium on soi optical chips", Physica E: Low-dimensional Systems and Nanostructures, vol.41, no.6, pp. 1090-1093 2009.

[2.6] E. Fitzgerald, Y. Xie, M. Green, D. Brasen, A. Kortan, J. Michel, Y. Mii and B. Weir, "Totally relaxed gesi layers with low threading dislocation densities grown on si substrates", Applied Physics Letters, vol.59, pp. 811 1991.

[2.7] J. Fan, B. Tsaur, R. Gale and F. Davis, "Reducing dislocations in semiconductors utilizing repeated thermal cycling during multistage epitaxial growth", US Patents, 1986.

[2.8] L. Colace, G. Masini, F. Galluzzi, G. Assanto, G. Capellini, L. Di Gaspare, E. Palange and F. Evangelisti, "Metal–semiconductor–metal near-infrared light detector based on epitaxial ge/si", Applied Physics Letters, vol.72, pp. 3175 1998.

[2.9] J. M. Hartmann, A. Abbadie, A. M. Papon, P. Holliger, G. Rolland, T. Billon, J. M. Fedeli, M. Rouviere, L. Vivien and S. Laval, "Reduced pressure--chemical vapor deposition of ge thick layers on si(001) for 1.3--1.55-mu m photodetection", Journal of Applied Physics, vol.95, no.10, pp. 5905-5913 2004.

[2.10] M. Jutzi, M. Berroth, G. Wohl, M. Oehme and E. Kasper, "Ge-on-si vertical incidence photodiodes with 39-GHz bandwidth", IEEE PHOTONICS TECHNOLOGY LETTERS, vol.17, no.7, pp. 1510-1512 2005.

[2.11] H. Luan, D. Lim, L. Colace, G. Masini, G. Assanto, K. Wada and L. Kimerling, "Germanium photodetectors for silicon microphotonics by direct epitaxy on silicon", pp. 279-284, Warrendale, Pa.; Materials Research Society; 1999, 2000.

[2.12] H. Luan, D. Lim, K. Lee, K. Chen, J. Sandland, K. Wada and L. Kimerling, "High-quality ge epilayers on si with low threading-dislocation densities", Applied Physics Letters, vol.75, pp. 2909 1999.

[2.13] S. Fama, L. Colace, G. Masini, G. Assanto and H. Luan, "High performance germanium-on-silicon detectors for optical communications", Applied Physics Letters, vol.81, pp. 586 2002.

[2.14] L. Colace, M. Balbi, G. Masini, G. Assanto, H. Luan and L. Kimerling, "Ge on si PIN photodiodes operating at 10 gbit/ s", Applied Physics Letters, vol.88, pp. 101111 2006.

[2.15] N. Feng, P. Dong, D. Zheng, S. Liao, H. Liang, R. Shafiiha, D. Feng, G. Li, J. Cunningham and A. Krishnamoorthy, "Vertical PIN germanium photodetector with high external responsivity integrated with large core si waveguides", Opt. Express, vol.18, pp. 96-101 2010.

[2.16] L. Vivien, J. Osmond, J. Fédéli, D. Marris-Morini, P. Crozat, J. Damlencourt, E. Cassan, Y. Lecunff and S. Laval, "42 GHz PIN germanium photodetector integrated in a silicon-on-insulator waveguide", Optics Express, vol.17, no.8, pp. 6252-6257 2009.

[2.17] M. Morse, O. Dosunmu, G. Sarid and Y. Chetrit, "Performance of ge-on-si PIN photodetectors for standard receiver modules", Photonics Technology Letters, IEEE, vol.18, no.23, pp. 2442-2444 2006.

[2.18] G. Dehlinger, S. Koester, J. Schaub, J. Chu, Q. Ouyang, A. Grill, I. Technologie and A. Villach, "High-speed germanium-on-soi lateral PIN photodiodes", IEEE Photonics Technology Letters, vol.16, no.11, pp. 2547-2549 2004.

[2.19] D. Ahn, C. Hong, J. Liu, W. Giziewicz, M. Beals, L. Kimerling, J. Michel, J. Chen and F. K rtner, "High performance, waveguide integrated ge photodetectors", Opt. Express, vol.15, pp. 3916-3921 2007.

[2.20] G. Masini, G. Capellini, J. Witzens and C. Gunn, "A 1550nm, 10Gbps monolithic optical receiver in 130nm cmos with integrated ge waveguide photodetector", in Group IV Photonics, 2007 4th IEEE International Conference on, pp. 1-3, 2007.

[2.21] D. Suh, S. Kim, J. Joo and G. Kim, "36-GHz high-responsivity ge photodetectors grown by rpcvd", IEEE Photonics Technology Letters, vol.21, no.10 2009.

[2.22] Z. Huang, J. Oh and J. Campbell, "Back-side-illuminated high-speed ge photodetector fabricated on si substrate using thin sige buffer layers", Applied Physics Letters, vol.85, pp. 3286 2004.

[2.23] J. Nakatsuru, H. Date, S. Mashiro and M. Ikemoto, "Growth of high quality ge epitaxial layer on si (100) substrate using ultra thin sige buffer", in Mater. Res. Soc. Symp. Proc., pp. 315-320, 2006.

[2.24] T. Loh, H. Nguyen, C. Tung, A. Trigg, G. Lo, N. Balasubramanian, D. Kwong and S. Tripathy, "Ultrathin low temperature sige buffer for the growth of high quality ge epilayer on si (100) by ultrahigh vacuum chemical vapor deposition", Applied Physics Letters, vol.90, pp. 092108 2007.

[2.25] D. Choi, Y. Ge, J. S. Harris, J. Cagnon and S. Stemmer, "Low surface roughness and threading dislocation density ge growth on si (0 0 1)", Journal of Crystal Growth, vol.310, no.18, pp. 4273-4279 2008.

[2.26] J. Osmond, G. Isella, D. Chrastina, R. Kaufmann, M. Acciarri and H. v. Kanel, "Ultralow dark current ge/si(100) photodiodes with low thermal budget", Applied Physics Letters, vol.94, no.20, pp. 201106 2009.

[2.27] H. Zang, W. Loh, J. Ye, T. H. Loh, G. Lo and B. Cho, "Integration of dual channels mosfet on defect-free, tensile-strained germanium on silicon", International Conference on Solid State Devices and Materials (SSDM), pp. 32-33 2007.

[2.28] T. Muoi, "Receiver design for high-speed optical-fiber systems", Lightwave Technology, Journal of, vol.2, no.3, pp. 243-267 1986.

[2.29] K. Kato, "Ultrawide-band/high-frequency photodetectors", IEEE Transactions on Microwave Theory and Techniques, vol.47, no.7, pp. 1265-1281 1999.

[2.30] S. Sze and K. Ng, Physics of semiconductor devices, Wiley-Blackwell, 2007.

[2.31] O. Dosunmu, D. Cannon, M. Emsley, L. Kimerling and M. Unlu, "High-speed resonant cavity enhanced ge photodetectors on reflecting si substrates for 1550-nm operation", IEEE Photonics Technology Letters, vol.17, no.1, pp. 175-177 2005.

[2.32] O. Dosunmu, M. K. Emsley, D. D. Cannon, B. Ghyselen, L. C. Kimerling and M. S. Unlu, "Germanium on double-soi photodetectors for 1550 nm operation", in Lasers and Electro-Optics Society, 2003. LEOS 2003. The 16th Annual Meeting of the IEEE, pp. 853-854 vol.852, 2003.

[2.33] L. Colace, G. Masini, G. Assanto, H. Luan, K. Wada and L. Kimerling, "Efficient high-speed near-infrared ge photodetectors integrated on si substrates", Applied Physics Letters, vol.76, pp. 1231 2000.

[2.34] J. Liu, J. Michel, W. Giziewicz, D. Pan, K. Wada, D. Cannon, S. Jongthammanurak, D. Danielson, L. Kimerling and J. Chen, "High-performance, tensile-strained ge PIN photodetectors on a si platform", Applied Physics Letters, vol.87, pp. 103501 2005.

[2.35] L. Vivien, M. Rouvière, J. Fédéli, D. Marris-Morini, J. Damlencourt, J. Mangeney, P. Crozat, L. El Melhaoui, E. Cassan and X. Le Roux, "High speed and high responsivity germanium photodetector integrated in a silicon-on-insulator microwaveguide", Optics Express, vol.15, no.15, pp. 9843-9848 2007.

[2.36] T. Yin, R. Cohen, M. Morse, G. Sarid, Y. Chetrit, D. Rubin and M. Paniccia, "31 GHz ge nip waveguide photodetectors on silicon-on-insulator substrate", Optics Express, vol.15, no.21, pp. 13965-13971 2007.

[2.37] J. Wang, W. Loh, K. Chua, H. Zang, Y. Xiong, S. Tan, M. Yu, S. Lee, G. Lo and D. Kwong, "Low-voltage high-speed (18 GHz/1 v) evanescent-coupled thin-film-ge lateral PIN photodetectors integrated on si waveguide", IEEE Photonics Technology Letters, vol.20, no.17, pp. 1485 2008.

[2.38] L. Chen and M. Lipson, "Ultra-low capacitance and high speed germanium photodetectors on silicon", Optics Express, vol.17, no.10, pp. 7901-7906 2009.

[2.39] S. Klinger, M. Berroth, M. Kaschel, M. Oehme and E. Kasper, "Ge-on-si p-i-n photodiodes with a 3-db bandwidth of 49 GHz", Photonics Technology Letters, IEEE, vol.21, no.13, pp. 920-922 2009.

[2.40] S. Dongwoo, J. Jiho, K. Sanghoon and K. Gyungock, "High-speed rpcvd ge waveguide photodetector", in Group IV Photonics, 2009. GFP '09. 6th IEEE International Conference on, pp. 16-18, 2009.

[2.41] S. Assefa, X. Fengnian and Y. A. Vlasov, "Cmos-integrated low-noise germanium waveguide avalanche photodetector operating at 40Gbps", in Optical Fiber Communication (OFC), collocated National Fiber Optic Engineers Conference, 2010 Conference on (OFC/NFOEC), pp. 1-3, 2010.

[2.42] Y. Kang, H. Liu, M. Morse, M. Paniccia, M. Zadka, S. Litski, G. Sarid, A. Pauchard, Y. Kuo and H. Chen, "Monolithic germanium/silicon avalanche photodiodes with 340 GHz gain–bandwidth product", Nature Photonics, vol.3, no.1, pp. 59-63 2008.

[2.43] K. Ang, J. Ng, A. Lim, M. Yu, G. Lo and D. Kwong, "Waveguide-integrated ge/si avalanche photodetector with 105ghz gain-bandwidth product", in Optical Fiber Communication (OFC), collocated National Fiber Optic Engineers Conference, 2010 Conference on (OFC/NFOEC), 2010.

[2.44] S. Assefa, F. Xia and Y. Vlasov, "Reinventing germanium avalanche photodetector for nanophotonic on-chip optical interconnects", Nature, vol.464, no.7285, pp. 80-84 2010.

[2.45] L. Pavesi and D. Lockwood, "Silicon photonics, topics in applied physics, vol. 94", Berlin, Germany: Springer-Verlag, 2004.

[2.46] J. Wang, W. Loh, H. Zang, M. Yu, K. Chua, T. Loh, J. Ye, R. Yang, X. Wang and S. Lee, "Integration of tensile-strained ge PIN photodetector on advanced cmos platform", in Group IV Photonics, 2007 4th IEEE International Conference on, pp. 1-3, 2007.

[2.47] W. Loh, J. Wang, J. Ye, R. Yang, H. Nguyen, K. Chua, J. Song, T. Loh, Y. Xiong and S. Lee, "Impact of local strain from selective epitaxial germanium with thin si/sige buffer on high-performance PIN photodetectors with a low thermal budget", IEEE Electron Device Letters, vol.28, no.11, pp. 984-986 2007.

[2.48] T. Loh, H. Nguyen, R. Murthy, M. Yu, W. Loh, G. Lo, N. Balasubramanian, D. Kwong, J. Wang and S. Lee, "Selective epitaxial germanium on silicon-on-insulator high speed photodetectors using low-temperature ultrathin si 0.8 ge 0.2 buffer", Applied Physics Letters, vol.91, pp. 073503 2007.

[2.49] K. Ang, M. Yu, S. Zhu, K. Chua, G. Lo and D. Kwong, "Novel nige msm photodetector featuring asymmetrical schottky barriers using sulfur co-implantation and segregation", IEEE Electron Device Letters, vol.29, no.7 2008.

[2.50] G. Masini, L. Colace, G. Assanto, H. Luan and L. Kimerling, "High-performance PIN ge on si photodetectors for the near infrared: From model to demonstration", IEEE Transactions on Electron Devices, vol.48, no.6, pp. 1092-1096 2001.

[2.51] M. Rouvière, L. Vivien, X. Le Roux, J. Mangeney, P. Crozat, C. Hoarau, E. Cassan, D. Pascal, S. Laval and J. Fédéli, "Ultrahigh speed germanium-on-silicon-on-insulator photodetectors for 1.31 and 1.55 m operation", Applied Physics Letters, vol.87, pp. 231109 2005.

[2.52] J. Liu, D. Cannon, K. Wada, Y. Ishikawa, S. Jongthammanurak, D. Danielson, J. Michel and L. Kimerling, "Tensile strained ge PIN photodetectors on si platform for c and l band telecommunications", Applied Physics Letters, vol.87, pp. 011110 2005.

[2.53] M. Jutzi, M. Berroth, G. Wöhl, M. Oehme and E. Kasper, "Zero biased ge-on-si photodetector on a thin buffer with a bandwidth of 3.2 GHz at 1300 nm", Materials science in semiconductor processing, vol.8, no.1-3, pp. 423-427 2005.

[2.54] M. Oehme, J. Werner, E. Kasper, M. Jutzi and M. Berroth, "High bandwidth ge PIN photodetector integrated on si", Applied Physics Letters, vol.89, pp. 071117 2006.

[2.55] J. F. Liu, D. Pan, S. Jongthammanurak, D. Ahn, C. Y. Hong, M. Beals, L. C. Kimerling, J. Michel, A. T. Pomerene, C. Hill, M. Jaso, K. Y. Tu, Y. K. Chen, S. Patel, M. Rasras, A. White and D. M. Gill, "Waveguide-integrated ge p-i-n photodetectors on soi platform", in Group IV Photonics, 2006. 3rd IEEE International Conference on, pp. 173-175, 2006.

[2.56] A. Donghwan, H. Ching-yin, L. Jifeng, M. Beals, C. Jian, F. X. Kaertner, L. C. Kimerling and J. Michel, "Ge photodetectors integrated with waveguides for electronic-photonic integrated circuits on cmos platform", in Optical Fiber Communication and the National Fiber Optic Engineers Conference, 2007. OFC/NFOEC 2007. Conference on, pp. 1-3, 2007.

[2.57] J. Liu, D. Ahn, C. Hong, D. Pan, S. Jongthammanurak, M. Beals, L. Kimerling, J. Michel, A. Pomerene and D. Carothers, "Waveguide integrated ge PIN photodetectors on a silicon-on-insulator platform", pp. 1-4, 2006.

[2.58] J. Michel, J. Liu, D. Ahn, D. Sparacin, R. Sun, C. Hong, W. Giziewicz, M. Beals, L. Kimerling and A. Kopa, "Advances in fully cmos integrated photonic devices", pp. 64770P, 2007.

[2.59] J. Wang, W. Loh, K. Chua, H. Zang, Y. Xiong, T. Loh, M. Yu, S. Lee, G. Lo and D. Kwong, "Evanescent-coupled ge PIN photodetectors on si-waveguide with seg-ge and comparative study of lateral and vertical PIN configurations", IEEE Electron Device Letters, vol.29, no.5, pp. 445 2008.

[2.60] H. Zang, S. Lee, W. Loh, J. Wang, M. Yu, G. Lo, D. Kwong and B. Cho, "Application of dopant segregation to metal-germanium-metal photodetectors and its dark current suppression mechanism", Applied Physics Letters, vol.92, pp. 051110 2008.

[2.61] Z. Shiyang, A. Kah-Wee, S. C. Rustagi, J. Wang, Y. Z. Xiong, G. Q. Lo and D. L. Kwong, "Waveguided ge/si avalanche photodiode with separate vertical seg-ge absorption, lateral si charge, and multiplication configuration", Electron Device Letters, IEEE, vol.30, no.9, pp. 934-936 2009.

[2.62] Y. Tao, R. Cohen, M. M. Morse, G. Sarid, Y. Chetrit, D. Rubin and M. J. Paniccia, "40gb/s ge-on-soi waveguide photodetectors by selective ge growth", in Optical Fiber communication/National Fiber Optic Engineers Conference, 2008. OFC/NFOEC 2008. Conference on, pp. 1-3, 2008.

[2.63] S. Assefa, F. Xia, S. Bedell, Y. Zhang, T. Topuria, P. Rice and Y. Vlasov, "Cmos-integrated high-speed msm germanium waveguide photodetector", Opt. Express, vol.18, pp. 4986-4999 2010.

[2.64] F. Dazeng, L. Shirong, D. Po, F. Ning-Ning, Z. Dawei, L. Hong, R. Shafiiha, L. Guoliang, J. Cunningham, K. Raj, A. V. Krishnamoorthy and M. Asghari, "Horizontal p-i-n high-speed ge waveguide detector on large cross-section soi waveguide", in Optical Fiber Communication (OFC), collocated National Fiber Optic Engineers Conference, 2010 Conference on (OFC/NFOEC), pp. 1-3, 2010.

[2.65] D. Suh, J. Joo, S. Kim and G. Kim, "High-speed RPCVD Ge waveguide photodetector", in Group IV Photonics, 6th IEEE International Conference on, pp. 16-18, 2009.

CHAPTER 3

3. Integration of Tensile-Strained Ge PIN Photodetector on Advanced CMOS Platform

3.1 Introduction

As discussed in Chapter 1 and 2, heteroepitaxy of SiGe/Ge and Ge-on-SOI are highly desired for near-infrared photodetection application due to its CMOS-process compatibility and its intrinsic bandgap at 0.8 eV and thus large absorption coefficient [3.1] . To further broaden the detection range, tensile-strained Ge photodetectors have been fabricated using either backside silicidation-induced strain effect [3.2] and/or two-step Ge-method [3.3] . The two-step Ge growth induces tensile-strain (~0.20%) in Ge [3.3] . When coupled with backside silicidation, Liu et al. have shown that the tensile-strain in Ge can be increased to 0.24% with resulting bandgap of 0.765 eV, which is sufficient for detection up to 1620 nm [3.4] . Nevertheless, these tensile-strains were incorporated on the devices globally, instead of locally, on the whole substrate. Local strain would allow us to engineer the devices selectively, for instance, only on photodetectors among all associated photonic devices on the same substrate.

In this study, the effects of selective epitaxially grown (SEG) Ge on a Si/SiGe buffer layer are investigated in terms of in-plane strain, defect density, dark current, photo responsivity and speed of the fabricated photodetectors. Unlike Refs [3.3, 3.4]

the strain effects in this work are incorporated locally based on the selective growth scheme without cyclic anneal. It is found that a Si buffer layer coupled with $Si_{0.8}Ge_{0.2}$ buffer is critical for low leakage, photoresponse and device speed due to its better film qualities and higher tensile-strain induced in the Ge layer.

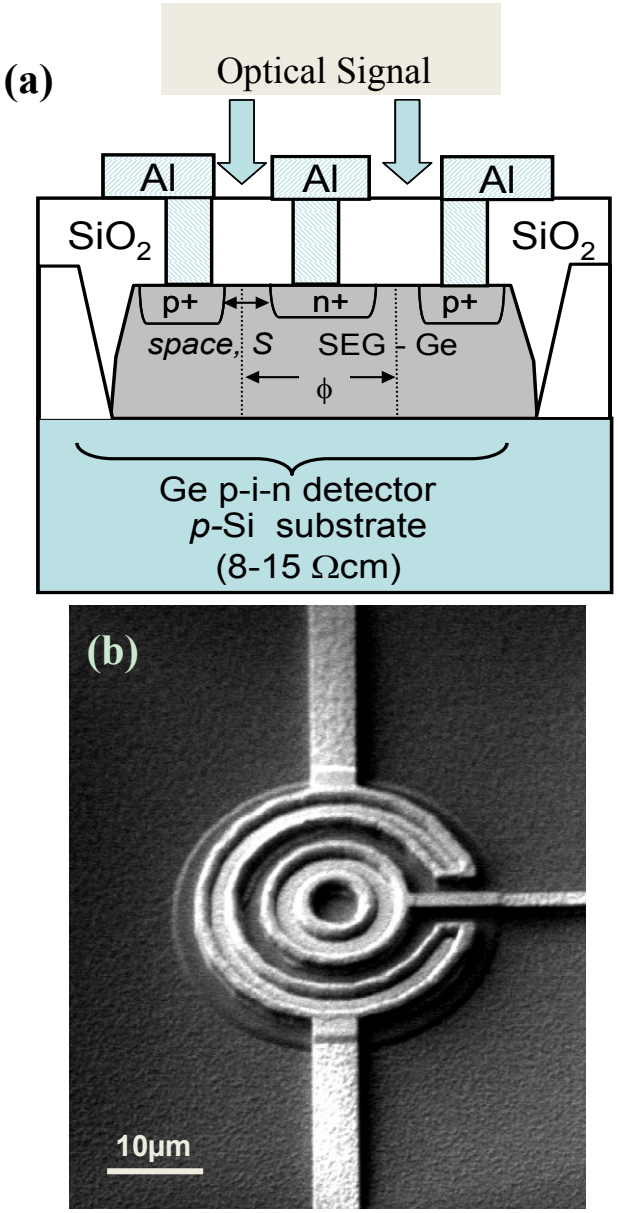

Fig. 3.1: (a) Schematic diagram of normal incidence photodetector with SEG Ge on Si substrate for circular ring structure with lateral spacing, S and diameter, ϕ. (b) SEM image of the photodetector.

3.2 Experimental

The schematic device structure as well as the SEM image are shown in Fig. 3.1 (a), (b), respectively, with two concentric ring-shaped n+/p+ implant with spacing S = 1.5 and 2 μm and diameter ϕ of 10, 20 and 28 μm. Starting with 8" Si p-(001) substrate (~8-15 Ω-cm), 120 nm of PECVD oxide were deposited and patterned by RIE (with ~10 nm oxide remaining) and wet DHF (1:200) etch to form oxide window. The wafers were subsequently cleaned with standard SC1 ($NH_4OH:H_2O_2:H_2O$=1:2:10 at 60˚C), DHF clean and IPA dry. All samples were then submitted for epi deposition in a UHVCVD chamber (with base pressure <10^{-8} Torr). Beginning with *in-situ* N_2-bake at 800˚C, after ramp-down and stabilizing at 500˚C, a thin Si-buffer layer (<2 nm) was selectively grown with SiH_4/HCl, followed by a selective $Si_{0.8}Ge_{0.2}$-buffer layer (10-15 nm) deposition with SiH_4/GeH_4 at 400˚C. The Ge concentration ~21.8% was measured by EDX as shown in Fig. 3.2. Two different types of samples with different buffer layers were prepared: Si/SiGe and SiGe buffer only. For samples with Si/SiGe buffer, the Si-buffer thickness was increased to ~6 nm followed by the same $Si_{0.8}Ge_{0.2}$-buffer. Those with SiGe buffer only have a thin Si-buffer of <2 nm. All samples were then subjected to SEG low-temperature Ge seed (10 nm) growth at 400 ˚C followed by SEG Ge (150 nm) at 600 ˚C and subsequently capped with 5 nm Si with SiH_4 [3.5] . The Ge film surface was then patterned, implanted with As (1×10^{15} cm^{-2}/15 keV) and BF_2 (1×10^{15} cm^{-2}/15 keV), and annealed at 600 ˚C for 10 s to form

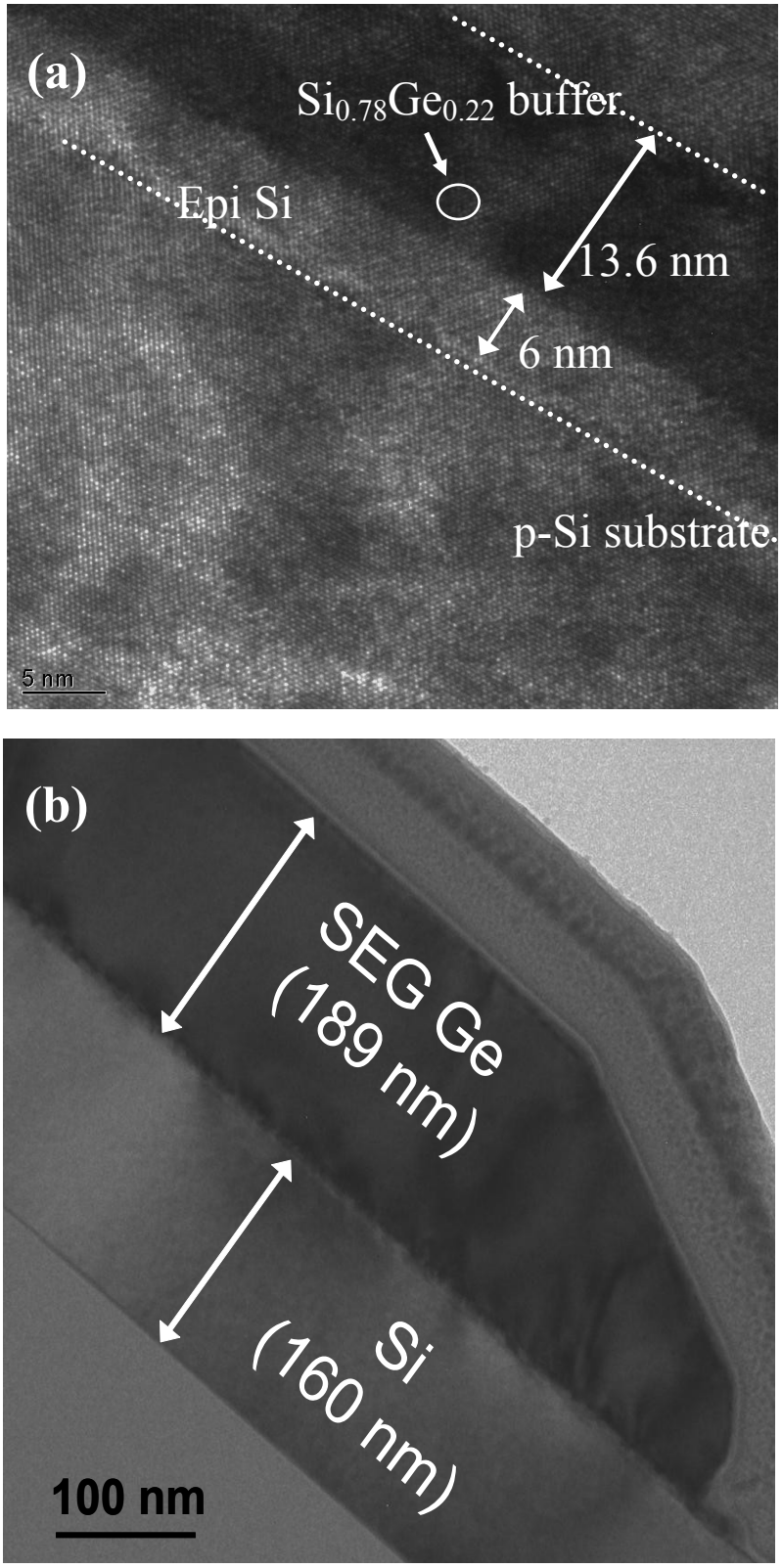

Fig. 3.2: (a) High-resolution TEM of the interfacial layers for samples with Si/SiGe buffer layer (6 nm of Si and 12 nm of SiGe). (b) The cross-sectional TEM view of the corner of the SEG-Ge on $Si/Si_{0.8}Ge_{0.2}$ buffer layer on p-type silicon substrate.

the n+ and p+ junctions. Ohmic contacts to the Ge n+/p+ were formed with Al metallization (25 nm TaN/600 nm Al) on 320 nm of PECVD oxide.

3.3 Results and Discussions

Fig. 3.2 (a) shows the high-resolution TEM of the SEG-Ge with Si/SiGe buffer. EDX showed very consistent Ge concentration (~92.1-94%) across the Ge film with Si/SiGe buffer without trace of Si migration at various locations. For both splits, no cross-hatch pattern was observed on the Ge top surfaces. Samples with Si/SiGe buffer show smoother surface, for scanning area of 5×5 μm^2, root-mean square roughness ~0.68 nm is obtained, whereas SiGe buffer shows ~1.068 nm. Although the epi-deposition in this study was conducted in SEG scheme, the beneficial effect of Si-buffer on subsequent Ge surface condition is consistent with that reported for blanket deposition as in [3.6] . Threading dislocation (TD) is evaluated by subjecting the Ge surface to selective etchant composing of ~55% CrO_3 and DHF (~49%). The estimated etch pits density (EPD) is 3.8×10^6 cm^{-2} for sample with Si/SiGe buffer and ~9.6×10^6 cm^{-2} for SiGe buffer sample. These EPD results are comparable to the defect density ~2.3×10^6 cm^{-2} obtained by Luan et al, using two-steps Ge deposition but with additional high temperature cyclic anneal [3.7] .

In Fig. 3.2 (b), the image of the Ge mesa's edge is shown. This selective Ge growth on patterned SiO_2/Si wafer was achieved by the same epi-growth method. From the image, a smooth surface o f the Ge layer can be observed. It also can be seen

that Ge layer was only grown on the Si region. There is no Ge growth on the SiO_2 region. The main reason of this selective Ge growth is that the reaction between GeH4 and SiO2 growth forms volatile GeO and retards the nucleation of poly Ge on SiO2. At the same time, the facets are visible on the edge of Ge mesas. The three types of facets on the edge are (311), (111) and (113). The facets play the role of strain relaxation during selective Ge growth.

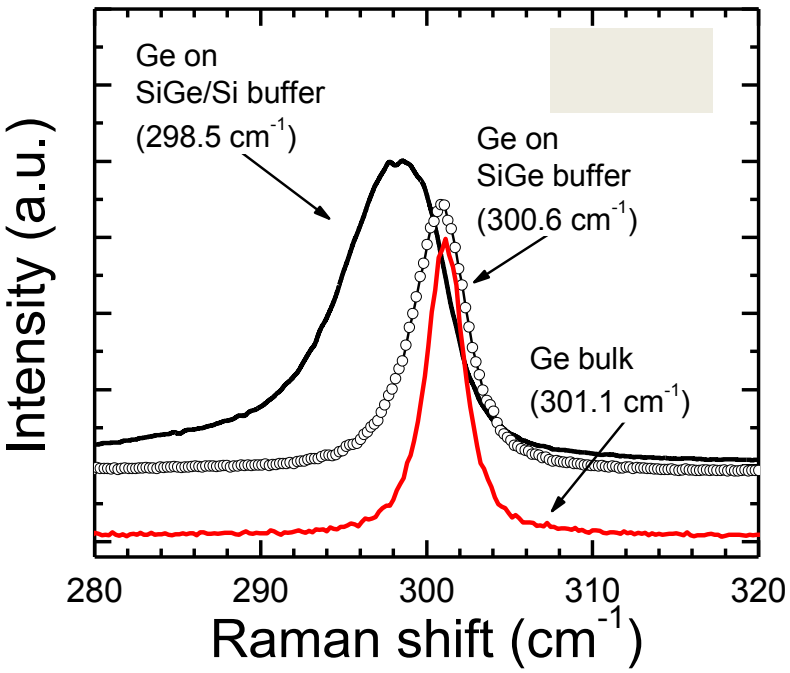

Fig. 3.3: Micro-Raman spectroscopy on Ge films selectively grown on different buffer layers on Si(001) substrate compared to bulk Ge substrate. SEG Ge on Si/SiGe buffer shows peak shift of 2.6 cm^{-1} which corresponds to tensile strain of 0.63% while that on SiGe buffer alone shows lower peak shift of 0.5 cm^{-1}, corresponding to tensile strain of 0.12%. Asymmetric broadening of the Raman spectra observed is due to tensile strain which causes a splitting of the threefold degeneracy of the zone center phonons into a singlet and doublet [3.8] .

Film quality and in-plane strain in the Ge layers were evaluated using Raman spectroscopy with 514.5 nm Ar^+-laser in the $z(\chi,\chi)\bar{z}$ backscattering configuration

as shown in Fig. 3.3 (a). Both SiGe and Si/SiGe buffer samples show red-shift of Ge-Ge vibrational mode compared to bulk Ge, indicating tensile strain in the SEG-Ge film. The in-plane strain component can be calculated from $\Delta\omega = b\varepsilon_{||}$ where b = -415 cm^{-1} using the elastic and strain tensor constant from [3.9] . From Fig. 3.3(a), it can be observed that samples with SEG-Ge grown on Si/SiGe buffer layer experience an in-plane tensile strain of 0.63%. Our strain results for Si/SiGe buffer are significantly higher than [3.4] . The major difference is the presence of the LT-Si and SEG-Ge in the current study, which is expected to form a primary misfit-dislocation (MD) network [3.10] due to the stress field during SEG Ge growth. The underlying MD network due to the compliant micro-crystalline Si layer is expected to have an even lower thermal coefficient of expansion (TCE) [3.11] compared to Si bulk. In contrast, samples with SiGe buffer (13.6 nm) have lower tensile strain of 0.12%. The enhanced tensile strain in Ge using Si/SiGe buffer results in bandgap narrowing, which will increase photon absorption and responsivity at a longer wavelength region [3.3].

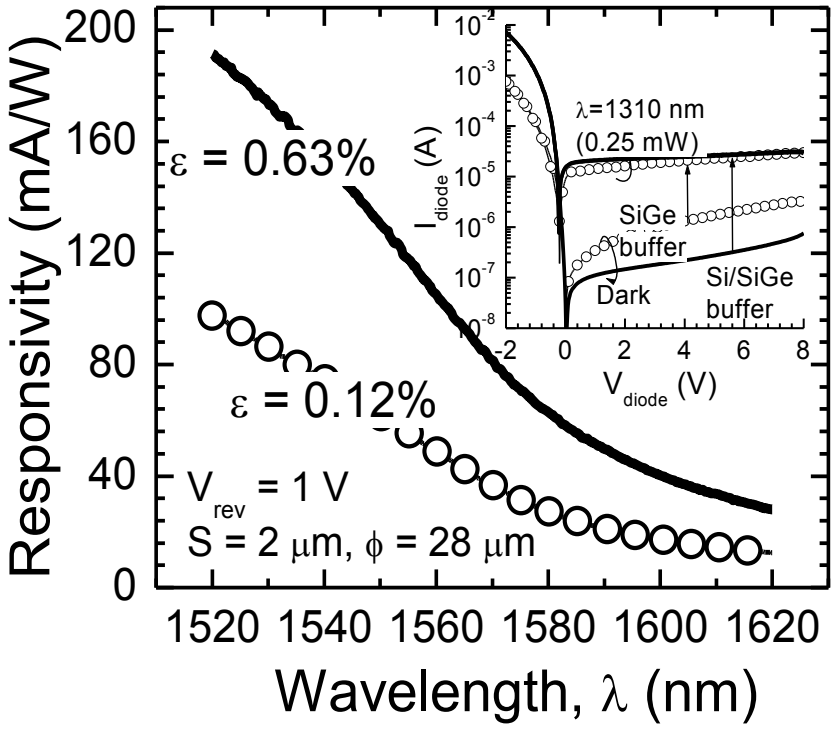

Fig. 3.4: Photocurrent spectral response for tensile-strained Ge PIN photodetectors with Si/SiGe buffer (ε=0.63%) and SiGe buffer (ε=0.12%). Inset shows the light and dark current leakage of SEG Ge on SiGe and Si/SiGe buffer layers for detectors with diameters of 28 μm and lateral spacing of 0.2 μm. Laser with wavelength of 1310 nm is coupled via fiber (m.f.d = 8 μm) onto the photodetector. Si/SiGe buffer shows significant improvement in dark current, photoresponse and spectral range due to enhanced tensile strain and better Ge film quality.

Fig. 3.4 shows the responsivity spectra of the lateral Ge PIN photo detector (circular ring with ϕ = 28 μm and finger spacing S = 2 μm) under normal incidence illumination using laser diode with multi-mode fiber probe at λ=1.52 to 1.62 μm. Samples with Si/SiGe buffer show wider and higher photoresponse of ~190 mA/W at 1.52 μm compared to those with SiGe buffer which could be attributed to the enhanced tensile strain. The responsivity is reasonable considering the thickness of Ge ($\leq$ 0.2 μm) and inherent mismatch between the multi-mode fiber and photodiode

aperture during testing. In comparison, Colace et al. have obtained responsivity of 240 mA/W at 1.32 μm for 0.4 μm thick Ge [3.12] . Fig. 3.4 inset shows the leakage current of the PIN photodetector at 25 °C. Samples with Si/SiGe buffer show lower dark current and higher photocurrent (λ = 1310 nm) compared to samples with SiGe buffer, due to better Ge film quality with lower threading dislocations.

The temporal response of several ring-shaped lateral detectors (ϕ = 9 μm, electrode spacing S = 1.5 μm between the n^+ and p^+ regions) were measured using 1.55 μm pulsed fiber laser (optical pulse width of 80 fs), microwave probes and a 15 GHz sampling oscilloscope. Fig. 3.5 shows the pulsed response and the Fast-Fourier-Transform (FFT) for Ge PIN with Si/SiGe buffer and SiGe buffer. The 3-dB bandwidth is estimated to be ~5.2 GHz (Si/SiGe buffer) and ~1.17 GHz (SiGe buffer) at 1-V. Carrier mobility calculated from the transit time for photocurrent at full-width at half maximum (FWHM) pulse [3.12] shows mobility of μ = 3084 cm^2/Vs and 377 cm^2/Vs for samples with Si/SiGe and SiGe buffer respectively. Bandwidth for Si/SiGe buffer is limited by the transit time with carrier mobility close to theoretical Ge mobility. In contrast, those of SiGe buffer shows significant speed degradation with long transient tail. Possible reasons are carrier interactions with higher density of slow traps in Ge on SiGe buffer, and slow carriers from underlying Si. In this case, as SIMS analysis for SiGe and Si/SiGe shows similar Si profile, it is confirmed that the degraded speed and responsivity in SiGe samples are not due to Si-Ge interdiffusion. Rather, it is speculated that the MD network present in Si/SiGe buffer may prevent

the underlying Si from interacting, resulting in enhanced speed even on Si substrate.

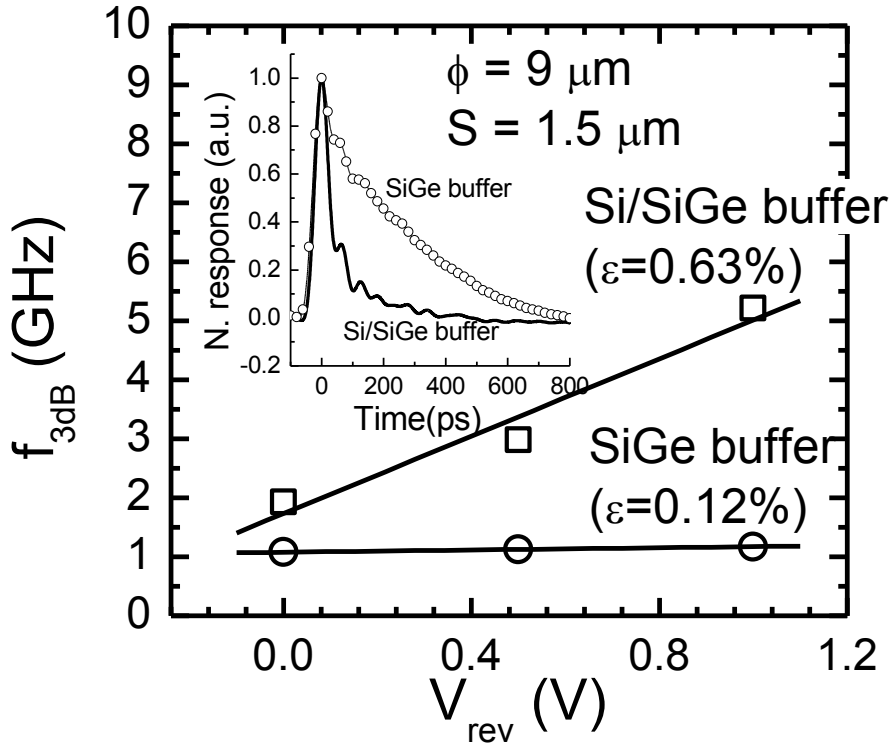

Fig. 3.5: Fast Fourier transform of the temporal response with bandwidth of 5.2 GHz (Si/SiGe buffer) and 1.17 GHz (SiGe buffer) is obtained at -1 V under normal incidence pulse from 1550 nm fiber laser with optical pulse width of 80 fs. The mobility calculated from FWHM transit time $\Delta\tau_{FWHM} = \frac{d}{\mu\xi}$ for Si/SiGe and SiGe buffer are 3084 cm^2/Vs and 377 cm^2/Vs respectively. Inset shows the impulse response under 1 V reverse bias for Si/SiGe and SiGe buffer samples.

3.4 Conclusion

This chapter studies the electrical/optical characteristics of selectively grown Ge on SiGe and Si/SiGe buffer on Si for optical photodetection. Using an additional Si epitaxial layer as buffer layer, dark current is reduced by half to 0.12 μA (circular ring, area = 1230 μm^2 and spacing, S = 2μm) at 1 V with smooth surface and low dislocation density without cyclic anneal or additional chemical-mechanical polishing.

By leveraging on the misfit dislocation network in the Si/SiGe buffer, tensile strain in Ge layer is increased. Lateral PIN Ge photodetector fabricated on this Ge platform shows photoresponsivity of ~190 mA/W at 1.52 μm and extended photon detection to 1.62 μm wavelength with 3-dB bandwidth at 5.2 GHz at 1 V.

REFERENCES

[3.1] J. M. Hartmann, A. Abbadie, A. M. Papon, P. Holliger, G. Rolland, T. Billon, J. M. Fedeli, M. Rouviere, L. Vivien, and S. Laval, "Reduced pressure-chemical vapor deposition of Ge thick layer on Si (001) for 1.3 – 1.55 m photodetection", J. Appl. Phys., vol. 95, pp. 5905, 2004.

[3.2] J. F. Liu, D. D. Cannon, K. Wada, Y. Ishikawa, S. Jongthammanurak, D. T. Danielson, J. Michel, and L. C. Kimerling, "Silicidation-induced bandgap shrinkage in Ge epitaxial films on Si", Appl. Phys. Lett., vol. 84, pp. 660, 2004.

[3.3] Y. Ishikawa, K. Wada, D. D. Cannon, J. F. Liu, H. C. Luan, and L. C. Kimerling, "Strain-induced band gap shrinkage in Ge grown on Si substrate", Appl. Phys. Lett., vol. 82, pp. 2044, 2003.

[3.4] J. F. Liu, D. D. Cannon, K. Wada, Y. Ishikawa, S. Jongthammanurak, D. T. Danielson, J. Michel, and L. C. Kimerling, "Tensile strained Ge p-i-n photodetectors on Si platform for C and L band telecommunications", Appl. Phys. Lett., vol. 87, pp. 011110, 2005.

[3.5] A. Sakai, T. Tatsumi, and K. Aoyama, "Growth of strain-relaxed Ge films on Si(001) surfaces", Appl. Phys. Lett., vol. 71, pp. 3510, 1997.

[3.6] Y. H. Luo, J. Wan, R. L. Forrest, J. L. Liu, M. S. Goorsky, and K. L. Wang, "High-quality strain-relaxed SiGe films grown with low temperature Si buffer", J. Appl. Phys., vol. 89, pp. 8279, 2001.

[3.7] H. C. Luan, D. R. Lim, K. K. Lee, K. M. Chen, J. G. Sandland, K. Wada, and L. C. Kimerling, "High quality Ge epilayers on Si with low threading-dislocation densities", Appl. Phys Lett., vol. 75, pp. 2090, 1999.

[3.8] F. Cerdeira, C. J. Buchenauer, F. H. Pollak, and M. Cardona, "Stress-induced shifts of first-order Raman frequencies of diamond – and zinc-blende-type semiconductors", Phys. Rev. B., vol. 5(2), pp. 580, 1972.

[3.9] J. Zi, K.M. Zhang, X.D. Xie, "Vibrational Properties of Si/Ge superlattices", Prog. Surf. Sci., vol. 54, 69, 1997.

[3.10] Yu. B. Bolkhovityanov, A. K. Gutakovskii, V. I. Mashanov, O. P. Pchelyakov, M. A. Revenko, and L. V. Sokolov, "Plastic relaxation of solid GeSi solution grown by molecular-beam epitaxy on the low temperature Si(100) buffer layer", J. Appl. Phys., vol. 91, pp. 4710, 2002.

[3.11] K. Takimoto, A. Fukuta, Y. Yamamoto, N. Yoshida, T. Itoh and S. Nonomura, "Linear thermal expansion coefficients of amorphous and microcrystalline silicon films", J. Non-Crystalline Solids, vol. 299, pp. 314, 2002.

[3.12] L. Colace, G. Masini and G. Assanto, " Ge-on-Si approaches to the detection of near-infrared light", IEEE J. Quatum Elect., vol. 35, pp. 1843, 1999.

CHAPTER 4

4. Evanescent-Coupled Ge-PIN Photodetectors on Si-Waveguide with SEG-Ge and Comparative Study of Lateral and Vertical PIN Configurations

4.1 Introduction

As discussed in Chapter 3, from the results of normal incidence Ge photodiodes, it is found that a Si buffer layer coupled with $Si_{0.8}Ge_{0.2}$ buffer is critical for low leakage, high photoresponse and device speed due to its better film qualities and higher tensile-strain induced in the Ge layer. In this chapter, waveguide-integration structure is utilized to leverage the trade-off between sensitivity and speed. Unlike normal incidence scheme, to decouple the light absorption and photo-carrier collection, light is delivered into the photodetector from the Si waveguide underneath the Ge layer. Therefore, it is of interest to examine the impact of the buffer layers on the waveguided photodetectors.

4.2 Background

Ge-on-Si photodiodes are critical for low-cost Si-based optical-electronic-integrated-circuit; integration of Ge on Si however has been very challenging due to Ge/Si lattice mismatch. Nonetheless, low-defect Ge was demonstrated by many

groups [4.1-4.3], with improved device performance in terms of dark current, responsivity and speed. To further improve, structure of the photodetector becomes important as well. Waveguide geometry is considered to be one of the key solutions, where high absorption efficiency and high speed can be realized simultaneously due to the light absorption perpendicular to current collection and thus de-coupling of efficiency from the active region thickness [4.4]. Different coupling schemes, e.g., evanescent- and butt-coupling, and different detector structures, e.g., Metal-Semiconductor-Metal (MSM) [4.5] and vertical Ge PIN [4.6-4.7], have been demonstrated.

This study reports on results of evanescent-coupled waveguided lateral Ge PIN photodetectors (LPD) and its comparative analysis with vertical Ge p-Si/i-Ge/n-Ge PIN (VPD).

4.3 Experimental

Starting with (100) SOI with 180-nm-thick p-type Si (~8-15 Ωcm) and 1-μm-thick SiO_2 insulator, waveguide (width 0.6 μm/height 180 nm) and detector region were defined by lithography and dry etch. For VPD, detector region was implanted with BF_2 1×10^{15} cm^{-2}/15 keV and annealed at 1000 °C to form p+ region. Subsequently, PECVD oxide ~150 nm was deposited on all samples, patterned and dry/wet etched to form 4.4-μm-wide 80-μm-long square windows for Ge deposition. Then ultra-thin Si seed (~10 nm, 500 °C), $Si_{0.8}Ge_{0.2}$ (~25 nm, 350-400 °C) buffer,

low-temperature Ge seed (~10 nm, 400 ˚C), and high-temperature strain-relaxed Ge (~100 nm, 600 ˚C) were sequentially deposited in a UHVCVD chamber with base pressure of 7×10^{-9} Torr [4.3]. The samples were implanted with BF_2 or As of the same condition (dose 1×10^{15} cm^{-2}, energy 15 keV) and thermally activated at 600 °C for 10 s to form p+/n+ region for LPD (i-region ~2.6 μm) and n+ region for VPD. Finally, ohmic contacts were formed by a thin layer of TaN (25 nm) and Al (0.75 μm) deposition and patterning. Fig. 4.1 illustrates the schematic of lateral and vertical PIN configurations. Fig. 4.2 (a) & (b) show the TEM image of the SEG-Ge on Si and the SEM image of LPD, respectively.

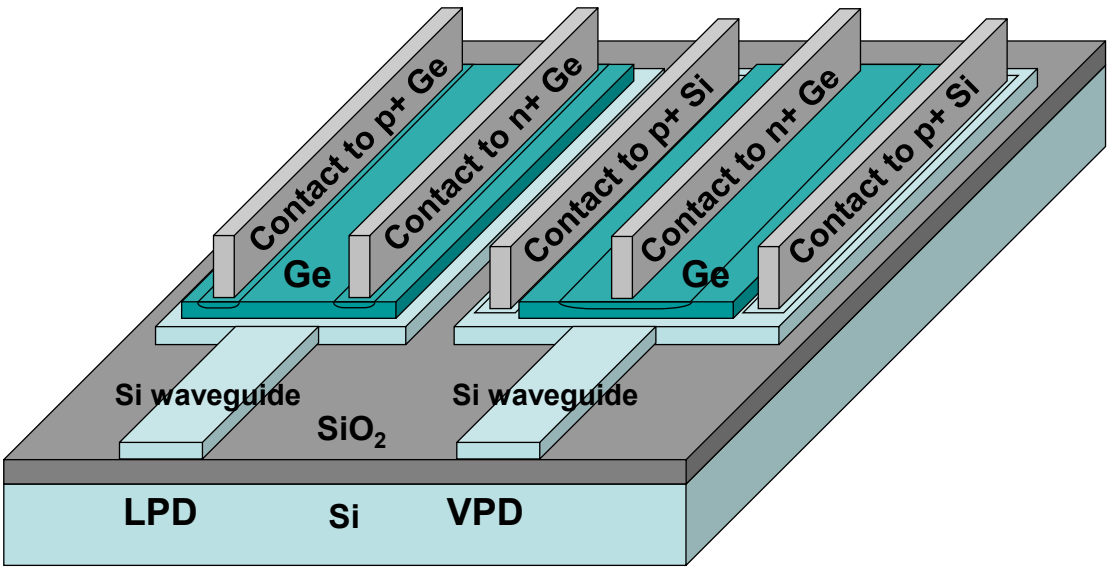

Fig. 4.1: The schematic structure of both lateral and vertical PIN configurations.

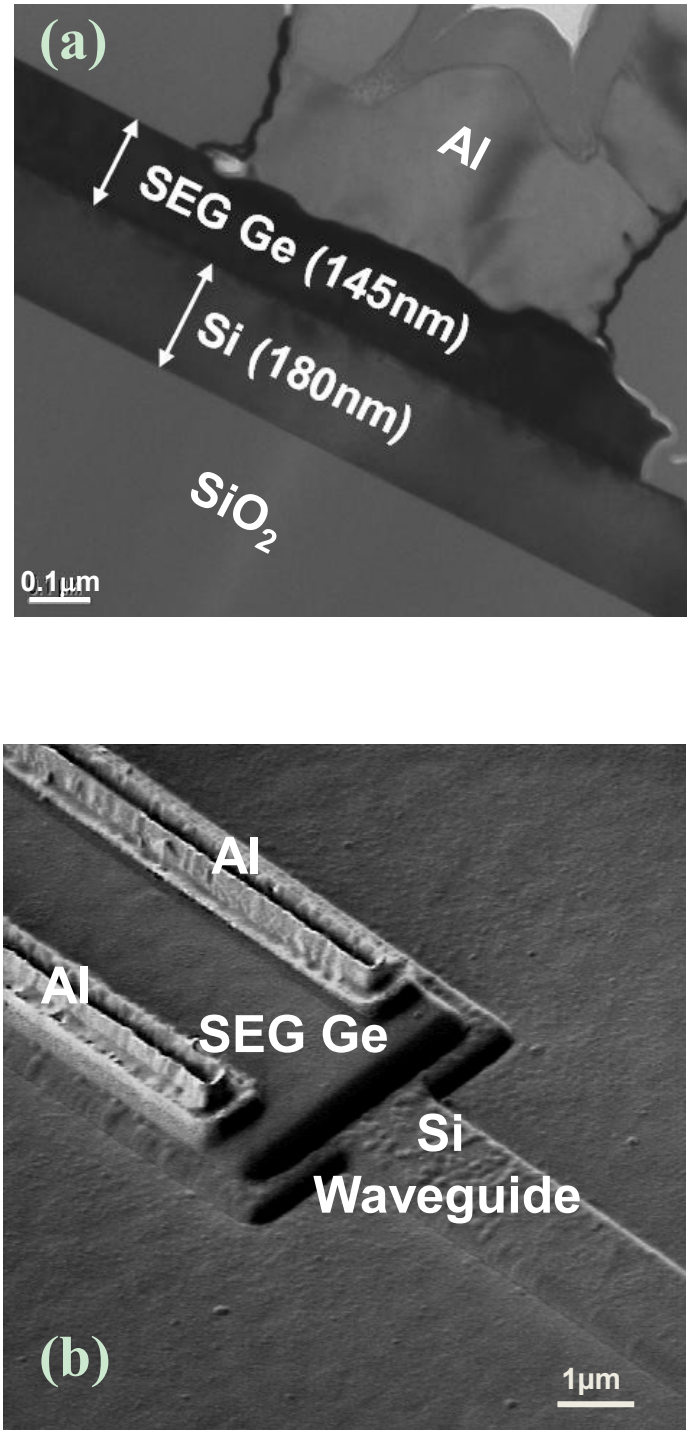

Fig. 4.2: (a) TEM image of the selective epi grown (SEG) Ge on Si/SiGe buffer on Si. The observed Ge surface roughness beneath the metal contact is due to the process non-ideality in the contact-etch step that causes over-etch to the Ge layer. The original as-deposited Ge-surface was smooth (rms~ 0.4 nm) as verified by AFM. (b) SEM image of LPD.

4.4 Sample Measurement Setup and Optical Simulations

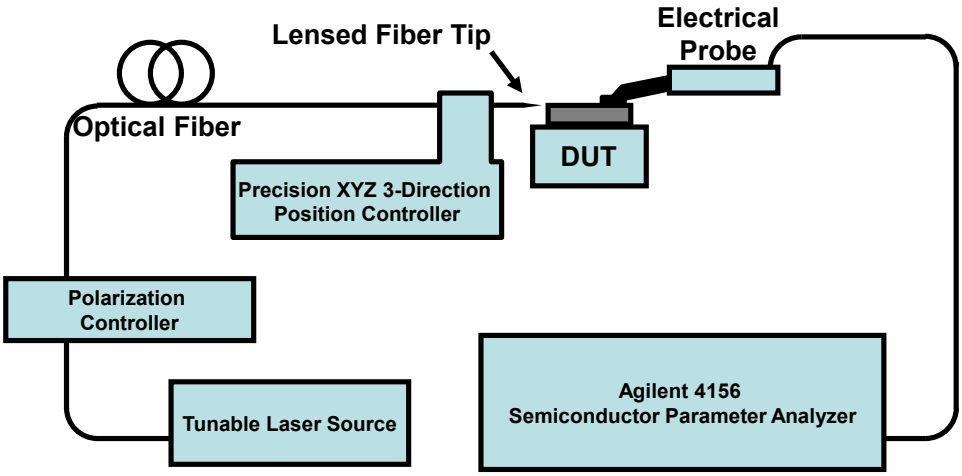

Fig. 4.3: Schematic of waveguided photodetector measurement setup.

The waveguided photodetector measurement is conducted on an optical bench whose configuration is schematically shown in Fig. 4.3. The Device-Under-Test (DUT) is held on stage with backside vacuum. An electrical probe contacts the probe pad on chip. An Agilent 4156 parameter analyzer connects the probe and monitors the current/voltage of the DUT. Tunable laser source generates the laser with optical wavelength in the range of 1520-1620 nm. The output laser power is tunable from 10^{-3} dBm to 8 dBm. A piezoelectric polarization controller is used to adjust the laser polarization without affecting the laser power. The laser is then coupled into on-chip waveguide through an optical fiber and lensed fiber (spot size 2.5±0.3 μm) whose position is controlled by precision XYZ 3-direction controller.

Before measurement, the samples are diced and polished. After sample placement, the fiber-waveguide coupling was optimized by adjusting the position of

the fiber to maximize responsivity which is monitored by parameter analyzer. Once fiber adjustment is done, the photocurrent of photodetector at bias was measured.

To estimate the fiber-to-waveguide mode-conversion loss, the simulation of the optical structure is performed by Beam Propagation Method (BPM) using commercial software (RSoft ^{TM}). The result is presented in Fig. 4.4.

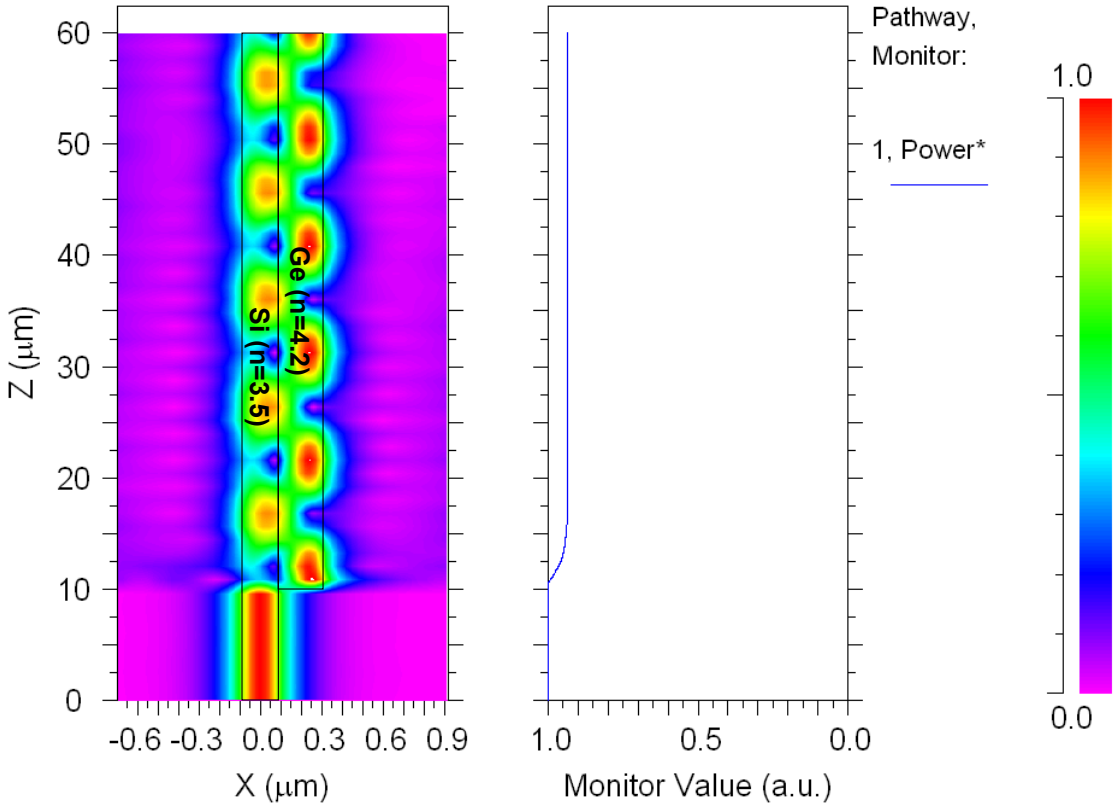

Fig. 4.4: Simulated light power distribution and total integrated power along the propagation direction. Ge's absorption is set to be zero.

For the study of coupling loss only, Si waveguide (refractive index n=3.5, height 180 nm) and non-absorptive Ge layer (refractive index n=4.2, height 220 nm) are used and the total light power in the simulated space is monitored. As can be seen,

the normalized total light power drop from 1 to 0.94 due to mode incontinuity. So it is calculated that the mode-conversion loss for the Si-waveguide/Ge-layer is -0.27 dB.

To check whether the 220 nm Ge layer is thick enough for complete evanescent-coupling, the same structure is used but with absorptive Ge layer (n=3.5+0.05j, the imaginary part of n corresponds to absorption coefficient of 4000 cm^{-1} for tensile strained Ge). As shown in Fig. 4.5, light couples up effectively into Ge layer. And only less than 5% of light power remains at the end of 20-μm-long Ge layer.

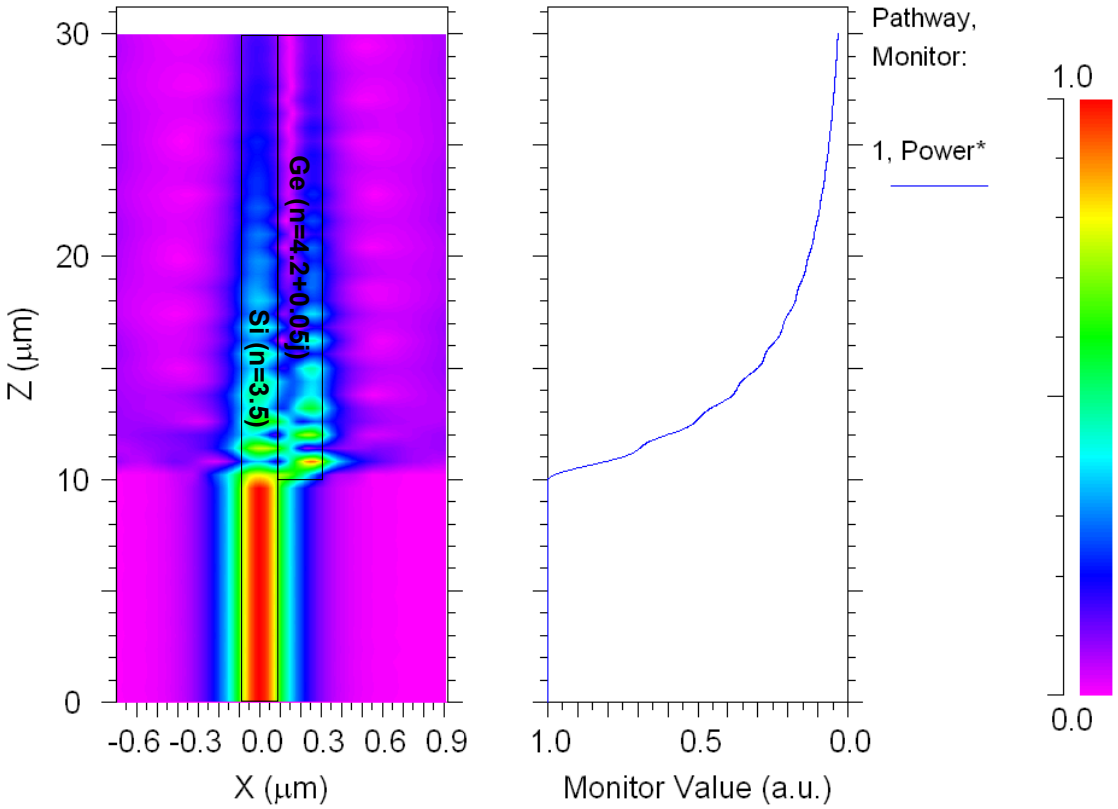

Fig. 4.5: Simulated light power distribution and total integrated power along the propagation direction.

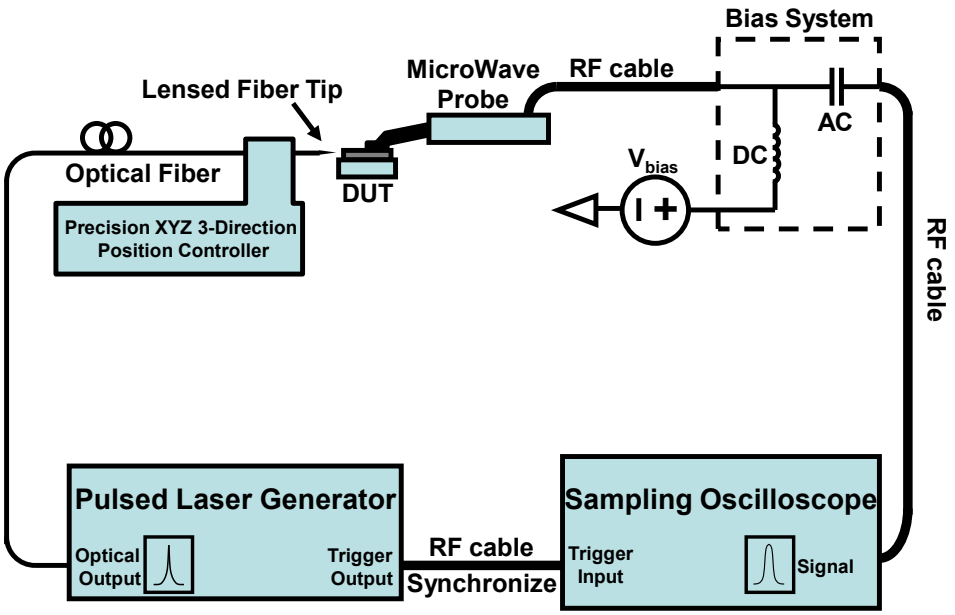

Fig. 4.6: Schematic of temporal response measurement setup.

Time-domain pulse response measurement was used for bandwidth extraction. The configuration of the measurement system is plotted in Fig 4.6. By examination of the response electrical pulse as a result of the incoming optical pulse, the response speed of the device can be derived. The excitation optical pulse is generated with pulse width ~ 80 fs and wavelength of 1550 nm. The electrical pulse from photodetector was measured by a system comprising digital sampling oscilloscope with nominatal 50 GHz bandwidth, bias network and high speed micromave probe.

Regarding the data collection procedure, in the 50 GHz oscilloscope showing the electrical pulse generated from the photodetector, the temporal resolution is adjusted to be the smallest (0.05 ps) and the data sampling window the largest (0.05 ps*4096 data points=205 ps). In this way, for the typical electrical response pulse with ~30 ps foot-to-foot width, there will be 600 sampled points in the pulse region and the 200 ps sampling window is 5 times wider than the pulse. Practically, it is

expected that the high resolution will avoid the possibility of ignoring of details in the pulse and by FFT analyzing the complete length of the sampled 205-ps-long curve; long tail will also be included for the bandwidth calculation.

4.5 Results and Discussion

4.5.1 I-V Characteristics

The current-voltage (I-V) measurement was carried out on both LPD and VPD. Fig. 4.7 (a) shows the typical I-V curves of the devices, demonstrating low leakage current at -1 V bias of 0.44 μA and 0.74 μA for VPD and LPD, respectively, which are both below the 1 μA limit for high speed receiver application [4.8]. For I_{dark} mechanism, each type of device was fitted to more than one mechanism including band-to-band generation [4.8], Shockley-Hall-Read (SHR) effect [4.8] and Poole-Frenkel process [4.9-4.13]. The dark current mechanism of VPD is determined to be trap-assisted generation in the depletion region, the so-called SHR process; while the I-V-temperature behavior of LPD only fits Poole-Frenkel effect which describes the attenuation of the Coulombic potential barrier under the influence of electric field. Fig. 4.7 (b) shows the field dependency of the I_{dark} of LPD considering Poole-Frenkel effect which can be modeled by the following expression:

$$I_{dark} = CE \exp(-\frac{q\Phi - q\Delta\Phi_{PF}}{kT}) \qquad \text{(Eq 4.1)}$$

$$q\Delta\Phi_{PF} = \left(\frac{q^3}{\pi\varepsilon_0 K}\right)^{1/2} E^{\gamma} = \beta_{PF} E^{\gamma} \qquad \text{(Eq 4.2)}$$

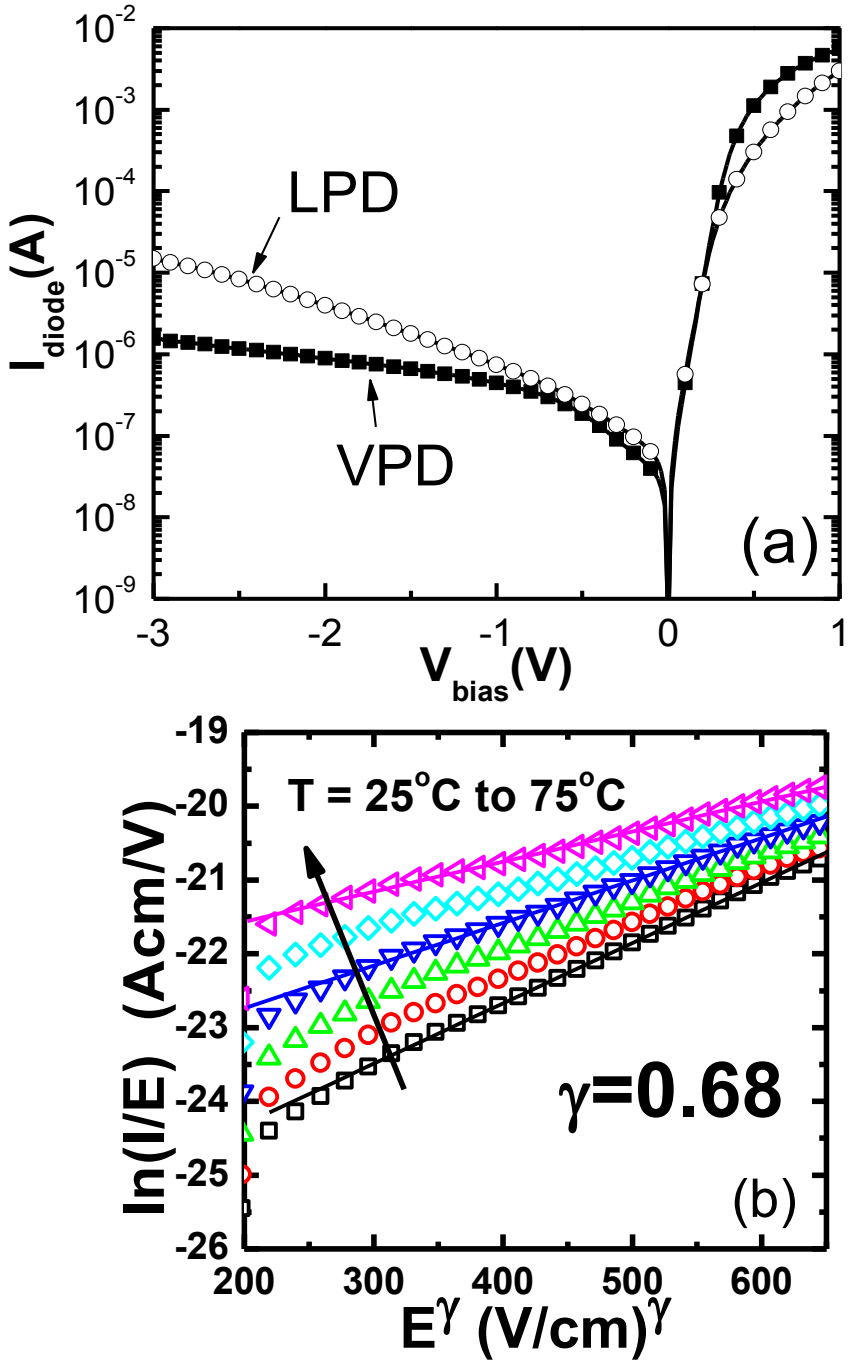

Fig. 4.7: (a) I-V curve of LPD and VPD at room temperature. The I-V characteristics have good uniformity as confirmed by testing more than 20 devices of VPD and LPD, respectively. (b) logarithm of LPD's conductivity ln(I/E) as a function of E^{γ} where γ=0.68. The temperature increment step is 10 °C. Good fit is observed for modified Poole-Frenkel barrier lowering thermal emission model with $E^{0.68}$ dependency.

where C is constant, E is the electric field in i-region, $q\Phi$ is zero-field ionization energy from Coulombic traps , k is Boltzmann const, T is temperature, K is the dielectric const of Ge and γ is a constant ranging from 0.5 to 1 [4.13]. Using the above equation with γ=0.68, the dielectric constant of K=13~21 is extracted at T=298 K to 348 K which is in the range of the theoretical dielectric constant of 16~16.2 for Ge. A field power exponent γ>0.5 for the modified Poole-Frenkel conduction is required due to non-uniform spatial distribution of the traps as well as influence of the electrode on bulk charge [4.13]. From Fig. 4.7 (b), it can be observed that I_{dark} in the LPD can be very well described by the modified Poole-Frenkel effect with a field power exponent of 0.68.

4.5.2 Responsivity Measurement

The method of the responsivity calculation is the same as what is described in [4.7] by Ahn et al.

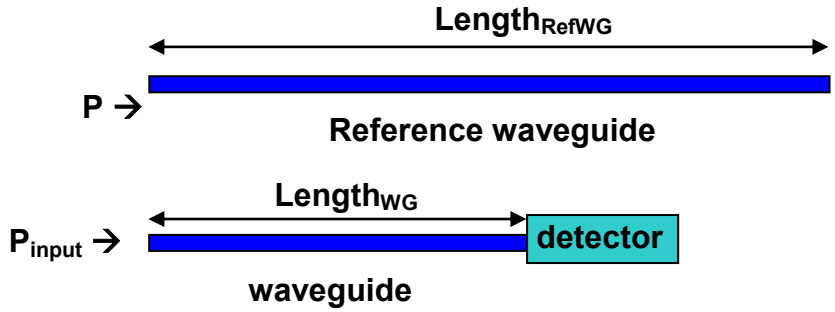

Fig. 4.8: Schematic of responsivity measurement

1. Optical propagation loss α_{WG} is extracted from the adjacent reference waveguide using cut-back method.

2. Fiber-waveguide coupling loss $Loss_{FB\text{-}WG}$ is calculated by subtracting the total propagation loss from the overall loss.

$$Loss_{FB\text{-}WG} = Loss_{total} - \alpha_{WG} * Length_{RefWG.} \quad \text{(Eq 4.3)}$$

3. The power sent into the detector is calculated as follows:

$$P_{detector} = P_{input} \times 10^{(Loss_{FB-WG} + \alpha_{WG} \times Length_{WG})/10} \quad \text{(Eq 4.4)}$$

Where $P_{detector}$ is the power at the input facet of the photodetector; P_{input} is the input light power of the laser equipment; $Length_{WG}$ is the length of the waveguide under test.

4. The responsivity is calculated by the equation below:

$$R_{detector} = \frac{I_{response}}{P_{detector}} \quad \text{(Eq 4.5)}$$

For optical characterization, since the waveguide (width 0.6 μm/height 180 nm) favors Transverse Electric (TE) -mode transmission [4.6], the TE polarization of input laser is chosen to transmit the maximum power to the detector. The fiber-waveguide coupling loss and waveguide propagation loss at λ=1550 nm were estimated 4.0±0.5 dB/facet and 10±1 dB/cm respectively as characterized on adjacent reference waveguides. The responsivity was extracted in a method similar to [4.7]. Fig. 4.9 compares the detectors' responsivity corrected for the losses. For VPDs, responsivity reaches plateau of 0.29 A/W at low onset bias of -0.5 V. The low responsivity is possibly attributed to the large overlap between the optical mode and the highly-doped n+ region in Ge layer since the light absorbed beyond the diffusion

length in Ge n+ region does not contribute to detection. The reasoning is illustrated in the optical mode in Fig. 4.10.

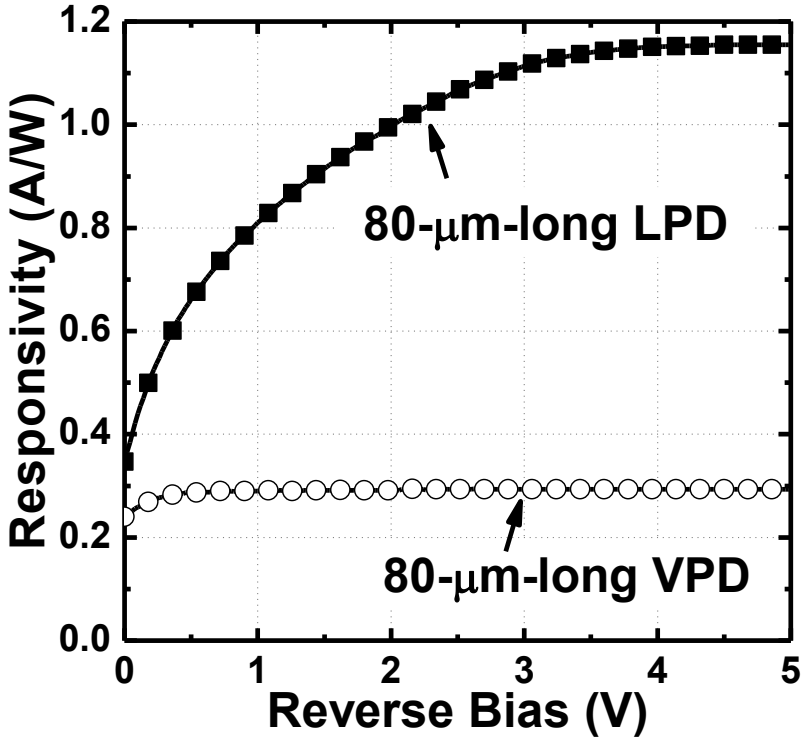

Fig. 4.9: Plot of responsivity of LPD and VPD as a function of reverse bias. The 1.16 A/W responsivity of LPD corresponds to ~90% quantum efficiency. (The theoretical 100%-quantum-efficiency responsivity is 1.25 A/W at wavelength of 1550 nm)

The optical modes for both VPD and LPD are calculated. The optical mode overlap with the highly-doped-region of VPD is seemingly much larger than that of LPD as confirmed by simulation (using beam propagation method (BPM)). To quantify that, the light intensity over the highly-doped (n+, p+) region is integrated; the results show the overlapped light power in VPD is 5 times of that in LPD. This may suggest that the optical mode overlap could be one reason of the lower responsivity of VPD.

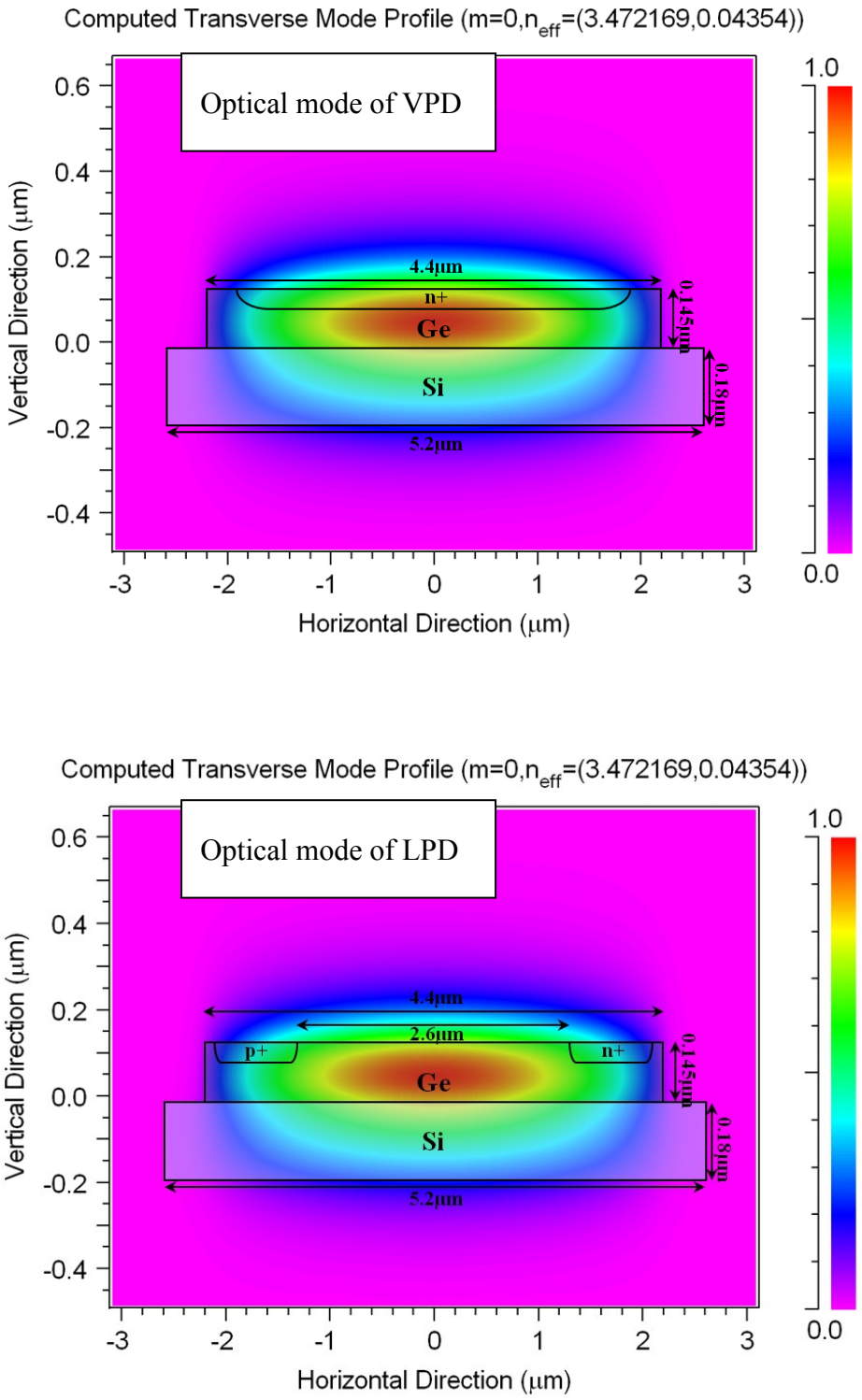

Fig. 4.10: Calculated optical mode of VPD and LPD. The result reveals larger optical mode overlap with highly-doped Ge region in VPD.

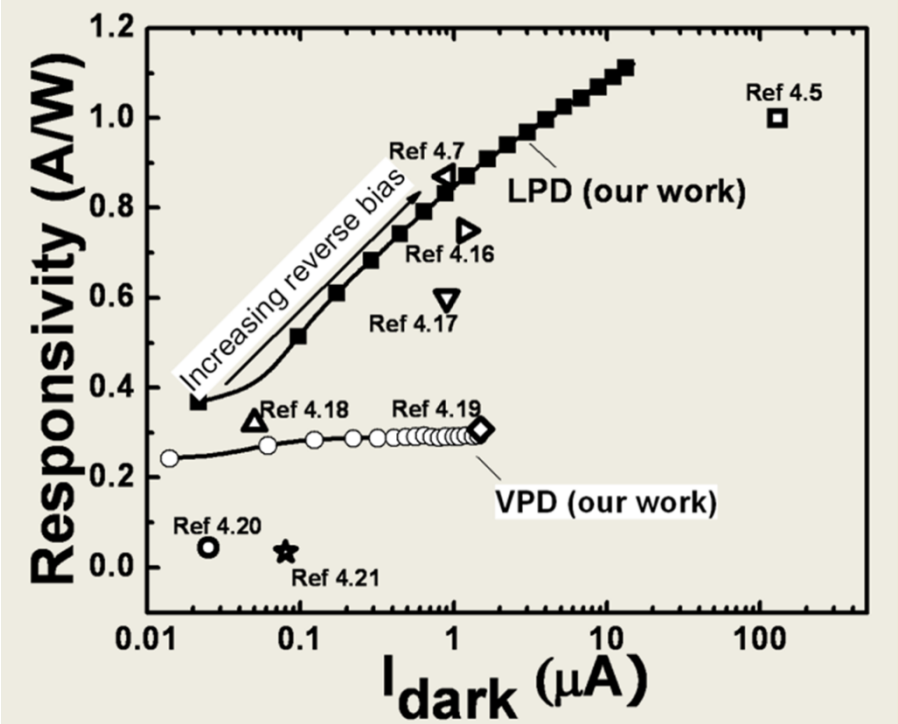

Fig. 4.11: Comparison of the various photodetectors' responsivity and dark current Idark.

Another possible reason is the defects in the Ge/Si interface which could act as recombination centers [4.14] and consume a portion of photogenerated electron/hole. On the other hand, responsivity of LPDs reaches as high as 1.16 A/W which corresponds to ~90% quantum efficiency at -5 V under high electric field across the long intrinsic Ge region horizontally, suggesting low defects in the bulk and surface of the Ge layer. Fig. 4.11 benchmarks current results with previously reported where responsivity is plotted against the logarithm of dark current. By considering both dark current and responsivity, it can be observed that the evanescent-coupled LPD matches to one of the best responsivities for given dark current. For clarity, Table 4.1 shows the comparison of the investigated devices with other groups' work.

Table 4.1: Comparison of the various photodetectors' performance indices.

Reference	structure	Idark(uA)	Responsivity@1550(A/W)	3dB bandwidth (GHz)
Ref [4.5]	waveguided Ge MSM	130@1V	1±0.2@1V	10@1V
Ref [4.7]	waveguided Ge PIN	0.9@1V	0.87@1V	7.2@1V
Ref [4.15]	normal incidence Ge PIN	1.2@1V	0.75@1V	2.5@1V
Ref [4.16]	Ge interdigited lateral PIN	0.9@5V	~0.6 bias condition unknown	1.8@5V
Ref [4.17]	waveguided AlGaInAs-silicon hybrid	0.05@1V	0.32@1V	0.467@4V
Ref [4.18]	waveguide poly-Ge	1.5@30V	0.076@30V	1@30V
Ref [4.19]	waveguide SiGe/Ge multiquantum well	0.1@10V	0.08@10V	---
Ref [4.20]	normal incidence Ge PIN	0.08@1V	0.035@0V	39@2V
This Work VPD	waveguided Ge PIN	0.44@1V	0.29@1V	4.4@1V
This Work LPD	waveguided Ge PIN	0.74@1V	0.81@1V	2.8@1V

*If not mentioned, the data listed is at reverse bias of 1V.

4.5.3 Detector Response Speed

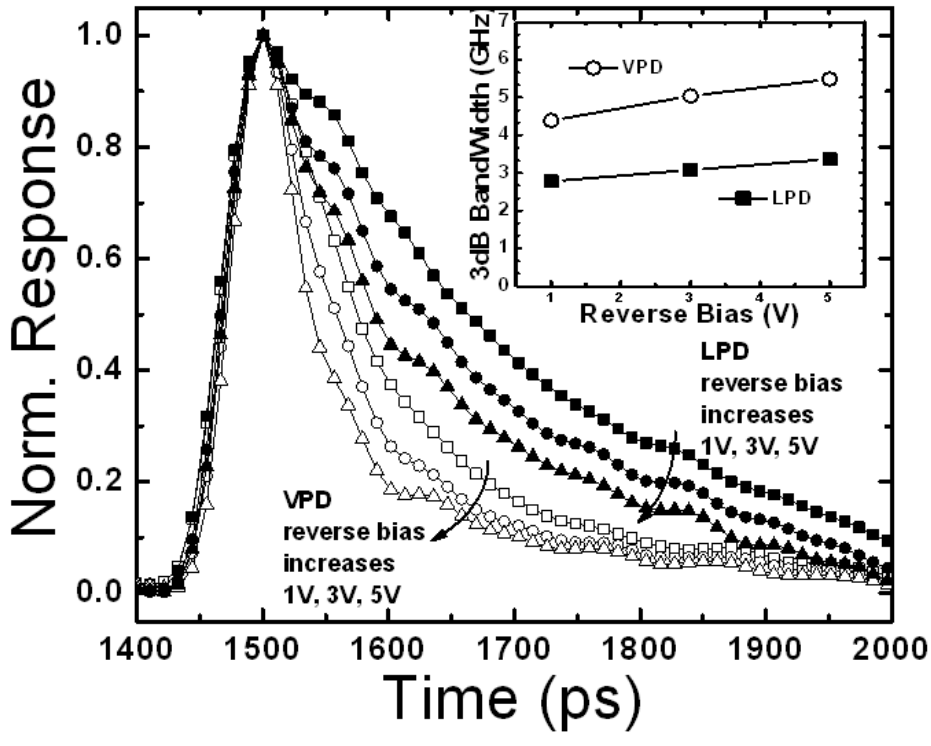

Fig. 4.12: Temporal impulse response of LPD and VPD at 1V, 3V, and 5V reverse bias. Inset shows the 3dB bandwidth of the devices.

The temporal response of both LPD and VPD were measured using 1.55 μm pulsed laser with 80 fs pulse width. Devices were probed with microwave probes and measured with a 15 GHz sampling oscilloscope. DC bias was coupled through a 50 GHz bias tee. Fig. 4.12 shows the pulsed response. The 3-dB bandwidth is 2.8 (LPD) and 4.4 GHz (VPD) at -1 V bias. When reverse bias rose to -5 V, 3dB bandwidth increases to 3.4 (LPD) and 5.5 GHz (VPD). The bandwidth is limited by effects of large parasitic capacitance (~500 fF) from large probe pad [4.7] and large inductance/series-resistance from the narrow metal lines (~4 μm) connecting the devices and the probe pads. The following section discusses the degradation of speed in details.

4.5.4 Speed Degradation Analysis

The overall 3dB bandwidth can be expressed following the equation

$$f_{3dB} = \frac{1}{\frac{1}{f_{RC}} + \frac{1}{f_{transit}}} \qquad \text{(Eq 4.6)}$$

Where f_{RC} is the RC delay limited bandwidth and $f_{transit}$ is the transit time limited bandwidth.

For our device, the layout of the probing pads in the devices is shown schematically in Fig. 4.13. The isolation oxide below the metal pad is 1.5 μm thick.

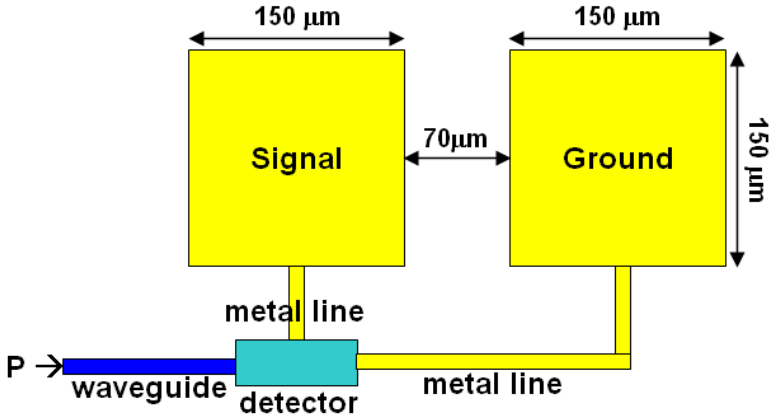

Fig. 4.13: Probing pads for photodetectors bandwidth measurement.

Using a first order approximation, the capacitance of the probe pad can be calculated from a parallel-plate capacitor with the same metal area and 1.5 um oxide in between the plates.

$$C_{pad} = \frac{\varepsilon_{SiO_2}\varepsilon_0 \times A}{d_{SiO_2}} = \frac{3.9 \times 8.85 \times 10^{-12} F/m \times 150 \times 10^{-6} m \times 150 \times 10^{-6} m}{1.5 \times 10^{-6} m} = 518 fF \quad \text{(Eq 4.7)}$$

Accordingly, the Resistance-Capacitance (RC) delay limited speed is then given by

$$f_{RC} = \frac{1}{2\pi RC} = \frac{1}{2 \times 3.14 \times 50\Omega \times 518 fF} = 6\ GHz \quad \text{(Eq 4.8)}$$

On the other hand, the transit time limit bandwidth can be calculated using equation 2.1 as follows,

For VPD:

$$f_{transit} = 0.45 \times \frac{v}{d} = 0.45 \times \frac{6 \times 10^6\ cm/s}{120\ nm} = 225\ GHz \quad \text{(Eq 4.9)}$$

For LPD:

$$f_{transit} = 0.45 \times \frac{v}{d} = 0.45 \times \frac{6 \times 10^6\ cm/s}{2.6\ \mu m} = 10\ GHz \quad \text{(Eq 4.10)}$$

As can be seen, the RC delay limited 3dB frequency is much than transit time limited cut-off frequency for both cases of VPD and LPD. Therefore, large capacitance induced by the large area of the probe pads is one of the major limiting factors of the devices' speed.

Using equations 4.6 to 4.10, the overall 3dB frequency can be calculated to be 5.8 GHz for VPD and 3.4 GHz for LPD. This is in agreement with our experimental results.

The low speed of the devices is not at all unexpected given the fact that the devices are our first attempt which is designed only for resolving the problems of (material) Ge epi growth on Si and (DC performance) higher responsivity. As a result, the high-speed-required design is not included in this batch, such as Ground-Signal-Ground (GSG) metal line configuration, proper microwave transmission line, and small probe pad.

4.6 Conclusion

In this chapter, it is demonstrated lateral Ge PIN with comparison to the vertical p-Si/i-Ge/n-Ge PIN photodetectors, both monolithically integrated with Si-waveguides on a SOI platform. From the results and analysis, given sufficiently low dark current, optimizing the probe pads' and metal lines' design, and shortening the p/n spacing in lateral PIN configuration are expected to achieve higher detector speed with maintained high responsivity.

REFERENCES

[4.1] L. Colace, G. Masini, and F. Galluzi, G. Assanto, "Ge-on-Si approaches to the detection of near-infrared light", IEEE J. Quantum Electron., vol. 35, pp. 1843-1852, Dec. 1999.

[4.2] H. -C. Luan, D. R. Lim, K. K. Lee, K. M. Chen, J. G. Sandland, K. Wada and L. C. Kimerling, "High-quality Ge epilayers on Si with low threading-dislocation densities", Appl. Phys. Lett., vol. 75, pp. 2909-2911, Nov. 1999.

[4.3] W. Y. Loh, J. Wang, J. D. Ye, R. Yang, H. S. Nguyen, K. T. Chua, T. H. Loh, Y. Z. Xiong, S. J. Lee, M. B. Yu, G. Q. Lo, and D. L. Kwong, "Impact of Local Strain from Selective-Epitaxial-Germanium with Thin Si/SiGe-Buffer for High-Performance p-i-n Photodetector with Low-Thermal Budget", IEEE Electron Dev. Lett., vol 28, pp. 984-986, Nov. 2007.

[4.4] L. C. Kimerling, D. Ahn, A. B. Apsel, M. Beals, D. Carothers, Y-K. Chen, T. Conway, D. M. Gill, M. Grove, C-Y Hong, M. Lipson, J. Liu, J. Michel, D. Pan, S. S. Patel, A. T. Pomerene, M. Rasras, D. K. Sparacin, K-Y. Tu, A. E. White and C. W. Wong, "Electronic-photonic integrated circuits on the CMOS platform", Proc. SPIE, vol. 6125, pp. 612502-612511, Mar. 2006.

[4.5] L. Vivien, M. Rouvière, J.-M. Fédéli, D. M.-Morini, J.-F. Damlencourt, J. Mangeney, P. Crozat, L. E. Melhaoui, E. Cassan, X. L. Roux, D. Pascal and S. Laval, "High speed and high responsivity germanium photodetector integrated in a Silicon-On-Insulator microwaveguide", Opt. Express, vol. 15, pp. 9843-9848, Jul. 2007.

[4.6] J. F. Liu, D. Ahn, C. Y. Hong, D. Pan, S. Jongthammanurak, M. Beals, L. C. Kimerling, J. Michel, A. T. Pomerene, D. Carothers, C. Hill, M. Jaso, K. Y. Tu, Y. K. Chen, S. Patel, M. Rasras, D. M. Gill and A. E. White, "Waveguide Integrated Ge p-i-n Photodetectors on a Silicon-on-Insulator Platform", Optoelectronics, 2006 Optics Valley of China International Symposium, pp. 1-4, Nov. 2006.

[4.7] D. Ahn, C. Y. Hong, J. F. Liu, W. Giziewicz, M. Beals, L. C. Kimerling, J. Michel, J. Chen and F. X. Kärtner, "High performance waveguide integrated Ge photodetectors", Opt. Express, vol. 15, pp. 3916-3921, Apr. 2007.

[4.8] S. J. Koester, L. Schares, C. L. Schow, G. Dehlinger, and R. A. John, "Temperature-dependent analysis of Ge-on-SOI photodetectors and receiver", Proc. Group IV Photonics Conference, pp. 179-181, Sep. 2006.

[4.9] J. G. Simmons, "Conduction in thin dielectric films", J. Phys. D: Appl. Phys., vol. 4, pp. 613-657, May. 1971.

[4.10] A. IIie and B. Equer, "Field-enhanced generation in hydrogenated amorphous silicon", Phys. Review B, vol. 57, pp. 15349-15359, Jun. 1998.

[4.11] W. R. Harrell and J. Frey, "Observation of Poole-Frenkel effect saturation in SiO2 and other insulating films", Thin Solid Films, vol. 352, pp. 195-204, Sep. 1999.

[4.12] M. M. Abdul-Gader jafar, “High-bias current-voltage-temperature characteristics of undoped rf magnetron sputter deposited boron carbide (B5C) / p-type crystalline silicon heterojunctions”, Semicond. Sci. Technol., vol. 18, pp. 7-22, Jan. 2003.

[4.13] P. C. Arnett and N. Klein, “Poole-Frenkel conduction and neutral trap”, J. Appl. Phys., Vol. 46, pp. 1399-1400, Mar. 1975.

[4.14] L. M. Giovane, H.-C. Luan, A. M. Agarwal, and L. C. Kimerling, “Correlation between leakage current density and threading dislocation density in SiGe p-i-n diodes grown on relaxed graded buffer layers”, Appl. Phys. Lett., vol. 78, pp. 541-543, Jan. 2001.

[4.15] S. Fama, L. Colace, G. Masini, G. Assanto, H.-C. Luan, “High performance germanium-on-silicon detectors for optical communications”, Appl. Phys. Lett., vol. 81, pp. 586-588, Jul. 2002.

[4.16] J. Oh, S. Csutak, and J. C. Campbell, “High-Speed Interdigitated Ge PIN Photodetectors”, IEEE Photonics Technol. Lett., vol. 14, pp. 369-371, Mar. 2002.

[4.17] H. Park, A. W. Fang, R. Jones, O. Cohen, O. Raday, M. N. Sysak, M. J. Paniccia, and J. E. Bowers, “A hybrid AlGaInAs-silicon evanescent waveguide photodetector”, Opt. Express, vol. 15, pp. 6044-6052, May. 2007.

[4.18] L. Colace, G. Masini, and G. Assanto, “ Guided-wave near-infrared detector in polycrystalline germanium on silicon”, Appl. Phys. Lett., vol. 87, pp. 203507 (3 pages), Nov. 2005.

[4.19] B. Li, G. Li, E. Liu, Z. Jiang, J. Qin and X. Wang, “Monolithic integration of a SiGe/Si modulator and multiple quantum well photodetector for 1.55 um operation”, Appl. Phys. Lett., vol. 73, pp. 3504-3505, Dec. 1998.

[4.20] M. Jutzi, M. Berroth, G. Wöhl, M. Oehme, and E. Kasper, “Ge-on-Si vertical incidence photodiodes with 39-GHz bandwidth”, IEEE Photonics Technol. Lett., vol. 17, pp. 1510-1512, Jul. 2005.

CHAPTER 5

5. Low-Voltage High-Speed Evanescent-Coupled Thin-film-Ge Lateral PIN Photodetectors Integrated on Si-Waveguide

5.1 Introduction

From the first attempt of waveguided Ge photodetector fabrication demonstrated in Chapter 4, it is found that the detector's 3dB bandwidth is limited by the large device capacitance due to relatively long device length of 100 μm together with parasitic effects. In the second attempt presented in this chapter, much higher speed was obtained by employing new device designs.

5.2 Background

Si-based electronic-photonic integrated circuit has gained increasing attention as a promising candidate for next generation semiconductor technology [5.1]. Being an important part of the building blocks, Ge is the best choice for photodetection (1.3-1.55 μm) for its process compatibility with the Si platform. In spite of 4.2% lattice mismatch between Ge and Si substrate, high quality Ge growth on Si has been demonstrated [5.1-5.5]. Taking advantage of selective-epitaxy growth in small area, a modified two-step Ge epitaxy procedure is developed where an ultra-low temperature

SiGe buffer is introduced in additional to the low/high temperature prepared Ge layer, with dislocation density in Ge as low as 6×10^{6} cm^{-2} without subsequent anneal [5.6]. As device performance is improved in terms of dark current and responsivity and speed, the key to further improvement lies in the optimization of the detector structure. Waveguided detection scheme, where the light absorption is perpendicular to current collection, is capable to achieve high absorption efficiency and high speed simultaneously due to the de-coupling of the efficiency from thickness [5.1]. Different coupling schemes, e.g., evanescent- and butt-coupling, and different detector structures, e.g., Metal-Semiconductor-Metal (MSM) [5.7] and vertical Ge PIN [5.2, 5.8] have been reported. In Chapter 4, another typical Ge detector structure, i.e., lateral PIN-integrated with Si waveguide is demonstrated, and the vertical PIN and lateral PIN waveguided photodetectors are compared, both exhibiting reasonably good device performance. It is shown that when Ge photodetection layer thickness is reduced to ~ 200 nm for effectively cost saving, lateral PIN structure can achieve much higher quantum efficiency as compared to vertical PIN due to less light consumption in the highly-doped region while achieving similar response speed [5.10].

In this chapter, the excellent scalability of the waveguided lateral PIN Ge detectors is further demonstrated targeting for low voltage operation (-1 V). With shrunk detector dimensions, the device with thin Ge (~220 nm) showed low dark

current (~0.06 μA), high internal responsivity (~0.65 A/W) with speed as high as ~18 GHz.

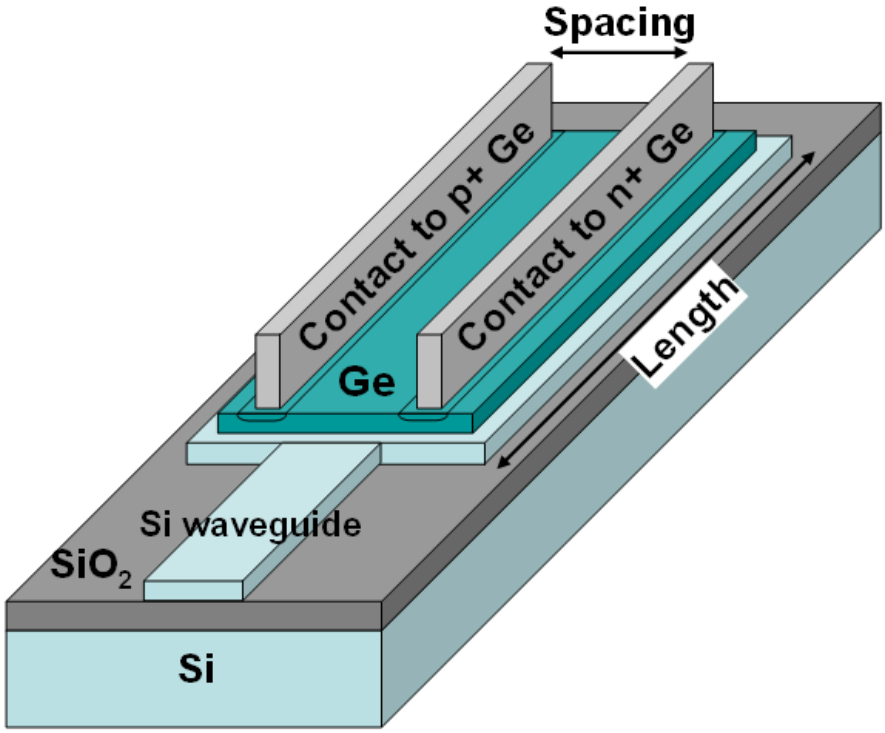

Fig. 5.1: The schematic structure of lateral PIN configurations.

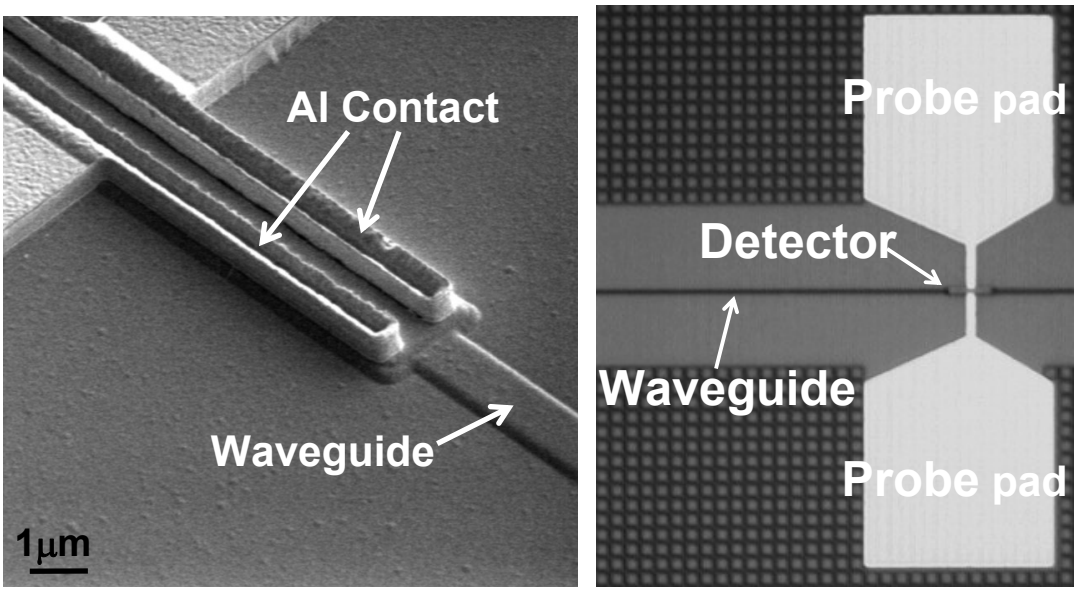

Fig. 5.2: The schematic structure of lateral PIN configurations.

5.3 Experimental

The process started with 8" (100) silicon-on-insulator (SOI) wafer with 180-nm-thick top p-type Si (~8-15 Ωcm) on 1 μm buried oxide. Si-waveguide and detector regions were patterned by 248 nm deep-ultra-violet lithography and reactive-ion-etching. Subsequently, plasma enhanced chemical vapor deposition (PECVD) oxide (~150 nm) was deposited, patterned and dry/wet etched to form square windows for later selective Ge epitaxial growth. The square windows defined the Ge-photodetector area, with width of 2.4 μm and length in range of 5-20 μm. After standard cleaning, Si seed layer (~10 nm, 500 °C), $Si_{0.8}Ge_{0.2}$ (~25 nm, 350-400 °C) buffer layer, low-temperature Ge seed (~10 nm, 400 °C), and high-temperature Ge (~180 nm, 600 °C) were sequentially deposited in a ultra-high vacuum chemical vapor deposition (UHVCVD) chamber with base pressure of 7×10^{-9} Torr [5.5]. The samples were implanted with BF_2 or As of the same condition (dose 1×10^{15} cm^{-2}, energy 15 keV) to the corresponding area to form p+/n+ regions. The dopants were thermally activated at 600 °C for 1s. After SiO_2 deposition and contact formation, TaN (25 nm) and Al (0.75 μm) were deposited and patterned. Fig. 5.1 illustrates the schematic of the lateral PIN detector. The light propagates through the Si waveguide into the detector region, and then couples evanescently into the overlying Ge region where absorption occurs. A scanning-electron-microscope (SEM) picture of the fabricated device is shown in Fig. 5.2.

5.4 Results and Discussion

For the devices with length of 20 μm and spacing of 0.8 μm, Fig. 5.3 shows the typical temperature-dependant current-voltage characteristics. At room temperature, the device has a good rectifying characteristic with low leakage current of 0.06 μA. The low leakage renders the devices more-than-acceptably suitable for high speed receiver application which requires dark current below 1 μA [5.9]. Fig. 5.4 shows the Arrhenius plot of the dark current $I_{dark}/T^{3/2}$ with activation energy of Ea ~ 0.31 eV, which corresponds to roughly half of the Ge bandgap (~ 0.66 eV), suggesting thermal generation and recombination of carriers in the intrinsic Ge layer as the major dark current mechanism.

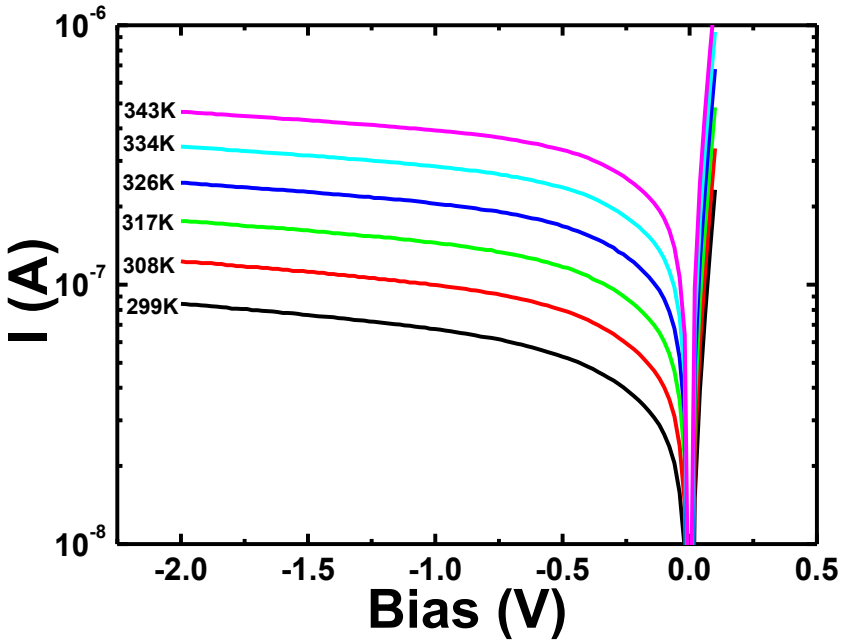

Fig. 5.3: Dark current for lateral Ge PIN photodiodes.

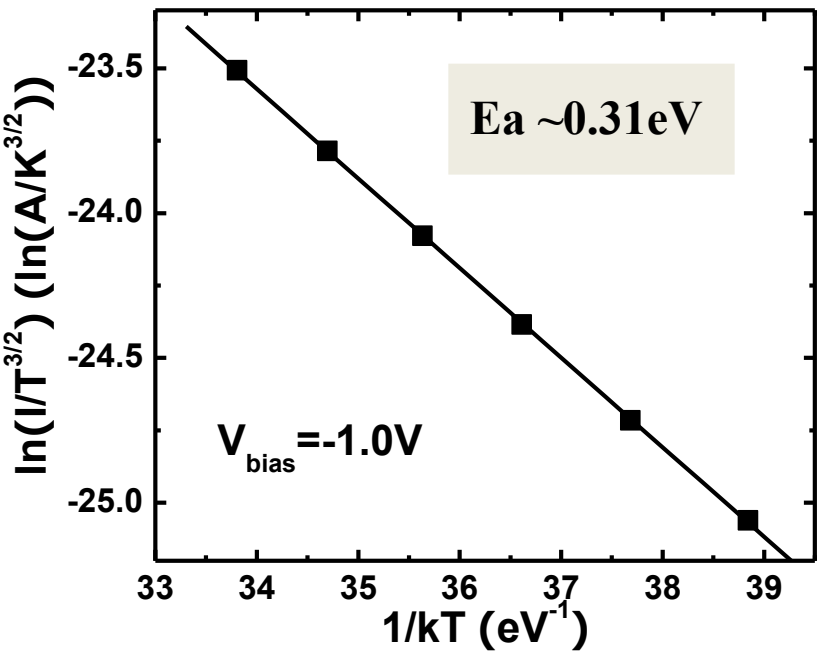

Fig. 5.4: Arrhenius plot of dark current for lateral PIN Ge photodiodes on SOI substrates. Selective epitaxial Ge on SOI substrate shows trap assisted tunneling due to Shockley-Hall-Read (SHR) process with activation energy ~ 0.31 eV.

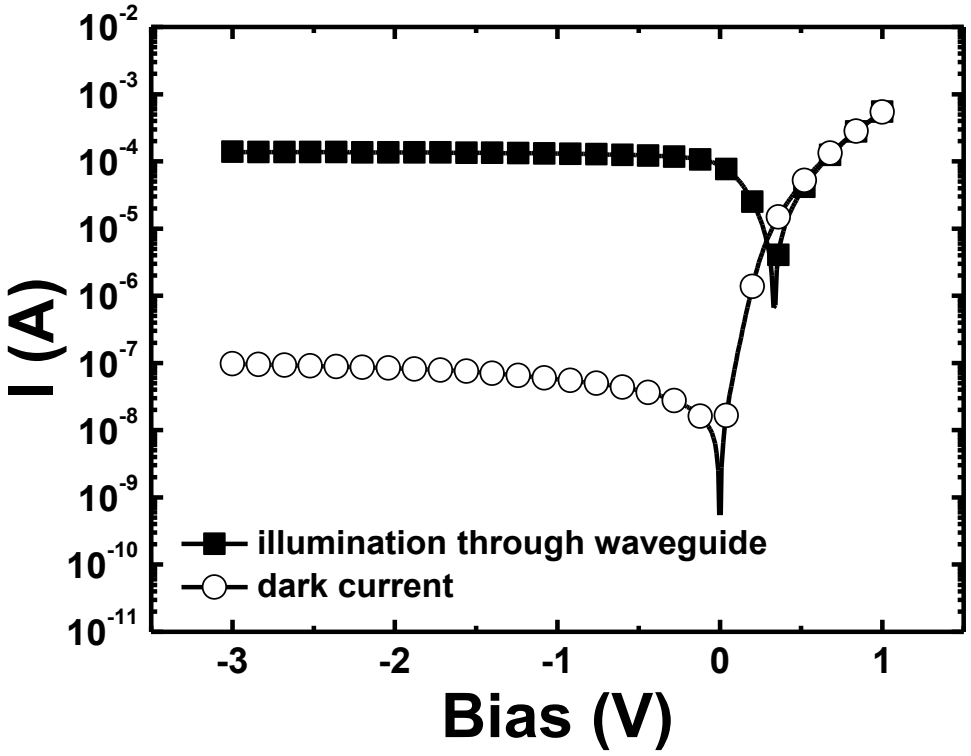

Fig. 5.5: IV curve with and without 1550 nm illumination for a typical 20 µm-long device.

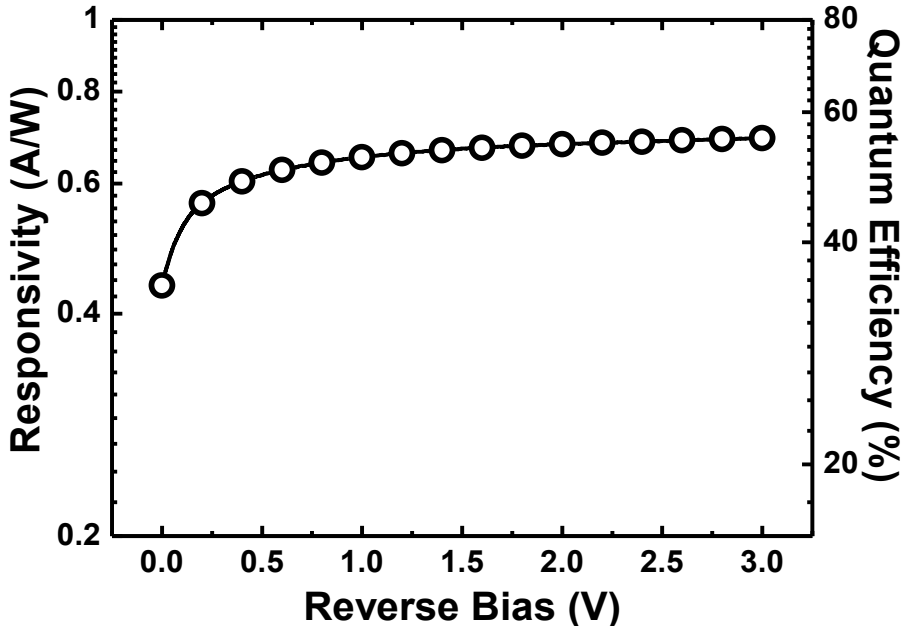

Fig. 5.6: 20 μm-long lateral Ge PIN photodiode's responsivity/quantum efficiency at wavelength of 1550 nm.

For the optical characterization, since the Si waveguide (width/height of 0.6 μm/180 nm) favors transverse electric (TE) mode transmission, to deliver high power to the detector, TE polarization of input laser was chosen. Fig. 5.5 shows I-V characteristics of a waveguide-integrated 20-μm-long Ge PIN diode, with and without 1550 nm laser coupled into the detector through the Si waveguide. Fig. 5.6 plots the device's responsivity together with the corresponding quantum efficiency. The photocurrent reaches maximum at reverse bias below 1 V, suggesting that even under low bias strong horizontal electric field exists in Ge intrinsic region indicating good Ge material quality. With the laser power of 1 mW at the end of the lensed fiber, the device under -1 V bias shows ~130 uA response current corresponding to an external responsivity of 0.13 A/W. Furthermore, the fiber-waveguide coupling loss and waveguide propagation loss at λ =1550 nm were estimated ~ -5± 0.5 dB/facet and ~ -

10±1 dB/cm respectively as characterized on adjacent reference waveguides. Using the same method described in [5.8], the power reaching the Ge detector was estimated to be ~200 μW. Thus the internal responsivity of the 20-μm-long detector is calculated to be ~ 0.65± 0.07 A/W. According to simulation using beam propagation method (BPM), the mode-conversion loss between Si waveguide and the Ge/Si region calculated to be -0.27 dB and 20 μm length is enough for ~90% quantum efficiency when absorption coefficient of 4000 cm^{-1} is assumed for tensile strained Ge [5.11]. The difference between simulation and experimental result could be attributed to the Si up-diffusion into Ge layer which results in reduced Ge absorption coefficient.

Table 5.1: Performance comparison of the fabricated photodetectors.

Source	Structure	Ge thickness (nm)	Spacing (μm)	Length (μm)	I_{dark} @-1 V (nA)	Resp. @λ=1.55 μm @-1V (A/W)	3dB BW @-1 V (GHz)
[5.8]	Normal incidence PIN	800	0.3	-	80	-	25@0 V 39@-2 V
[5.6]	WG vertical PIN	1100	1.1	10	900	0.87	7
[5.7]	WG MSM	330	1	10	10^5	1	10
[5.2]	WG vertical PIN	800	0.7	100	267 @-2 V	1.16@-2 V	10@0 V 29.4@-2 V
This Work	WG lateral PIN	220	0.8	5	15	0.4	18
				10	30	0.5	
				15	45	0.58	
				20	60	0.65	

It can be seen that, with comparable device performance, the detectors' Ge detection layer thickness is the thinnest which is critical for effective cost reduction in future industrialized massive integration.

The temporal response of the detector were measured using 1.55 μm pulsed laser with 80 fs pulse width. Devices were probed with microwave probe and measured with a 50 GHz sampling oscilloscope. DC bias was coupled through a 50 GHz bias tee. Fig. 5.7 shows the typical pulse response of a 20-μm-long detector under 1 V reverse bias. The full-width-at-half-maximum (FWHM) is 17 ps. The Fast Fourier Transform (FFT) of the temporal pulse curve indicates a 3dB electrical bandwidth of 18 GHz. Fig. 5.8 shows the bandwidth of the device with applied reverse voltage of 1, 3, 5, 10 V. As can be seen, the bandwidth saturates at 18.5 GHz with reverse bias voltage larger than 5 V.

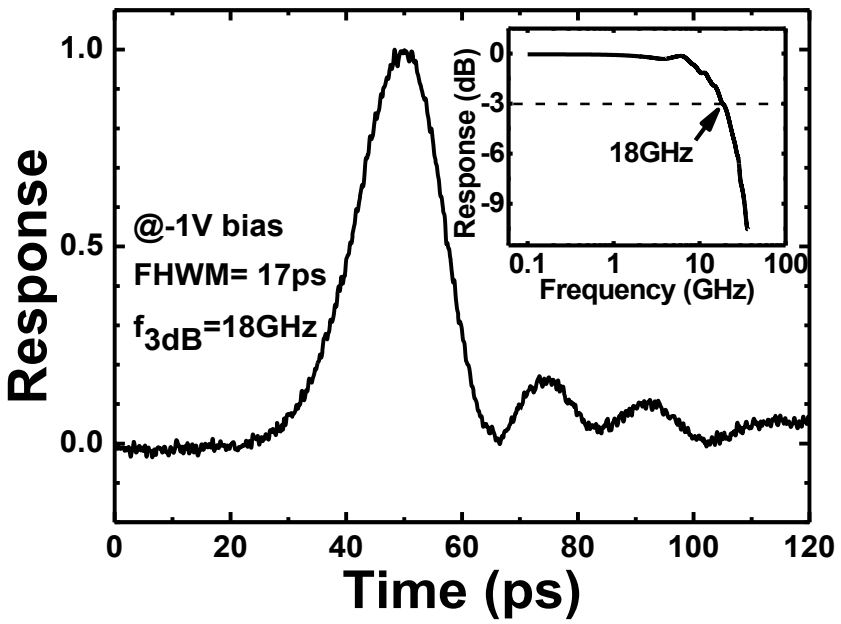

Fig. 5.7: Temporal impulse response of 20 μm-long detector at -1 V reverse bias. Inset shows Fourier transform of the data.

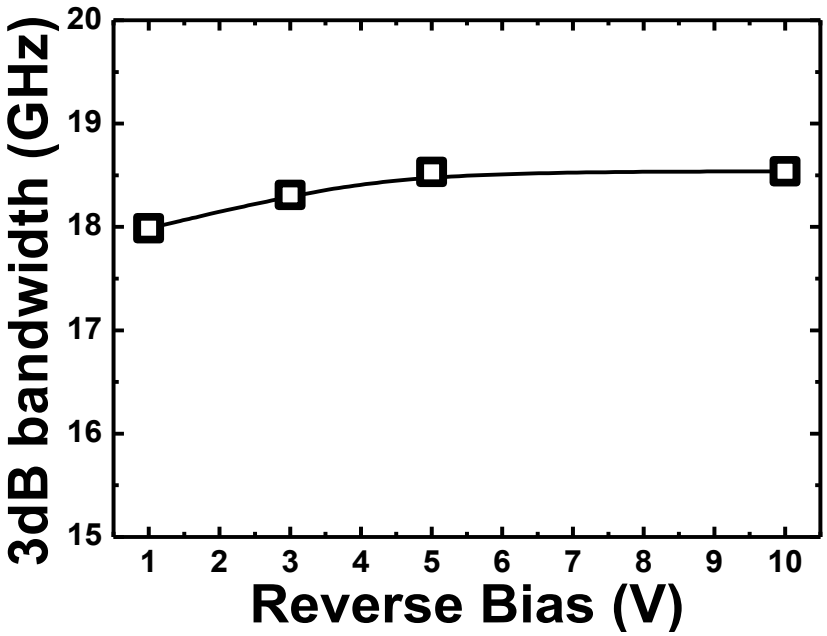

Fig. 5.8: 3dB bandwidth of the device vs. bias voltage.

The experimental speed results agree well with the estimation considering both resistance-capacitance (RC) delay and transit time limitations. It is worth noting that due to the lateral layout of P and N regions, the device's PN junction area was determined by the detector length and Ge thickness. This difference from the vertical PIN structure makes the intrinsic depletion capacitance in lateral PIN diode much smaller than the capacitance from vertical structure due to the small junction area as a result of thin Ge layer. For 20-μm-long device, the intrinsic depletion capacitance is estimated to be 0.8 fF which is negligible compared with the calculated probe pad (80× 80 μm^2) capacitance of 133 fF. Therefore, the overall device capacitance mainly comes from the parasitic effect, namely the probe pad capacitance. Using R=50 Ω of the osillopscope, the estimated RC limited bandwidth is $f=(2\pi RC)^{-1}$=23.8 GHz. Using the electron and hole drift saturation velocities of 6× 10^6 cm/s [5.13, 5.14], the transit-

time limited bandwidth for the 0.8 μm-spacing detector is 33.2 GHz. Hence, combining these two factors, the estimated overall bandwidth is 19.3 GHz, which is close to the experiment. While the experiment fits well with the theory, further work is needed for direct frequency-domain measurement which is necessary for comprehensive analysis of the detectors' speed performance.

As suggested in the calculation above, excluding the probe pad capacitance effects, the detector's intrinsic speed is expected to be limited only by the carrier transit time and the expected bandwidth is ~30 GHz. In fact, due to the low intrinsic capacitance which is the merit of the lateral PIN structure, one can increase the responsivity by fabricating longer device with well remained high speed. According to the simulation, 100-μm-long photodiode with the same P/N spacing will show 90% quantum efficiency and maintained high speed with only 3.2 fF depletion capacitance larger than the 20-μm-long device.

Figs. 5.9 shows eye diagrams obtained with a 20-μm-long device at a reverse bias of 1 V using 10 Gbit/s Digital Communication Analyzer (DCA) and a commercially available 40 Gbit/s $LiNbO_3$ modulator. The eye aperture is satisfactory. It is worthwhile underlining that a low reverse bias is an important characteristic for electrical compatibility with silicon high-speed electronics.

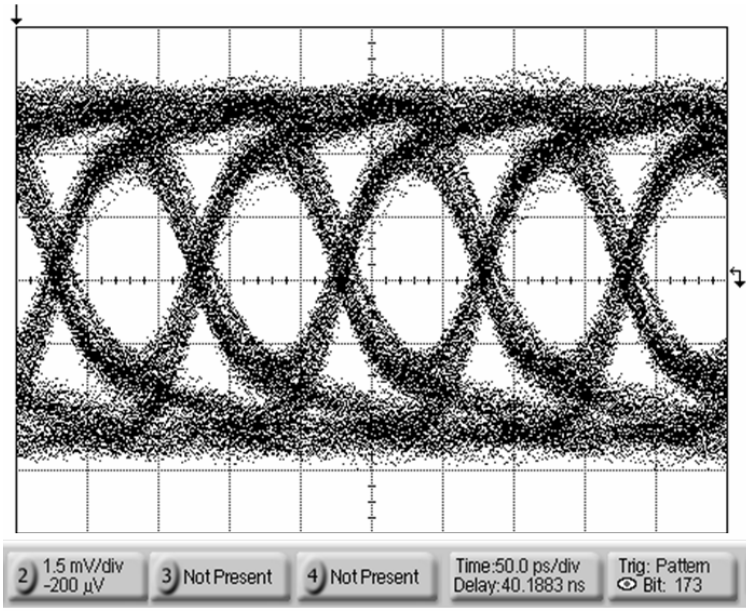

Fig. 5.9: Eye diagrams at 10 Gbit/s in a 20-µm-long detector reverse biased at 1 V.

5.5 Conclusion

In this chapter, scaled thin-film-Ge lateral PIN photodetectors monolithically integrated with Si-waveguides on a SOI platform is demonstrated. From the results and analysis, given thin Ge layer and sufficiently low dark current, increasing the device length and optimizing the probe pads' design are expected to achieve improved responsivity and much higher detector speed.

REFERENCES

[5.1] L. C. Kimerling, D. Ahn, A. B. Apsel, M. Beals, D. Carothers, Y-K. Chen, T. Conway, D. M. Gill, M. Grove, C-Y Hong, M. Lipson, J. Liu, J. Michel, D. Pan, S. S. Patel, A. T. Pomerene, M. Rasras, D. K. Sparacin, K-Y. Tu, A. E. White and C. W. Wong, "Electronic-photonic integrated circuits on the CMOS platform", Proc. SPIE, vol. 6125, pp. 612502-612511, Mar. 2006.

[5.2] T. Yin, R. Cohen, M. M. Morse, G. Sarid, Y. Chetrit, D. Rubin, and M. J. Paniccia, "31 GHz Ge n-i-p waveguide photodetectors on Silicon-on-Insulator substrate", Opt. Express, vol. 15, pp. 13965-13971, Oct. 2007.

[5.3] T. Yin, R. Cohen, M. M. Morse, G. Sarid, Y. Chetrit, D. Rubin, and M. J. Paniccia, "40Gb/s Ge-on-SOI waveguide photodetectors by selective Ge growth", Conf. Optical Fiber Communications, OFC 2008, paper OMK2, Feb. 2008.

[5.4] S. J. Koester, C. L. Schow, L. Schares, G. Dehlinger, J. D. Schaub, F. E. Doany, and R. A. John, "Ge-on-SOI-Detector/Si-CMOS-Amplifier Receivers for High-Performance Optical-Communication Applications", IEEE Journal of Lightwave Technology, vol.25, no.1, pp. 46-57, Jan. 2007.

[5.5] W. Y. Loh, J. Wang, J. D. Ye, R. Yang, H. S. Nguyen, K. T. Chua, J. F. Song, T. H. Loh, Y. Z. Xiong, S. J. Lee, M. B. Yu, G. Q. Lo, and D. L. Kwong, "Impact of Local Strain from Selective-Epitaxial-Germanium with Thin Si/SiGe-Buffer for High-Performance p-i-n Photodetector with Low-Thermal Budget", IEEE Electron Dev. Lett., vol. 28, pp. 984-986, Nov. 2007.

[5.6] T. H. Loh, H. S. Nguyen, C. H. Tung, A. D. Trigg, G. Q. Lo, N. Balasubramanian, and D. L. Kwong, "Ultrathin low temperature SiGe buffer for the growth of high quality Ge epilayer on Si(100) by ultrahigh vacuum chemical vapor deposition", Appl. Phys. Lett. , 90, pp. 092108, Feb. 2007.

[5.7] L. Vivien, M. Rouvière, J. -M. Fédéli, D. Marris-Morini, J. F. Damlencourt, J. Mangeney, P. Crozat, L. El Melhaoui, E. Cassan, X. Le Roux, D. Pascal, and S. Laval, "High speed and high responsivity germanium photodetector integrated in a Silicon-On-Insulator microwaveguide", Opt. Express, vol. 15, pp. 9843-9848, Jul. 2007.

[5.8] D. Ahn, C. Y. Hong, J. Liu, W. Giziewicz, M. Beals, L. C. Kimerling, J. Michel, J. Chen, and F. X. Kärtner, "High performance waveguide integrated Ge photodetectors", Opt. Express, vol. 15, pp. 3916-3921, Apr. 2007.

[5.9] S. J. Koester, L. Schares, C. L. Schow, G. Dehlinger, and R. A. John, "Temperature-dependent analysis of Ge-on-SOI photodetectors and receiver", Proc. Group IV Photonics Conference, pp. 179-181, Sep. 2006.

[5.10] J. Wang et al., "Evanescent-Coupled Ge-PIN Photodetectors on Si-Waveguide with SEG-Ge and Comparative Study of Lateral and Vertical PIN Configurations", accepted for publication in IEEE Electron Dev. Lett., 2008.

[5.11] J. Liu, D. D. Cannon, K. Wada, Y. Ishikawa, S. Jongthammanurak, D. Danielson, J. Michel, and L. C. Kimerling, "Tensile strained Ge p-i-n

photodetectors on Si platform for C and L band telecommunications," Appl. Phys. Lett. vol. 87, pp. 011110, Jul. 2005.

[5.12] M. Jutzi, M. Berroth, G. Wohl, M. Oehme, and E. Kasper, "Ge-on-Si vertical incidence photodiodes with 39-GHz bandwidth", IEEE Photonics Technology Lett., vol. 17, pp. 1510-1512, Jul. 2005.

[5.13] Jacoboni, F. Nava, C. Canali and G. Ottaviani, "Electron dirft velocity and diffusivity in germanium", Phys. Rev. B, vol. 24, pp. 1014-1026, Jul. 1981.

[5.14] E. J. Ryder, "Mobility of Holes and Electrons in High Electric Fields", Phys. Rev., vol. 90, pp. 766-769, Jun. 1953.

CHAPTER 6

6. Enhanced Sensitivity of Small Size Junction-Field-Effect-Transistor-Based Germanium Photodetector

6.1 Introduction

In the previous chapters, high performance Ge-on-Si photodiodes are fabricated and characterized. In this chapter, to address the issues related to photodiodes' further scalability, novel structures of photodetectors, namely Junction-Field-Effect-Transistor (JFET)-Based photodetectors, are demonstrated.

6.2 Background

State-of-the-art electronics technology requires integration with photonics as clock delivery system and data bus to quench the increasing speed degradation and heat dissipation issues of conventional metal interconnections [6.1]. Ge photodetectors, being one of the critical components for low-cost Si-based OEIC (Opto-Electronics Integrated Circuit), have been successfully demonstrated by many with good performance [6.2, 6.3]. However, due to its inherent limitations, current PN/PIN diode based Ge photodetectors suffer from serious scalability issues where further scaling-down of photodiodes inevitably leads to insufficient light absorption

and reduced quantum efficiency [6.4]. Thus, novel structures of photodetectors, which employ optical gain to maintain detection efficiency even with small detector size, have attracted increasing research interest based on both group IV [6.5, 6.6] and III-V materials [6.7-6.9]. Sahni et al. [6.6] demonstrated a highly scalable Ge photodetector based on a junction field-effect-transistor (JFET) structure whose dimensions are comparable with that of modern MOSFETs (Metal-Oxide-Semiconductor Field-Effect Transistor). However, the reported device sensitivity (I_{on}/I_{off} ratio: ~1.33) and response time (FWHM: ~3 ns) are behind that of typical large area photodiode. It was suggested the poor performance is mainly due to the low-temperature MBE-grown Ge gate where high density of defects act as recombination centers and thus reduce the photocarrier collection efficiency.

In this chpater, a novel Ge epi-growth technique of two-step Ge growth combining with a SiGe buffer was applied in Ge gate formation. With the high quality Ge gate, a JFET-based Ge photodetector is demonstrated with dramatically improved sensitivity (I_{on}/I_{off} = 185) and response time (FWHM=110 ps, rise time=10 ps). Together with the maintained merit of large scalability, the device suggests a promising solution to image sensor integrated with CMOS circuit and future small-footprint-area photodetector for optical interconnections.

6.3 Experimental

Starting with 8" (100) p-type (~6-9 Ωcm) Si-substrate, active regions were defined by optical lithography and dry etch. The wafer was implanted with Boron 1×10^{11} cm^{-2}/20 keV and source/drain were patterned and implanted with Boron 1×10^{15} cm^{-2}/7 keV. After 1000 °C/5s activation, the junction depth in channel region is estimated to be ~150 nm. Subsequently, plasma-enhanced-chemical-vapor-deposition oxide of ~150 nm was deposited on the surface, patterned and dry/wet etched to form square windows on the top of channel region for Ge epi-growth. After standard cleaning, using Selective Area Growth (SAG) method, ultra-thin Si seed (~10 nm, 500 °C), $Si_{0.8}Ge_{0.2}$ (~25 nm, 350-400 °C) buffer, low-temperature Ge seed (~10 nm, 400 ˚C), and high-temperature Ge (~100 nm, 600 ˚C) were sequentially deposited in a UHVCVD (ultrahigh vacuum chemical vapor deposition) chamber with base pressure of 7×10^{-9} Torr [6.10]. Due to the dislocations in the epitaxy layer, Ge region is estimated to be p-type (~1×10^{17} cm^{-3}). Since at the interested wavelength pure Ge has much higher absorption coefficient than $Si_{0.8}Ge_{0.2}$ [6.2], $Si_{0.8}Ge_{0.2}$ buffer layer's contribution to the device's optical performance can be neglected. Finally, ohmic contacts were formed by TaN (25 nm)/Al (0.75 μm) deposition and patterning. Fig.6.1 illustrates the cross section structure of the Ge JFET photodetector, while the SEM image of the device's top-down view is shown in Fig. 6.2. The length/width of the channel region are 1 μm/100 μm. Fig. 6.3 shows the TEM image of the Ge layer on Si.

6.4 Results and Discussion

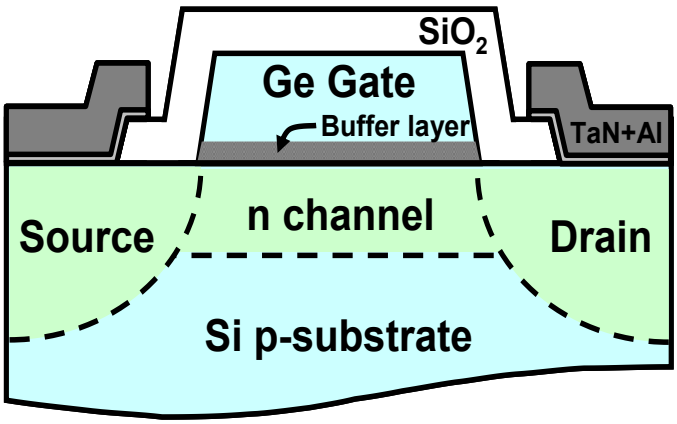

Fig. 6.1: The cross-section schematic of Ge JFET photodetector.

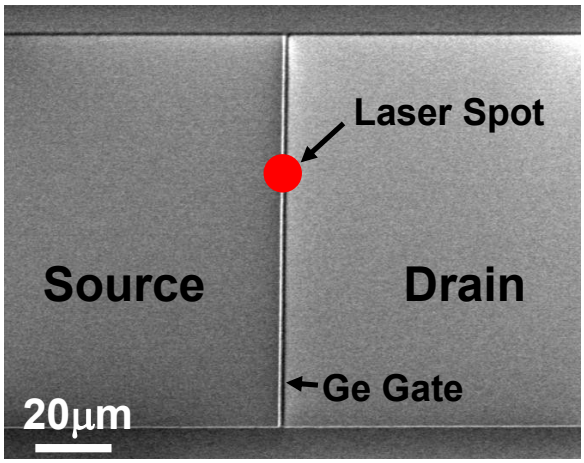

Fig. 6.2: SEM image of the device. The laser spot shinned on the Ge gate through cleaved single mode fiber is shown together. To obtain the intrinsic characteristics of the Ge JFET, the contribution of source-drain current of the un-illuminated part of the channel in I_D calculation is eliminated.

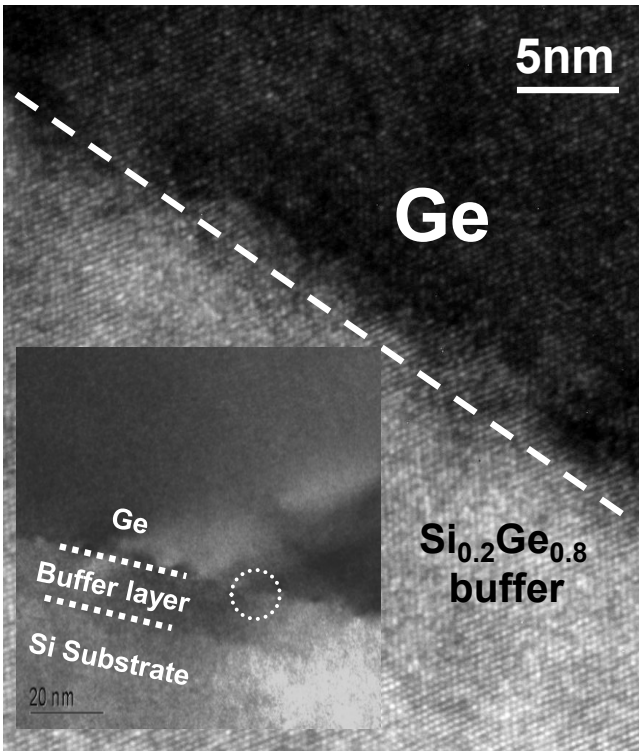

Fig. 6.3: TEM image of the selective area grown (SAG) Ge on Si/SiGe buffer on Si.

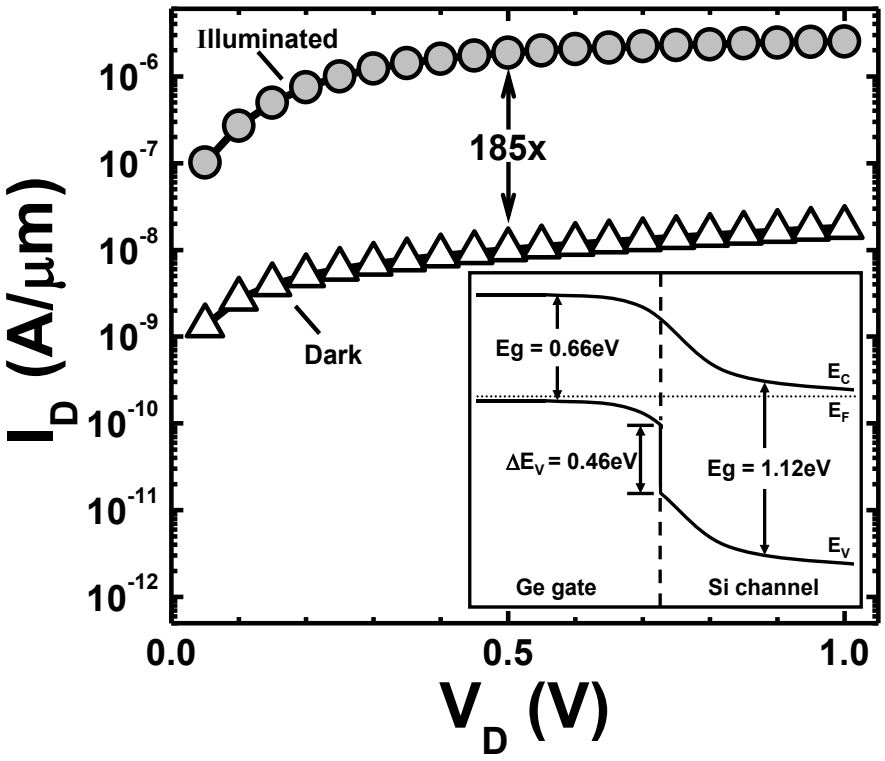

Fig. 6.4: I_D-V_D curve of Ge JFET with and without illumination. Inset shows the band diagram of Ge gate on Si channe.

The current-voltage (I-V) measurements were carried out on the Ge JFET. These characterizations were limited to source-drain bias below 1 V, as in the application of highly integrated inter-/intra-chip signal communication, low power consumption is much desirable. Fig.6.4 shows the typical I_D-V_D curves of the devices, both with and without illumination. As can be seen, without illumination, the device demonstrates low leakage current density of 10.1 nA/μm at 0.5 V bias, which corresponds to the channel "off" state as a result of the depletion formed in the junction region between the n-Si Channel and p-Ge gate. For optical characterization, light was coupled onto the device via cleaved single-mode fiber (core diameter ~8.2 μm). Due to the large valence band offset (~0.46 eV) between Ge and Si (band diagram shown in Fig.6.4 inset), photo-generated holes are confined in the Ge side at the Ge/Si interface. The accumulated holes attract electrons in the Si channel underneath and thus reduce the width of the depletion region, which leads to enhanced source-drain conductance. For the device with 1550 nm laser of 3-mW-power, at low bias of V_D = 0.5 V, I_D is increased from dark current by 185× to 1.86 μA/μm corresponding to an internal responsivity of ~2.36 A/W using the calculation method described in [6.2, 6.6] with coupling loss of 0.0558 between the optical fiber and small-area device taken into account. The lower responsivity of this work compared to previous III-V HEMT photodetectors is due to the difference in device structure, material properties and characterization method.

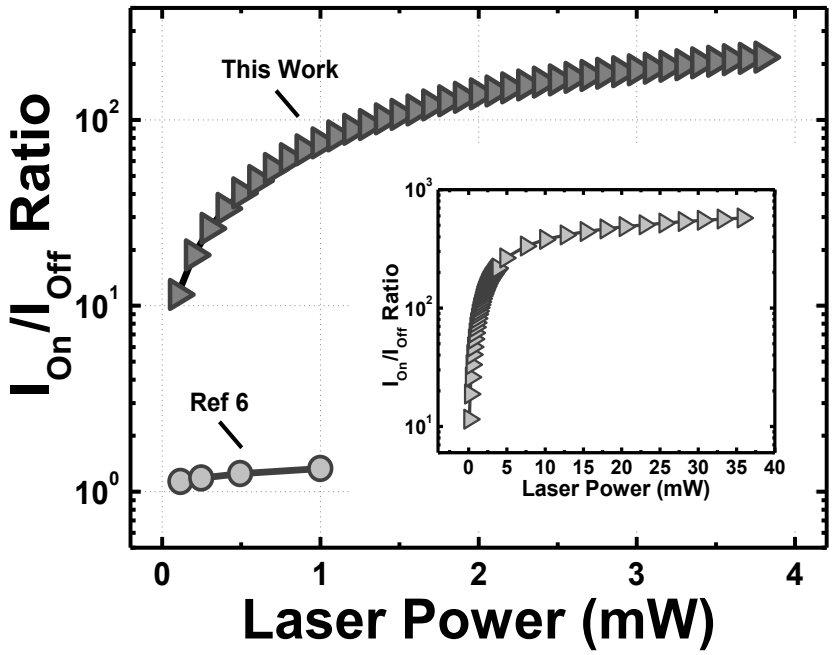

Fig. 6.5: I_{on}/I_{off} ratio versus laser power in comparison with the prior arts. Inset is the saturation behavior for the device with laser power up to 35.8 mW.

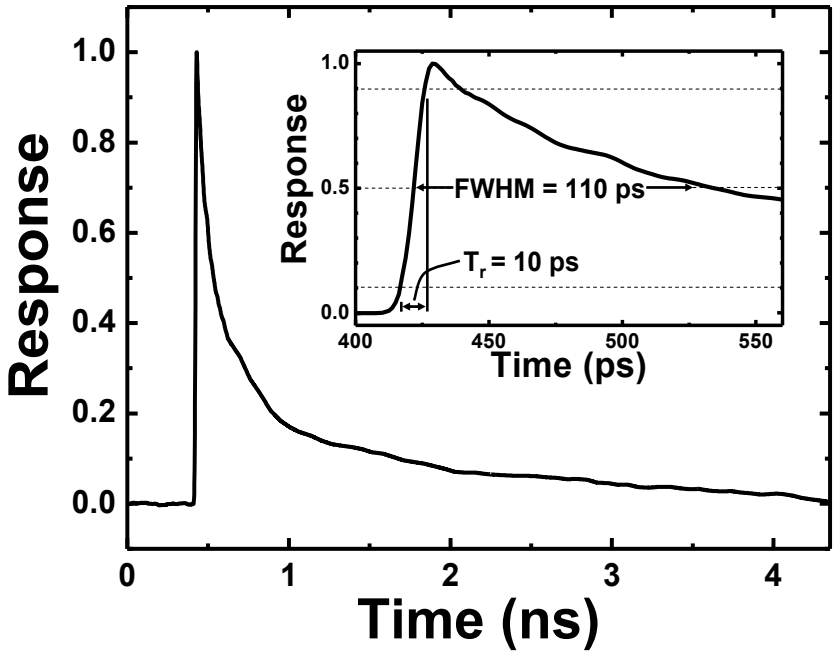

Fig. 6.6: Temporal impulse response of Ge JFET at 0.5 V source-drain bias. Inset shows the zoomed details of the pulse's rising part.

In Fig. 6.5, the I_{on}/I_{off} ratio (ratio of source-drain current under illumination and dark current) at a fixed source-drain bias of 0.5 V versus the laser power is shown together with previously reported data from [6.6]. Compared with the up to 1.33× I_{on}/I_{off} ratio observed by Sahni et al., the device from this work demonstrates more than ten times' enhancement over the whole light power range. The main reason for the sensitivity boost-up is believed to be the enhanced quality of the Ge film by our novel Ge epi-growth technique of two-step Ge growth combining with a SiGe buffer, which results in low density of defects in Ge top layer, thus high photo-carrier collection efficiency can be achieved. Fig. 6.5 inset shows Ge JFET's saturation behavior. Similar to conventional JFET [6.11], with increasing incident laser power, the device eventually enters saturation region. With the highest available laser power of 35.8 mW, I_{on}/I_{off} reaches as high as 575 corresponding to I_D = 5.79 μA/μm. This value is in close consistency with the classic JFET theory, from which a saturation source-drain current of ~7 μA/μm is estimated.

The temporal response of the Ge JFET was measured using 1.55 μm pulsed laser (pulse width 80 fs, repetition rate 20 MHz). Devices were probed with microwave probes and measured with a 50 GHz sampling oscilloscope. DC bias of 0.5 V was coupled through a 50 GHz bias tee. The pulsed response is shown in Fig.6.6. The inset zooms in on the rising part of the pulse. Worth noticing is that the rise time (tr) of the device is 10 ps which is comparable with the advanced Ge-on-Si photodiodes and suitable for high-speed applications. The FWHM (Full Width at Half

Maximum) and fall time (tf) are 110 ps and 1.4 ns, respectively. Similar to the HEMT photodetectors [6.7], the long tail in the impulse response's falling portion is due to the long lifetime of the accumulated holes. The speed performance is higher than the previous best results for Ge JFET (tf =20 ns and FWHM=3 ns from [6.6]), which could be attributed to the low-temperature defective buffer layers between Ge and Si where dislocations act as recombination centers and thus reduce the lifetime of the accumulated photo-holes in the Ge/Si interface [6.12]. Therefore, optimizations, such as defect engineering [6.13, 6.14] on the buffer layer between Ge and Si, are expected to extend the bandwidth further. A gate electrode in contact with the Ge island is also a possible way for speed enhancement similar to a base terminal in heterojunction phototransistor (HPT) [6.15, 6.16].

6.5 Conclusion

In this chapter, the enhanced performance of Ge JFET photodetector is demonstrated using the Ge epi-growth technique of two-step Ge growth combining with a SiGe buffer. The I_{on}/I_{off} ratio achieves as high as 575 in saturation region. The device shows a fast temporal response of 10 ps rise time with FWHM=110 ps. Together with its large scalability, the Ge JFET photodetector suggests an attractive solution to replace large size photodiode in future waveguide-based opto-electronics integrated circuit.

REFERENCES

[6.1] L. C. Kimerling, D. Ahn, A. B. Apsel, M. Beals, D. Carothers, Y-K. Chen, T. Conway, D. M. Gill, M. Grove, C-Y Hong, M. Lipson, J. Liu, J. Michel, D. Pan, S. S. Patel, A. T. Pomerene, M. Rasras, D. K. Sparacin, K-Y. Tu, A. E. White and C. W. Wong, "Electronic-photonic integrated circuits on the CMOS platform", Proc. SPIE, vol. 6125, pp. 612502-612511, Mar. 2006.

[6.2] L. Colace, G. Masini, and F. Galluzi, G. Assanto, "Ge-on-Si approaches to the detection of near-infrared light", IEEE J. Quantum Electron., vol. 35, no. 12, pp. 1843-1852, Dec. 1999.

[6.3] H. Zang, S. J. Lee, W. Y. Loh, J. Wang, K. T. Chua, M. B. Yu, B. J. Cho, G. Q. Lo, and D.-L. Kwong, "Dark-Current Suppression in Metal–Germanium–Metal Photodetectors Through Dopant-Segregation in NiGe Schottky Barrier," IEEE Electron Device Lett., vol. 29, no. 2, pp. 161–164, Feb. 2008.

[6.4] J. Wang, W. Y. Loh, K. T. Chua, H. Zang, Y. Z. Xiong, S. M. F. Tan, M. B. Yu, S. J. Lee, G. Q. Lo, and D. L. Kwong, "Low-Voltage High-Speed (18 GHz/1 V) Evanescent-Coupled Thin-Film-Ge Lateral PIN Photodetectors Integrated on Si Waveguide", IEEE Photonics Technol. Lett., vol. 20, no. 17, pp. 1485-1487, Sep. 2008.

[6.5] Ali K. Okyay, Duygu Kuzum, Salman Latif, David A. B. Miller, and Krishna C. Saraswat, "Silicon Germanium CMOS Optoelectronic Switching Device: Bringing Light to Latch", IEEE Trans. Electron. Device, vol. 54, no. 12, pp. 3252-3259, Dec. 2007.

[6.6] Subal Sahni, Xi Luo, Jian Liu, Ya-hong Xie, and Eli Yablonovitch, "Junction field-effect-transistor-based germanium photodetector on silicon-on-insulator," Opt. Lett., vol. 33, no. 10, pp. 1138-1140, May. 2008.

[6.7] Murilo A. Romero, M. A. G. Martinez, and Peter R. Herczfeld, "An Analytical Model for the Photodetection Mechanisms in High-Electron Mobility Transistors", IEEE Trans. Microw. Theory Tech., vol. 44, no. 12, pp. 2279–2287, Dec. 1996.

[6.8] D. M. Kim, S.H. Song, H. J. Kim, and K. N. Kang, "Electrical Characteristics of an Optically Controlled N-Channel AlGaAs/GaAs/InGaAs Pseudomorphic HEMT", IEEE Electron Device Lett., vol. 20, no. 2, pp. 73–76, Feb. 1999.

[6.9] M. Marso, M. Wolter, and P. Kordos, "A Novel Two-Color Photodetector Based on an InAlAs–InGaAs HEMT Layer Structure", IEEE Photonics Technol. Lett., vol. 16, no. 11, Nov. 2004.

[6.10] W. Y. Loh, J. Wang, J. D. Ye, R. Yang, H. S. Nguyen, K. T. Chua, T. H. Loh, Y. Z. Xiong, S. J. Lee, M. B. Yu, G. Q. Lo, and D. L. Kwong, "Impact of Local Strain from Selective-Epitaxial-Germanium with Thin Si/SiGe-Buffer for High-Performance p-i-n Photodetector with Low-Thermal Budget", IEEE Electron Dev. Lett., vol. 28, no. 11, pp. 984-986, Nov. 2007.

[6.11] S. M. Sze, Physics of Semiconductor Devices, 3rd ed., Wiley, 2007.

[6.12] A. D. Kurtz, S. A. Kulin, and B. L. Averbach, "Effect of Dislocations on the Minority Carrier Lifetime in Semiconductors", Phys. Rev., vol. 101, no.4, pp. 1285-1291, Feb. 1956.
[6.13] T. A. Langdo, C. W. Leitz, M. T. Currie, E. A. Fitzgerald, A. Lochtefeld and D. A. Antoniadis, "High quality Ge on Si by epitaxial necking", Appl. Phys. Lett., vol. 76, no. 25, pp. 3700-3702, Jun. 2000.
[6.14] L. C. Kimerling, "Silicon microphotonics", Appl. Surf. Sci, vol. 159-160, pp. 8-13, Jun. 2000.
[6.15] T. F. Carruthers, M. Y. Frankel, and C. S. Kyono, "Ultrafast photodetection with an AlInAs/GaInAs heterojunction bipolar transistor", Appl. Phys. Lett., vol. 63, no. 14, pp. 1921-1923, Oct. 1993.
[6.16] Z. Pei, J.-W. Shi, Y.-M. Hsu, F. Yuan, C. S. Liang, S. C. Lu, W. Y. Hsieh, M.-J. Tsai, and C. W. Liu, "Bandwidth Enhancement in an Integratable SiGe Phototransistor by Removal of Excess Carriers", IEEE Electron Device Lett., vol. 25, no. 5, pp. 286-288, May 2004.

CHAPTER 7

7. Silicon Waveguide Integrated Germanium JFET Photodetector with Improved Speed Performance

7.1 Introduction

In Chapter 6, the two-step Ge epi-growth technique combining with a SiGe buffer was applied in Ge gate formation in JFET photodetectors, resulting considerably enhanced sensitivity. However, the speed performance of the JFET is still inadequate for GHz-range Si photonics applications. Therefore, in this chapter, SOI wafers are used as the fabrication substrate of the JFET photodetectors, cancelling the bulk diffusion effects that resulted in the long response tail, leading to ~GHz bandwidth JFETs. Furthermore, waveguide-feeding structure is utilized to facilitate the integration of JFET into Si photonics circuits.

7.2 Background

Si-based OEIC, which employs optical signal as data deliverer, has been considered as a promising candidate to solve the delay and heat problems related to the global metallic interconnects [7.1] and to maintain the microelectronics scale-down roadmap known as Moore's Law [7.2]. Therefore, the development of

photonics building blocks such as silicon light-emitting diode and laser diode [7.2, 7.3], low loss optical waveguides [7.4], high-speed integrated modulators [7.5, 7.6] and detectors [7.7, 7.8] are under intensive study.

Although Ge waveguided photodiodes have been demonstrated with improved device performances [7.9, 7.10], to address the issues related to photodiodes' further scalability, novel structures of photodetectors has to be introduced. As a result, different groups are focusing on the investigation and new structures were proposed and demonstrated based on group IV [7.11, 7.12] or III-V materials [7.13]. In Chapter 6, a scalable Ge-photodetector based on junction field-effect-transistor (JFET) structure was successfully demonstrated with I_{on}/I_{off} ratio of 185 [7.14]. To overcome the low detection efficiency issue of conventional JFET photodetectors, modified two-step high/low temperature epitaxy technique [7.15] was utilized to grow a high quality Ge epi-layer as the gate of JFET. However, the reported temporal response (full width at half maximum (FWHM)) of 110 ps severely limits JFET's application in GHz-domain Si photonics. Carrier generation and diffusion in the bulk Si region beneath the device is a possible reason for the pulse response's long decaying tail.

In this work, a considerably enhanced bandwidth of 8 GHz is found in the Ge JFET photodetectors built on silicon-on-insulator (SOI) wafers, which play a major role in eliminating the carrier generation and diffusion far away from the intrinsic device region thus boost up the detection speed. While the merit of JFET's large scalability is maintained, the results suggest a promising solution to replace large-size

photodiodes in future OEIC through small-footprint-area photodetector for optical interconnections.

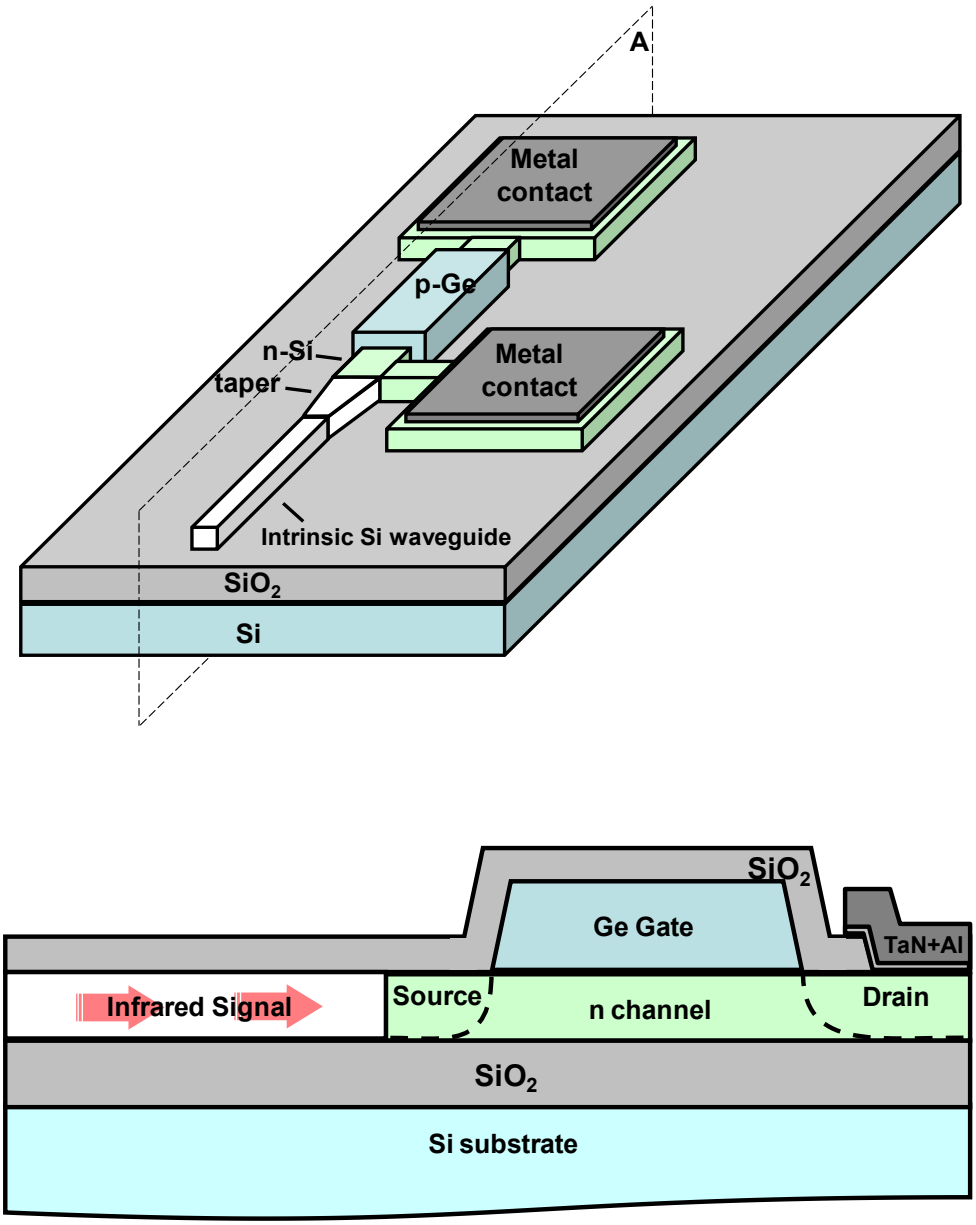

Fig. 7.1: (a) Schematic of Germanium JFET photodetector integrated with Si waveguide on SOI platform; (b)cross-section structure of JFET along plain A.

7.3 Experimental

Fig. 7.1(a) shows the schematic of the fabricated JFET-based photodetectors with the feeding Si waveguide. Starting from (100) SOI with 400-nm-thick p-type Si (8~15 Ωcm) and 2-μm-thick SiO2 insulator, waveguide (width 400 nm) and detector region were defined by lithography and dry etch. Subsequently, JFET channel region was implanted with Phosphorus 1×10^{11} cm^{-2}/20 keV and the source/drain was implanted with Phosphorus 1×10^{15} cm^{-2}/15 keV. After spike annealing at 1000 °C/5 s to activate n-/n+ region, plasma-enhanced chemical-vapor-deposition (PECVD) oxide of ~ 150 nm was deposited. This was followed by the patterning and etching to form 1.5-μm-wide 2-μm-long square windows for Ge deposition on top of the channel region. The etching process was carried out first by reactive ion etch. After removal of ~ 130 nm oxide, wet etching by 1% diluted HF was used to remove the remaining oxide in the window. Subsequently, the wafers were sent for cleaning in (NH_4OH : H_2O_2 : DI (de-ionized water) = 1 : 2 : 10) for 8 min, HF : DI (1 : 200) for 2 min followed by ultrasonic drying. Immediately after cleaning, the wafers were loaded into an ultra-high vacuum chemical vapor deposition chamber with base pressure of 7×10^{-9} Torr [7.15], where ultra-thin Si seed (~ 10 nm, 500 °C), $Si_{0.8}Ge_{0.2}$ (~ 25 nm, 350-400 °C) buffer, low-temperature Ge seed (~ 10 nm, 400 ˚C), and high-temperature strain-relaxed Ge (~ 300 nm, 600 ˚C) were sequentially deposited. Finally, after 750 nm PECVD oxide deposition and contact via etch, ohmic contacts were formed by a thin layer of TaN (25 nm) and Al (0.75 μm) deposition and patterning.

Fig. 7.1 (b) illustrates the cross-sectional structure of the device. The transmission electron microscope (TEM) image of the selective area grown Ge is shown in Fig. 7.2.

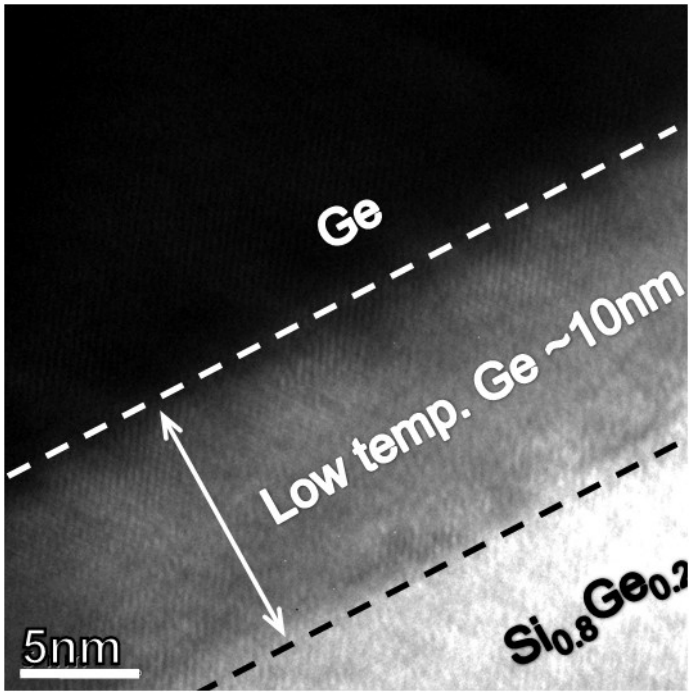

Fig. 7.2: TEM image of the Ge/Si interface.

7.4 Results and discussion

The photodetectors were first characterized in terms of dark current and light response. The current-voltage curve of the device is measured and plotted in Fig. 7.3. As can be seen, the device's dark current is 0.5 μA@1 V. It is previously suggested that dark current lower than 1 μA@-1 V is desirable for reduced standby power and acceptable detection noise [7.16].

For optical characterization, the samples were diced and polished. Then 1550-nm-wavelength laser was coupled into the waveguide by lensed-fiber (spot size 2.5±0.3 μm) mounted on precision XYZ stage. The coupling loss between the fiber

and the waveguide is calculated to be ~ 7 dB from the cutback structures near the actual devices. Therefore, for the input laser power of 8.3 mW, the power reaching the device is estimated to be ~ 1.7 mW.

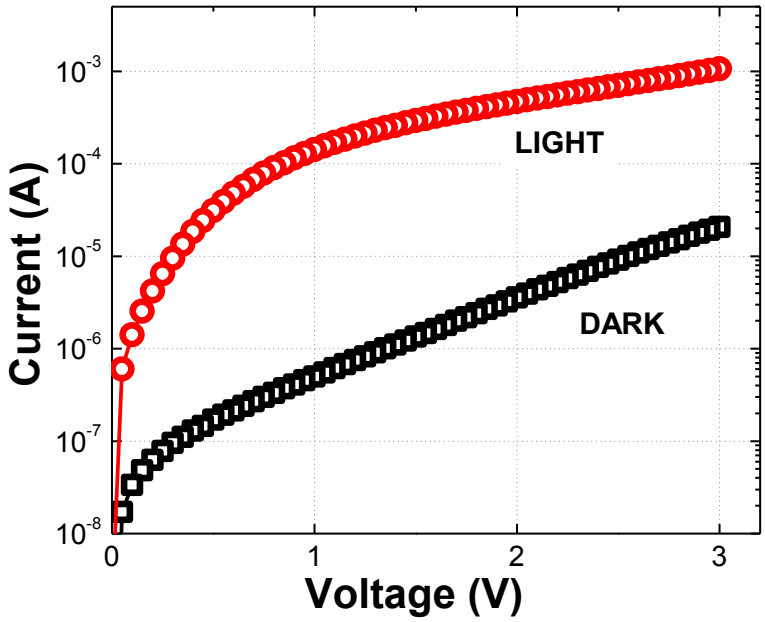

Fig. 7.3: IV characteristics of the waveguide JFET with and without laser input.

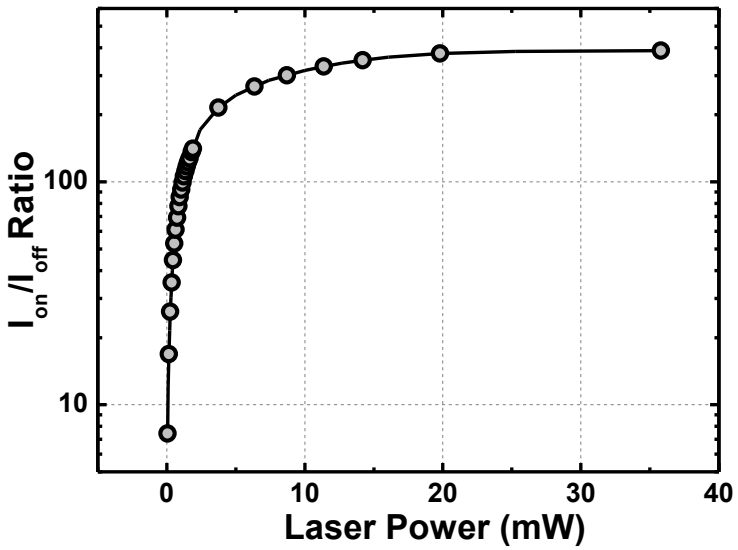

Fig. 7.4: I_{on}/I_{off} ratio versus input laser power showing the saturation behavior for the device similar as previously reported [7.14].

The external responsivity at 1 V is calculated to be 17 mA/W. At 3 V, the external responsivity is 128 mA/W, which corresponds to an internal responsivity of 642 mA/W with the coupling loss factored out. Since the theoretical responsivity for 1550 nm wavelength assuming 100% quantum efficiency (QE) is 1.2 A/W, the reported responsivity corresponds to QE of ~ 53%. The reported external responsivity is the highest for photodetectors with the detection material's footprint as small as 2 μm×2 μm. This could be attributed to the intrinsic gain mechanism from the device's working principle [7.12]. However, the total device area is still large taking into account the 5 μm×5 μm contact via, making further device design optimization necessary.

In Fig. 7.4, the I_{on}/I_{off} ratio at the source/drain bias of 1 V is plotted, which shows typical saturation behavior due to the balance between photocarrier generation and recombination, similar to previous report [7.14].

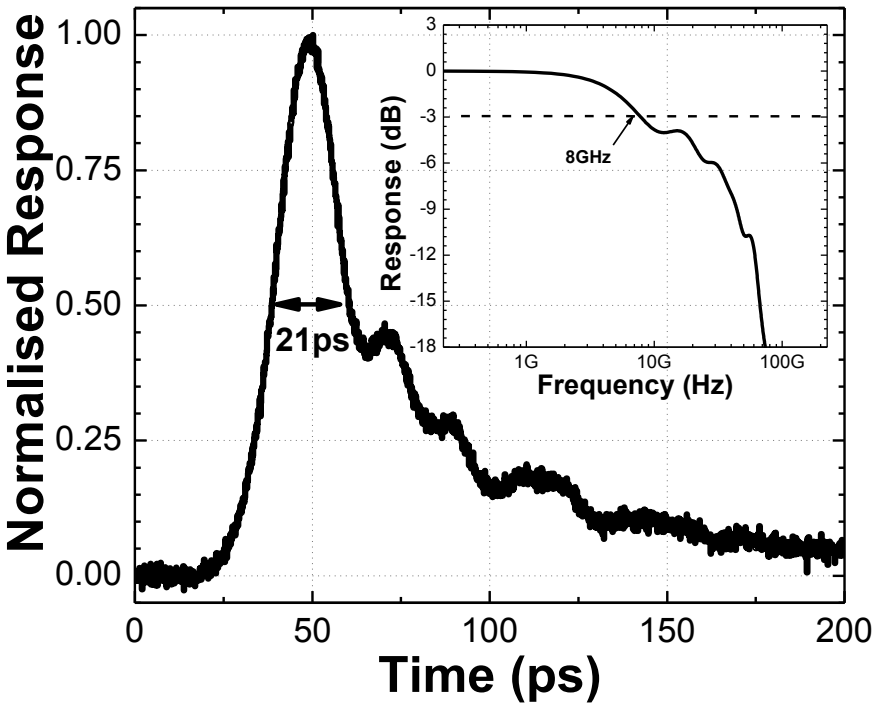

Fig. 7.5: Electrical response to the input laser pulse captured by high-speed oscilloscope. Inset is JFET photodetector's -3dB bandwidth. The device is biased at 1 V.

To measure the 3dB bandwidth of the reported device, ~ 80-fs-wide laser pulse was coupled into the detector and the generated electrical response pulse was captured by measurement system comprising 50-GHz-bandwidth sampling oscilloscope, RF microwave probe and high-speed RF cable.

Fig. 7.5 shows the obtained response pulse under source/drain bias of 1 V. The FWHM is 21 ps. The fast-fourier-transform (FFT) of the original pulse is plotted in Fig. 7.5 inset. It should be noted that the FFT was conducted over a window of 1000 ps, much larger than the 200 ps window shown in Fig. 7.5, to ensure correct data processing. An initial bandwidth of ~ 5 GHz was obtained. After correction to eliminate the impact of the measure system by deconvolving the system response

(20GHz limited by RF cable), the device demonstrates ~ 8 GHz bandwidth. Although the mechanism for the largely improved bandwidth is still being studied, one of the possible reasons is the use of the SOI substrate, which suppresses the carrier diffusion in the bulk Si, hence eliminating the long response tail following the initial impulse. Another possible mechanism is the higher leakage leading to further reduction of the carrier occupation time in the Ge layer [7.12], as the device shows an increased dark current as compared to [7.14].

7.5 Conclusion

In this chapter, waveguide-integrated Germanium infrared photodetector based on JFET was demonstrated with low dark current, high responsivity and large bandwidth. By the use of SOI wafers, parasitic effects is suppressed, which were previously believed to limit the detector's performance. The responsivity of 642 mA/W, bandwidth of 8 GHz may confirm Ge JFET's promise for the future small-foot-print photodetector.

REFERENCES

[7.1] L. C. Kimerling, D. Ahn, A. B. Apsel, M. Beals, D. Carothers, Y-K. Chen, T. Conway, D. M. Gill, M. Grove, C-Y Hong, M. Lipson, J. Liu, J. Michel, D. Pan, S. S. Patel, A. T. Pomerene, M. Rasras, D. K. Sparacin, K-Y. Tu, A. E. White and C. W. Wong, "Electronic-photonic integrated circuits on the CMOS platform", Proc. SPIE, vol. 6125, pp. 612502-612511, Mar. 2006.

[7.2] International Technology Roadmap for Semiconductors, 2009 edition.

[7.3] H. Rong, Richard Jones, Ansheng Liu, Oded Cohen, Dani Hak, Alexander Fang and Mario Paniccia, Nature, vol. 433, pp. 725-728, 2005.

[7.4] A. Fang, H. Park, O. Cohen, R. Jones, M, Paniccia and J. Bower, Opt. Express, vol. 14, pp. 9203-9210, 2006.

[7.5] Kevin K. Lee, Desmond R. Lim, Lionel C. Kimerling, Jangho Shin and Franco Cerrina, Optics Letters ,vol. 26, pp. 1888-1890, 2001.

[7.6] A. Liu, L. Liao, D. Rubin, H. Nguyen, B. Ciftcioglu, Y. Chetrit, N. Izhaky, and M. Paniccia, Opt. Express, vol. 15, pp. 660-668, 2007.

[7.7] Q. Xu, B. Schmidt, S. Pradhan, and M. Lipson, Nature, vol. 435, pp. 325-327, 2005.

[7.8] G. Dehlinger and S. J. Koester and J. D. Schaub and J. O. Chu and Q. C. Ouyang and A. Grill, "High-speed germanium-on-soi lateral PIN photodiodes", IEEE Photon. Technol. Lett., vol. 16, pp. 2547-2549, 2004.

[7.9] H. Luan, D. Lim, K. Lee, K. Chen, J. Sandland, K. Wada and L. Kimerling, "High-quality ge epilayers on si with low threading-dislocation densities", Applied Physics Letters, vol. 75, pp. 2909, 1999.

[7.10] L. Colace, G. Masini and G. Assanto, " Ge-on-Si approaches to the detection of near-infrared light", IEEE J. Quatum Elect., vol. 35, pp. 1843, 1999.

[7.11] Ali K. Okyay, Duygu Kuzum, Salman Latif, David A. B. Miller, and Krishna C. Saraswat, "Silicon Germanium CMOS Optoelectronic Switching Device: Bringing Light to Latch", IEEE Trans. Electron. Device, vol. 54, no. 12, pp. 3252-3259, Dec. 2007.

[7.12] Subal Sahni, Xi Luo, Jian Liu, Ya-hong Xie, and Eli Yablonovitch, "Junction field-effect-transistor-based germanium photodetector on silicon-on-insulator," Opt. Lett., vol. 33, no. 10, pp. 1138-1140, May. 2008.

[7.13] Murilo A. Romero, M. A. G. Martinez, and Peter R. Herczfeld, "An Analytical Model for the Photodetection Mechanisms in High-Electron Mobility Transistors", IEEE Trans. Microw. Theory Tech., vol. 44, no. 12, pp. 2279–2287, Dec. 1996.

[7.14] J. Wang, H. Zang, M. B. Yu, Y. Z. Xiong, G. Q. Lo, D. L. Kwong, and S. J. Lee, "Enhanced Sensitivity of Small-Size (With 1-μm Gate Length) Junction-Field-Effect-Transistor-Based Germanium Photodetector Using Two-Step Germanium Epitaxy by Ultrahigh Vacuum Chemical Vapor Deposition", IEEE Electron Dev. Lett., vol. 30, pp. 1066-1068, 2009.

[7.15] W. Y. Loh, J. Wang, J. D. Ye, R. Yang, H. S. Nguyen, K. T. Chua, T. H. Loh, Y. Z. Xiong, S. J. Lee, M. B. Yu, G. Q. Lo, and D. L. Kwong, “Impact of Local Strain from Selective-Epitaxial-Germanium with Thin Si/SiGe-Buffer for High-Performance p-i-n Photodetector with Low-Thermal Budget”, IEEE Electron Dev. Lett., vol. 28, no. 11, pp. 984-986, Nov. 2007.

[7.16] S. J. Koester, L. Schares, C. L. Schow, G. Dehlinger, and R. A. John, “Temperature-dependent analysis of Ge-on-SOI photodetectors and receiver”, Proc. Group IV Photonics Conference, pp. 179-181, Sep. 2006.

[7.17] N. Biyikli, I. Kimukin, O. Aytur, M. Gokkavas, M. Selim Unlu, and E. Ozbay, "45-GHz Bandwidth-Efficiency Resonant-Cavity-Enhanced ITO-Schottky Photodiodes", IEEE Photon. Technol. Lett., vol. 13, pp. 705-707, 2001.

CHAPTER 8

8. Conclusion and Outlook

This thesis focused on the research of integration of Ge photodiodes and Ge JFETs photodetectors on Si platform for OEIC.

In Chapter 2, the literature and technology review on recent progresses in the development and integration of Ge-photodetectors on Si-based photonics are reviewed. The remaining technological issues to overcome are also discussed.

Chapter 3 studies the electrical/optical characteristics of selectively grown Ge on SiGe and Si/SiGe buffer on Si for optical photodetection. Using an additional Si epitaxial layer as buffer layer, dark current is reduced by half to 0.12 μA at 1 V with smooth surface and low dislocation density without cyclic anneal or additional chemical-mechanical polishing. Lateral PIN Ge photodetector fabricated on this Ge platform shows photoresponsivity of ~190 mA/W at 1.52 μm and extended photon detection to 1.62 μm wavelength with 3-dB bandwidth at 5.2 GHz at 1 V.

Chapter 4 Si-waveguide-integrated lateral Ge-PIN photodetectors using novel Si/SiGe buffer and two-step Ge-process are demonstrated. Comparative analysis between lateral Ge PIN and vertical p-Si/i-Ge/n-Ge PIN are made. Light is evanescently coupled from Si waveguide to overlaying Ge-detector, achieving high responsivity of 1.16 A/W at 1550 nm with f_{3dB} bandwidth of 3.4 GHz for lateral Ge

PIN detector at 5 V reverse bias. In contrast, vertical p-Si/i-Ge/n-Ge PIN has lower responsivity of 0.29 A/W but higher bandwidth of 5.5 GHz at -5V bias.

Chapter 5 presents the device performance of the scaled thin-film-Ge lateral PIN photodetectors monolithically integrated with Si-waveguides on a SOI platform. With shrunk detector dimensions, the device with thin Ge (~220 nm) showed low dark current (~0.06 μA), high internal responsivity (~0.65 A/W) with speed as high as ~18 GHz. It is shown that with increasing detector length, devices' internal quantum efficiency can be further improved to ~90%.

In Chapter 6, the enhanced performance of Ge JFET photodetector is demonstrated using the Ge epi-growth technique of two-step Ge growth combining with a SiGe buffer. The I_{on}/I_{off} ratio achieves as high as 575 in saturation region. The device shows a fast temporal response of 10 ps rise time with FWHM=110 ps. Together with its large scalability, the Ge JFET photodetector suggests an attractive solution to replace large size photodiode in future waveguide-based opto-electronics integrated circuit.

Chapter 7 reports results on high-speed silicon-waveguided germanium junction-field-effect-transistor (JFET) -based photodetector with low stand-by current (0.5 μA@1V), high responsivity (642 mA/W) and high speed (8 GHz). The reported Ge JFET is a promising candidate for the further scale-downed photodetector in the next-generation Si photonics

There are several areas of work which can be studied in future research.

1) Pursuit of Higher Bandwidth

Nowadays, the reported Ge photodetectors' bandwidths are approaching 50 GHz, ready for near-future 40 Gb/s applications. On the other hand, in correspondence with III-V photodetectors whose speed has already exceed 100 GHz, it can be seen that there is still much room for enhancement. For bandwidths beyond 50 GHz, much thinner Ge intrinsic layers should be used. As in the high frequency region, undesirable parasitic effect such as contact resistance, stray capacitance and inductance may become the main limiting factors in bandwidth performance. Given the fact that reducing the intrinsic region's thickness for smaller carrier transition time at the same time leads to increase of device capacitance, the mushroom-mesa structure [8.1] may be of help for further bandwidth evolution, since it is capable of reducing the Rs and capacitance simultaneously.

2) Monolithic Integration of Ge Photodetectors with CMOS Circuits

Essential for future Si OEICs the co-integration of Ge photodetectors with functional CMOS circuits, which brings optical detection and further signal processing together. Therefore, there has been much effort in pursuing such integration. However, fabrication of high performance Ge photodetectors together with conventional CMOS devices comes with several technical issues that must be addressed, including the thermal budget issue, the cross contamination issues and the non-planarity issue due to Ge layer thickness. These issues could be one of the major research directions in the future study.

3) Plasmonics for Extreme Light Concentration

For higher speed, lower noise and suppressed power consumption, photodetectors are being fabricated in smaller dimensions [8.2]. However, previously the physical dimensions of the photodetectors were limited in the micrometer range by classical diffraction theory.

Recently, the amazing ability of plasmonic structures to concentrate light both laterally and in the depth of a semiconductor material beyond the diffraction limit into the deep-subwavelength-dimension was reported by Ishi et al. [8.3] A concentric grating surface plasmon antenna of 10 μm diameter was demonstrated to concentrate light into the center Si mesa Schottky diode of an active area of 300 nm in diameter. The observed more than 20-fold enhancement in photocurrent confirms the plasmonic effect. The estimated bandwidth of such small detector exceeds 100 GHz.

Because of its promise in Ge photodetector's drastic miniaturization into the nano-scale domain and expected high speed, plasmonics technology's application in Ge-based detectors should be pursued in the future.

REFERENCES

[8.1] K. Kato, "Ultrawide-band/high-frequency photodetectors", IEEE Transactions on Microwave Theory and Techniques, vol.47, no.7, pp. 1265-1281 1999.

[8.2] J. Schuller, E. Barnard, W. Cai, Y. Jun, J. White and M. Brongersma, "Plasmonics for extreme light concentration and manipulation", Nature materials, vol.9, no.3, pp. 193-204 2010.

[8.3] T. Ishi, J. Fujikata, K. Makita, T. Baba and K. Ohashi, "Si nano-photodiode with a surface plasmon antenna", Japanese Journal of Applied Physics, vol.44, pp. L364-L366 2005.

Appedix: List of Publications

Journal Publications

1. **J. Wang**, M. B. Yu, G. Q. Lo, D. L. Kwong and S. J. Lee, "Silicon Waveguide Integrated Germanium JFET Photodetector with Improved Speed Performance", *IEEE Photon. Tech. Lett.*, vol. 23, no. 12, pp. 765, Mar. 2011.

2. **J. Wang** and S. Lee, "Ge-photodetectors for Si-based Optoelectronic Integration", *Sensors*, vol. 11, no. 1, pp. 696-718, Jan. 2011.

3. **J. Wang**, H. Zang, M. B. Yu, Y. Z. Xiong, G. Q. Lo, D. L. Kwong, and S. J. Lee, "Enhanced Sensitivity of Small-Size (With 1-μm Gate Length) Junction-Field-Effect-Transistor-Based Germanium Photodetector Using Two-Step Germanium Epitaxy by Ultrahigh Vacuum Chemical Vapor Deposition", *IEEE Electron Device Lett.*, vol. 30, no. 10, pp. 1066-1068, Oct. 2009.

4. **J. Wang**, W. Y. Loh, K. T. Chua, H. Zang, Y. Z. Xiong, S. M. F. Tan, M. B. Yu, S. J. Lee, G. Q. Lo and D. L. Kwong, "Low-Voltage High-Speed (18 GHz/1 V) Evanescent-Coupled Thin-Film-Ge Lateral PIN Photodetectors Integrated on Si Waveguide," *IEEE Photon. Tech. Lett.*, vol. 20, no. 17, pp. 1485, Sep. 2008.

5. **J. Wang**, W. Y. Loh, K. T. Chua, H. Zang, Y. Z. Xiong, T. H. Loh, M. B. Yu, S. J. Lee, G. Q. Lo and D. L. Kwong, "Evanescent-Coupled Ge-PIN Photodetectors on Si-Waveguide with SEG-Ge and Comparative Study of Lateral and Vertical PIN Configurations," *IEEE Electron Device Lett*., vol. 29, no. 5, pp. 445-447, May 2008.

6. W. Y. Loh, **J. Wang**, J. D. Ye, R. Yang, H. S. Nguyen, K. T. Chua, T. H. Loh, Y. Z. Xiong, S. J. Lee, M. B. Yu, G. Q. Lo, and D. L. Kwong, "Impact of Local Strain from Selective- Epitaxial-Germanium with Thin Si/SiGe-Buffer for High-Performance p-i-n Photodetector with Low-Thermal Budget", *IEEE Electron Dev. Lett.*, vol 28, pp. 984-986, Nov. 2007

7. Ter-Hoe Loh, **J. Wang**, Hoai-Son Nguyen , B. Murthy , M. B. Yu , Wei Loh , Guo-Qiang Lo , Sung-Joo Lee , Balasubramanian Narayanan , D. Kwong, "Selective-Epitaxial Germanium on Silicon-on-insulator High Speed Photodetectors Using Low Temperature Ultra-thin Si0.8Ge0.2 Buffer ", *Appl. Phys. Lett.* 91, 073503, 2007

8. Shiyang Zhu, Kah-Wee Ang, Subhash C Rustagi, **J. Wang**, Y Z Xiong, G Q Lo and D L Kwong, "Waveguided Ge/Si Avalanche Photodiode with Separate Vertical SEG-Ge Absorption, Lateral Si Charge and Multiplication

Configuration", IEEE Electron Device Lett., vol. 30, no. 9, pp. 934–936, Sep. 2009

9. H. Zang, S. J. Lee, W. Y. Loh, **J. Wang**, M. B. Yu, G. Q. Lo and D. L. Kwong, "High-Speed Metal-Germanium-Metal Configured PIN-like Ge-Photodetector under Photovoltaic Mode and with Dopant-Segregated Schottky-Contact Engineering," *IEEE Photon. Tech. Lett.*, vol. 20. no. 23, pp. 165-167, 2008.

10. H. Zang, S. J. Lee, W. Y. Loh, **J. Wang**, M. B. Yu, G. Q. Lo, D. L. Kwong and B. J. Cho, "Application of Dopant Segregation to Metal–Germanium–Metal Photodetectors and its Dark Current Suppression Mechanism," *Appl. Phys. Lett.*, vol. 92, no. 1, 051110, 2008.

11. H. Zang, S. J. Lee, W. Y. Loh, **J. Wang**, K. T. Chua, M. B. Yu, B. J. Cho, G. Q. Lo and D. L. Kwong, "Dark-Current Suppression in Metal–Germanium–Metal Photodetectors Through Dopant-Segregation in NiGe Schottky Barrier," *IEEE Electron Device Lett.*, vol. 29, no. 2, pp. 161–164, Feb. 2008.

12. K W Ang, S Y Zhu, **J. Wang**, K T Chua, M B Yu, G Q Lo and D L Kwong, "Novel Silicon-Carbon (Si:C) Schottky Barrier Enhancement Layer for Dark Current Suppression in Ge-on-SOI MSM Photodetectors", *IEEE Electron Device Lett.*, vol. 29, no. 7, pp. 704–707, Jul. 2008.

Conference Presentations

13. **J. Wang**, W. Y. Loh, K. T. Chua, H. Zang, Y. Z. Xiong, T. H. Loh, M. B. Yu, S. J. Lee, G. Q. Lo and D. L. Kwong, "Evanescent-Coupled SEG-Ge Lateral and Vertical PIN Photodetectors integrated on Si-Waveguide," *International Conference on Solid State Devices and Materials (SSDM)*, pp. 966-967, Sep. 2008.

14. **J. Wang**, W. Y. Loh, H. Zang, M. B. Yu, K. T. Chua, T. H. Loh, J.D. Ye, R. Yang, X. L. Wang, S. J. Lee, B. J. Cho, G. Q. Lo and D. L. Kwong, "Integration of Tensile-Strained Ge p-i-n Photodetector on Advanced CMOS Platform," *4th IEEE International Group IV Photonics Conference (GFP)*, pp. 1-3, Sep. 2007.

15. **J. Wang**, Z. Xia, G. Du, X. Liu, and R. Han, "Simulation of Tri-Gate MOSFET Using 3D Monte Carlo Method Based on the Quantum Boltzmann Equation", *11st IEEE International Workshop on Computational Electronics (IWCE)*, P55, May 2006.

16. Ter-Hoe Loh, **J. Wang**, Hoai-Son Nguyen, Ramana Murthy, Ming-Bin Yu, Wei-Yip Loh, Guo-Qiang Lo, Balasubramanian Narayanan, Dim-Lee Kwong, "High Speed Selective-Area Epitaxial Ge-on-SOI P-I-N Photo-detector Using Thin Low-temperature $Si_{0.8}Ge_{0.2}$ Buffer by UHVCVD", *4th IEEE International Group IV Photonics Conference (GFP)*, pp. 1-3, Sep. 2007.